Self-Assembling Peptide Nanofibers RADA16 and IEIK13 for Rapid Hemostasis

by

Colin Bittner

B.S. Chemical Engineering
Virginia Tech, 2015

Submitted to the Department of Chemical Engineering
in partial fulfillment of the requirements for the degree of

Doctor of Philosophy

at the

MASSACHUSETTS INSTITUTE OF TECHNOLOGY

September 2022

Author _____
Department of Chemical Engineering
July 14, 2022

Certified by _____
Paula T. Hammond
Institute Professor
David H. Koch Professor
Head, Department of Chemical Engineering
Thesis Supervisor

Accepted by _____
Patrick S. Doyle
Robert T. Haslam (1911) Professor of Chemical Engineering
Singapore Research Professor
Graduate Officer

Self-Assembling Peptide Nanofibers RADA16 and IEIK13 for Rapid Hemostasis

by

Colin Bittner

Submitted to the Department of Chemical Engineering
on July 14, 2022, in partial fulfillment of the
requirements for the degree of
Doctor of Philosophy in Chemical Engineering

Abstract

Blood loss and trauma remain a significant cause of mortality in both the military and for civilians. This mortality can be reduced through the development of hemostatic bandages to reduce bleeding and prolong life in the prehospital setting. Many successful hemostat materials exist but there is still nothing that meets all the criteria of the ideal hemostat: easy to apply, no negative side effects, long term shelf stability, thermal stability, cost effective, and bioabsorbable. Self-assembling peptide nanofibers RADA16 and IEIK13 provide a unique possibility to create a hemostat that meets all of these criteria. These short peptides self-assemble into nanofibers that entangle and gel in solution. Through the use of layer-by-layer (LbL) we can apply these hemostatic peptides to a bioabsorbable substrate in thin conformal layers to produce a bandage that is lightweight and stable for long periods at room temperature.

In this thesis, we developed and optimized a new LbL system using the self-assembling peptide IEIK13 and validated it alongside a RADA16 based system. Dipping LbL on flat substrates was optimized and used to validate stability and film growth. These findings were translated into a spray LbL process allowing for coating of a three dimensional gelatin sponge substrate. These spray LbL methods were optimized to produce robust hemostatic films. We examined possible mechanisms for RADA16 and IEIK13 to accelerate hemostasis by examining the effects on the activity of several clotting factors as well as effects on clot formation. While some effects on the activity of individual clotting factors were observed, in vitro testing using whole blood showed no significant differences in clot formation. Finally, we developed entirely new LbL systems to through the addition of adhesive molecules, catechol functional groups and chitosan, to improve interaction between the coated dressings and wound tissue. We were able to show the application of these LbL films produced significant increase in tissue adhesion. These findings lay the groundwork for the development of a successful hemostatic bandage based on LbL films contain self-assembling peptide nanofibers.

Thesis Supervisor: Paula T. Hammond
Title: Institute Professor, David H. Koch Professor, and Department Head of Chemical Engineering, MIT

This doctoral thesis has been examined by the following committee:

Paula T. Hammond, PhD
Thesis Supervisor
Institute Professor, David H. Koch Professor, Department Head of Chemical Engineering, MIT

Bradley D. Olsen, PhD
Member, Thesis Committee
Professor of Chemical Engineering, MIT

Michael B. Yaffe, PhD
Member, Thesis Committee
Director, MIT Center for Precision Cancer Medicine, David H. Koch Professor in Science,
Professor of Biological Engineering, MIT

Shuguang Zhang, PhD
Member, Thesis Committee
Molecular Machine Group, Media Lab, MIT

Table of Contents

List of Figures

created using solutions with a polyelectrolyte concentration of either 0.1 g/L or 1.0 g/L. (B) Pilot test (n=1) comparing RADA16 and IEIK13 LbL coated surgifoam gelatin sponges. In both tests, surgical gauze was used as a control and uncoated surgifoam was used as a vehicle control. Blood loss was normalized to the mass of the animal. Pre-treatment blood loss represents the severity of the injury, post-treatment blood loss represents the effect of the applied treatment.

Figure 3.1 V-well clotting assay of RADA16 and IEIK13 in PBS. Gel formation assay mixing red blood cells with PBS containing different amounts of peptide RADA16 or IEIK13. When a gel is present in solution, red blood cells remain suspended and the color is spread throughout the well. When no gel is present, the red blood cells settle to the bottom creating a dark spot in the middle of the well. Arrows mark the gelation threshold for RADA16 (top) and IEIK13 (bottom).

Figure 3.2 Effects of LbL films on clotting factor activity. Fold Change in (A) factor IXa activity, (C) factor VII activity, (E) tissue factor activity, (G) thrombin activity with stock solutions of LbL components. Stock solutions are 1mg/mL added 1:10 with platelet poor plasma. Control for stock solutions is the vehicle control of 10mM HCl. Fold Change in (B) factor IXa activity, (D) factor VII activity, (F) tissue factor activity, (H) thrombin activity with solutions released from LbL formulations. Film releasates are added 1:10 with platelet poor plasma. Control for film releasate is the vehicle control of 1xPBS with gelatin sponge digested by collagenase. RADA/HA is $(RADA/HA)_{200}$, IEIK/HA is $(IEIK/HA)_{200}$. Statistical analysis conducted comparing each sample to the vehicle control using ordinary one way anova with Dunnett multiple comparison correction. (* $P \leq 0.05$, ** $P \leq 0.01$, *** $P \leq 0.001$, **** $P \leq 0.0001$).

Figure 3.3 Effects of LbL films on platelet aggregation. Platelet aggregation results showing fold change from vehicle control for aggregation of (A,D) non-activated platelets, (B,E) activated platelets, and (C,F) specific aggregation of platelets calculated as the activated platelet value minus the non-activated platelets. (A-C) shows results from stock solutions of 1mg/mL added 1:10 with platelet rich plasma. The vehicle control is 10mM HCl. (D-F) shows results from released sponge samples added 1:10 with platelet rich plasma and the vehicle control is 1xPBS with gelatin sponge digested by collagenase. RADA/HA is $(RADA/HA)_{200}$ and IEIK/HA is $(IEIK/HA)_{200}$. Statistical analysis conducted comparing each sample to the vehicle control using ordinary one way anova with Dunnett multiple comparison correction. (* $P \leq 0.05$, ** $P \leq 0.01$, *** $P \leq 0.001$, **** $P \leq 0.0001$).

Figure 3.4 Effects of LbL films on platelet rich plasma clot time. Absorbance assay to measure clot formation time in platelet rich plasma for (A) stock solutions and (B) film releasate samples. Stock solutions are 1mg/mL added 1:10 with platelet rich plasma. Material released from sponge samples added 1:10 with platelet rich plasma. The vehicle control for stock solutions is 10mM HCl. The vehicle control for film releasate is 1xPBS with gelatin sponge digested by collagenase. RADA/HA is $(RADA/HA)_{200}$ and IEIK/HA is $(IEIK/HA)_{200}$. Statistical analysis conducted comparing each sample to the vehicle control using ordinary one way anova with Dunnett multiple comparison correction. (* $P \leq 0.05$, ** $P \leq 0.01$, *** $P \leq 0.001$, **** $P \leq 0.0001$).

Figure 3.5 Effects of LbL films on whole blood clot time. Mechanical measurement of clot formation time in whole blood for (A) stock solutions and (B) film releasate samples. Stock solutions are 1mg/mL added 1:10 with citrated whole blood. Stock solutions are 1mg/mL added 1:10 with platelet rich plasma. Material released from sponge samples added 1:10 with citrated whole blood. The vehicle control for stock solutions is 10mM HCl. The vehicle control for film releasate is 1xPBS with gelatin sponge digested by collagenase. RADA/HA is $(RADA/HA)_{200}$ and IEIK/HA is $(IEIK/HA)_{200}$. Statistical analysis conducted comparing each sample to the vehicle control within each individual test using ordinary one way anova with Šídák's multiple comparisons

correction. Each test was compared within each individual test, bars show which samples are compared. (ns=not significant, * P ≤ 0.05, ** P ≤ 0.01, *** P ≤ 0.001, **** P ≤ 0.0001).

Figure 3.6 Peptide effects on whole blood clot formation and strength. Thromboelastography mechanical measurement of clot formation and strength for A) RADA16 and B) IEIK13. movement away from the center line denotes deflection of the measurement pin as a result of clot formation. A larger deflection is the result of a stiffer clot. Clot formation is triggered by the addition of $CaCl_2$ solution for clotting samples or saline solution for non-clotting samples. The vehicle control is deionized water. Brown- Clotting Blood with 150ug/mL Peptide, Pink- Clotting Blood with Vehicle Control, Green- Non-clotting Blood with 150ug/mL Peptide, White- Non-clotting Blood with Vehicle Control.

Figure 4.1 Reaction scheme and molecules for layer-by-layer film construction. (A) Reaction scheme to synthesize catechol modified hyaluronic acid (HACA) using EDC/Sulfo-NHS chemistry. (B)-(D) Polycations for LbL films. (B) Self-assembling peptide RADA16, (C) self-assembling peptide IEIK13, (D) Chitosan. Hyaluronic acid (HA) (A middle) and catechol functionalized hyaluronic acid (HACA) (A right) are polyanions for LbL films.

Figure 4.2 Film Growth of adhesive LbL formulations. LbL film growth measured by film thickness for a given number of (A) bilayers or (B) tetralayers. (A) Bilayer films contain the self-assembling peptide RADA16 or IEIK13 as a polycation and either hyaluronic acid (HA) or catechol modified hyaluronic acid (HACA) as a polyanion. (B) Tetralayer films contain chitosan (Chi) and either RADA16 or IEIK13 as polycations and hyaluronic acid (HA) as the polyanion. Each formulation is listed as follows: RADA/HA-$(RADA/HA)_n$, RADA/HACA-$(RADA/HACA)_n$, RADA/Chi-$(RADA/HA/Chi/HA)_n$, IEIK/HA-$(IEIK/HA)_n$, IEIK/HACA-$(IEIK/HACA)_n$, IEIK/Chi-$(IEIK/HA/Chi/HA)_n$.

Figure 4.3 Surface morphology of LbL coated gelatin sponges. SEM imaging of uncoated and LbL coated gelatin sponges. (A,B) uncoated gelatin sponge substrate (C,D) $(RADA/HA)_{200}$,(E,F) $(IEIK/HA)_{200}$, (G,H) $(RADA/HACA)_{200}$, (I,J) $(IEIK/HACA)_{200}$, (K,L) $(RADA/Chi)_{200}$, (M,O) $(IEIK/Chi)_{200}$. Images show a collapse of the gelatin sponge structure from the spray LbL process that is conserved for all LbL film formulations. Scale bars represent 100 μm (A,C,E,G,I,K,M) and 10 μm (B,D,F,H,J,L,O).

Figure 4.4 Peptide coverage of spray LbL coated sponge samples. Composite IVIS images of LbL coated gelatin sponge samples containing fluorescently labeled self assembling peptides. Color intensity denotes the peptide concentration. (A) RADA LbL formulations (B) IEIK LbL formulations. Each column shows multiple samples of the same formulation. Two replicate sponges are shown for each film treatment. $(RADA/HA)_{200}$ and $(IEIK/HA)_{200}$ images reproduced from Figure 2.7.

Figure 4.5 Total loading and release of LbL coated gelatin sponges. (A) Mass normalized total loading of LbL film formulations, mass of loaded peptide normalized to the mass of gelatin sponge substrate. (B) Area normalized total loading of LbL film formulations, mass of loaded peptide normalized to the area of the active LbL coated sponge surface. (C) Mass fraction of released RADA16 in PBS (solid line) and FBS (dashed line). (C, insert) mass fraction of RADA16 released over the first 3 hours. (D) Mass fraction of released IEIK13 in PBS (solid line) and FBS (dashed line). (D,insert) mass fraction of IEIK13 released over the first 3 hours. Total loadings obtained by digesting sponge samples with collagenase.

Figure 4.6 Effects of LbL films on clotting factor activity. Fold Change in (A) factor IXa activity, (B) factor VII activity, (C) tissue factor activity, (D) thrombin activity with stock solutions of LbL

components. Stock solutions are 1mg/mL added 1:10 with platelet poor plasma. Control is the vehicle control of 10mM HCl. Fold Change in (E) factor IXa activity, (F) factor VII activity, (G) tissue factor activity, (H) thrombin activity with solutions released from LbL formulations. Film releasates are added 1:10 with platelet poor plasma. Control is the vehicle control of 1xPBS with gelatin sponge digested by collagenase. RADA/HA is $(RADA/HA)_{200}$, RADA/HACA is $(RADA/HACA)_{200}$, RADA/Chi is $(RADA/HA/Chitosan/HA)_{200}$, IEIK/HA is $(IEIK/HA)_{200}$, IEIK/HACA is $(IEIK/HACA)_{200}$, IEIK/Chi is $(IEIK/HA/Chitosan/HA)_{200}$. Results for Stock Solution Control, RADA, IEIK, HA, Film Release Contol, RADA/HA, and IEIK/HA reproduced from figure 3.2. Statistical analysis conducted comparing each sample to the vehicle control using ordinary one way anova with Dunnett multiple comparison correction. (* $P \leq 0.05$, ** $P \leq 0.01$, *** $P \leq 0.001$, **** $P \leq 0.0001$).

Figure 4.7 Effects of LbL films on platelet aggregation. Platelet aggregation results showing fold change from vehicle control for aggregation of (A,D) non-activated platelets, (B,E) activated platelets, and (C,F) specific aggregation of platelets calculated as the activated platelet value minus the non-activated platelet. (A-C) shows results from stock solutions of 1mg/mL added 1:10 with platelet rich plasma. The vehicle control is 10mM HCl. (D-F) shows results from released sponge samples added 1:10 with platelet rich plasma and the vehicle control is 1xPBS with gelatin sponge digested by collagenase. RADA/HA is $(RADA/HA)_{200}$, RADA/HACA is $(RADA/HACA)_{200}$, RADA/Chi is $(RADA/HA/Chitosan/HA)_{200}$, IEIK/HA is $(IEIK/HA)_{200}$, IEIK/HACA is $(IEIK/HACA)_{200}$, IEIK/Chi is $(IEIK/HA/Chitosan/HA)_{200}$. Stock Solution Control, RADA, IEIK, HA, Film Release Contol, RADA/HA, and IEIK/HA reproduced from figure 3.3. Statistical analysis conducted comparing each sample to the vehicle control using ordinary one way anova with Dunnett multiple comparison correction. (* $P \leq 0.05$, ** $P \leq 0.01$, *** $P \leq 0.001$, **** $P \leq 0.0001$).

Figure 4.8 Effects of LbL films on clot formation time. (A,B) Absorbance assay to measure clot formation time in platelet rich plasma for (A) stock solutions and (B) film releasate samples. (A) Stock solutions are 1mg/mL added 1:10 with platelet rich plasma and the vehicle control is 10mM HCl. (B) Material released from sponge samples added 1:10 with platelet rich plasma and the vehicle control is 1xPBS with gelatin sponge digested by collagenase. (C,D) Mechanical measurement of clot formation time in whole blood for (C) stock solutions and (D) film releasate samples. (C) Stock solutions are 1mg/mL added 1:10 with citrated whole blood and the vehicle control is 10mM HCl. (D) Material released from sponge samples added 1:10 with citrated whole blood and the vehicle control is 1xPBS with gelatin sponge digested by collagenase. RADA/HA is $(RADA/HA)_{200}$, RADA/HACA is $(RADA/HACA)_{200}$, RADA/Chi is $(RADA/HA/Chitosan/HA)_{200}$, IEIK/HA is $(IEIK/HA)_{200}$, IEIK/HACA is $(IEIK/HACA)_{200}$, IEIK/Chi is $(IEIK/HA/Chitosan/HA)_{200}$. (A,B) Stock Solution Control, RADA, IEIK, HA, Film Release Contol, RADA/HA, and IEIK/HA reproduced from figure 3.4. (C,D) Stock Solution Control, RADA, IEIK, HA, Film Release Contol, RADA/HA, and IEIK/HA reproduced from figure 3.5. (A,B) Statistical analysis conducted comparing each sample to the vehicle control using ordinary one way anova with Dunnett multiple comparison correction. (C,D) Statistical analysis conducted comparing each sample to the vehicle control within each individual test using ordinary one way anova with Šídák's multiple comparisons correction. Each test was compared within each individual test, bars show which samples are compared. (ns=not significant, * $P \leq 0.05$, ** $P \leq 0.01$, *** $P \leq 0.001$, **** $P \leq 0.0001$).

Figure 4.9 Adhesive strength of LbL coated sponges. Mechanical test of shear force to measure the interfacial shear strength between sponge samples and porcine muscle tissue. RADA/HA is $(RADA/HA)_{200}$, RADA/HACA is $(RADA/HACA)_{200}$, RADA/Chi is $(RADA/HA/Chitosan/HA)_{200}$, IEIK/HA is $(IEIK/HA)_{200}$, IEIK/HACA is $(IEIK/HACA)_{200}$, IEIK/Chi is $(IEIK/HA/Chitosan/HA)_{200}$. n=6 for each formulation. Control is an uncoated gelatin sponge. Statistical analysis conducted

comparing each sample to the vehicle control using ordinary one way anova with Dunnett multiple comparison correction. (* $P \leq 0.05$, ** $P \leq 0.01$, *** $P \leq 0.001$, **** $P \leq 0.0001$).

Figure A.1 Visual depiction of time to equilibrium adsorption for RADA16 in 10mM HCl. (A) shows the first bilayer of adsorption. (B) shows the second bilayer of adsorption. A decrease in frequency translates to deposited mass. Black lines represent the start of the adsorption, 5 minutes of adsorption, and 10 minutes of adsorption. Each curve represents a different resonance point on the crystal. The second Bilayer adsorption takes longer than the first.

Figure A.2 Spray LbL setup optimization. (A) 3D model of sponge holder designed to hold and coat 8cm x 12.5cm x 10mm gelatin sponges. (B) LbL coated sponge front and back sprayed at full house vacuum pressure (Closed pressure of approximately -90kPa). (C) LbL coated sponge front and back sprayed at half house vacuum pressure (closed pressure of approximately -45kPa). The reduction in pressure helps keep the sponge from soaking through and being damaged after the LbL spraying process.

Figure A.3 NMR of different batches of catechol functionalized HA (HACA) used to determine the percent functionalization of hyaluronic acid side groups. NMR spectrum of Dopamine HCl (purple), HACA batch 3 (blue), HACA batch 3 (green), hyaluronic acid (HA) (red). Percent functionalization values for Batch 2 and Batch 3 are between 24-44% functionalization based on integration of different dopamine peaks.

Figure A.4 Optimization of adhesion shear test methods. (A) Testing different types of muscle tissue in a shear force test. (B)Testing effect different amounts of contact time between the sponge sample and chicken muscle tissue on shear strength in a shear force test. Control is an uncoated gelatin sponge control. RADA is $(RADA/HA)_{200}$ sponges made using 0.5 g/L RADA16 and HA solutions. (A) n=3 for all samples, (B) n=3 for 1hr and n=1 for 17hr. Pork was selected moving forward because of the larger effect observed from the coated sponge samples. Longer contact time between tissue and sponge samples showed a larger adhesion force, but one hour was used to stay relevant to the bleeding application.

Figure A.5 Rat Liver injury test model. Testing adhesive LbL formulations in a rat liver injury model. N=5. Blood loss normalized to rat total blood volume. Sponge control is an uncoated gelatin sponge. RADA/HA is $(RADA/HA)_{200}$, RADA/HACA is $(RADA/HACA)_{200}$, RADA/Chi is $(RADA/HA/Chitosan/HA)_{200}$, IEIK/HA is $(IEIK/HA)_{200}$, IEIK/HACA is $(IEIK/HACA)_{200}$, IEIK/Chi is $(IEIK/HA/Chitosan/HA)_{200}$. Statistical analysis conducted comparing each sample to the sponge control using ordinary one way anova with Dunnett multiple comparison correction, no significant differences in blood loss were observed.

Chapter 1. Introduction

1.1 Motivation

Hemorrhage is one of the leading causes of death amongst US military warfighters;[1] improved methods for achieving hemostasis in the field will transform the survivability of the injured solider. Blood loss remains not only the greatest cause of loss of life for warfighters in combat[2], but also the most preventable. If blood loss can be stopped in sufficient time for treatment there is a greatly improved chance of survival following gunshot, blast and other traumatic injuries. In fact, it was found in a recent study of 5000 deaths that almost 25% of battlefield deaths were possibly preventable and the majority (>87%) of such deaths were due to hemorrhage[2, 3]. For the wars in Iraq and Afghanistan, 50% of combat casualty deaths were due to exsanguination and even after the patient was transported to a medical facility, hemorrhage remained the primary cause of death[4]. This indicates the importance of maintaining the viability of the patient during the period of prolonged field care as well as transport to full scale medical facilities. If a patient suffering trauma can be stabilized until transport to a full scale surgical medical treatment center, the chances of survival for those suffering trauma is greater than 98%[3]. This problem exists even outside of the military; the leading cause of death in the US is trauma related hemorrhage for patients aged 1-46[4] and hemorrhage accounts for nearly 40% of these deaths[5]. This level has remained consistent over time and highlights the need for better hemostats.

1.2 Hemostasis mechanism

Hemostasis is the process by which blood clots and blood loss at a wound stops. It is generally broken down into two complimentary processes; primary and secondary hemostasis. In primary hemostasis, a platelet plug is formed at the wound site. The wound causes the exposure of collagen to platelets which become activated and stick to collagen and von Willebrand Factor.

These activated platelets are then able to bind to fibrinogen in the blood, leading to the formation of the platelet plug[3]. Secondary hemostasis describes the formation of a fibrin clot through a process often described as the clotting cascade. The clotting cascade involves two pathways of activation; the intrinsic pathway and the extrinsic pathway. The intrinsic pathway is activated by contact of the blood to a negatively charged surface and acts through coagulation factors XII, XI, IX, VII, and V. The extrinsic pathway is activated by the wound causing exposure of tissue factor to the blood and activating factor VII[6]. Tissue factor is expressed by cells surrounding blood vessels and present in very small amounts in the blood[7]. Both processes ultimately lead to the activation of factor X which is responsible for converting prothrombin into the active form thrombin. Thrombin is then responsible for converting fibrinogen into fibrin as well as further activating platelets. Fibrin then polymerizes and leads to the formation of the fibrin clot which is able to form around the original platelet plug[3, 6].

Hemostasis is a complex process that can often run into issues if various clotting factors are impaired or depleted. The levels of various clotting factors can range considerably, even within healthy patients. Thrombin levels in healthy patients can range as much as 4.5 fold[8]. Factor VII levels in healthy patients can range from 60-140%[9]. Factor VII clotting activity can range from 65-160 U/100mL and activated factor VII levels can range from 30-170 mU/mL in healthy individuals[10]. Normal levels of factor IX are 0.5-1.5 units/mL[11]. Variations outside of these normal ranges can indicate a disorder or the presence of coagulopathy. Coagulopathy refers to a state of impaired clot ability due to the depletion and dilution of clotting factors. This can significantly affect bleeding outcomes and often requires additional interventions to achieve clot formation[12].

1.3 Existing hemostat solutions

The ideal hemostat is easy to apply, has no negative side effects, long term shelf stability, thermal stability, cost effective, and bioabsorbable[13]. The last 20 years have yielded large growth in the number of hemostats, sealants, and adhesives available for surgery[14, 15], However, combat

and field hemostatic agents require significantly increased performance beyond those used in the common surgical setting. Combat materials must be lightweight and portable, durable, easy to apply with minimal skills, stable under a wide variety of temperature and humidity conditions for a period of months or years, and ready to use immediately (i.e. no thawing steps). These requirements make most surgical hemostats highly impractical for use in the field.

Several solutions have been developed for combat use in the past decade though none have met the criteria for an ideal hemostat. Previously utilized zeolite based powder materials have been abandoned due to an exotherm that can result in second and third degree burns, and smectite granular formulations have been shown to produce micro-emboli that create complications or tissue damage[4]. Current state of the art approaches for warfighter use in addressing hemostasis to prevent lethal blood loss are freeze-dried chitosan based bandages such as Hem-Con®, which rely on the natural blood clotting capability of the positively charged biopolymer chitosan which has some muco-adhesive properties[16, 17], and Quik-Clot Combat gauze®, which is based on kaolin clay that is able to rapidly absorb water from blood and activate local clotting factors[18-20]. In studies, chitosan bandages have been demonstrated to allow re-bleeding following initial hemostasis. Furthermore, chitosan bandages are costly, and some of these agents are not as effective under coagulopathic conditions, making them less applicable to severely injured patients suffering from both trauma- and crystalloid-induced coagulopathy. Gauze based material containing silicates, clays or other nondegradable components can create wound healing difficulties when they are ultimately removed. Particulate and granular based releasates from the bandages can leave residues on local blood vessels, which may later contribute to pathologic clot formation and venous thromboembolic phenomena[18, 21]. Although this system is cost-effective and has shown an advance over previous dressings, the Combat Gauze kaolin impregnated polyester/nylon is non-degradable, and must be removed at a later point during treatment which can lead to disruption of the original clot and re-bleeding[2]. Other dressings and treatments that have recently been developed include rapidly expanding microsponges

(XStat®)[3] which involves injection of the sponges into deep penetrating wounds in the extremities. Systemically delivered intravascular nanoparticles and artificial platelets have also been examined for internal bleeding.

The treatment of coagulopathic bleeding has generally only been addressed well by fibrin sealants that contain fibrin and thrombin proteins isolated in some form, and combined before or during application[4-5]. Such systems are typically costly and require refrigeration, making their use relatively prohibitive for large scale military use. Although several groups are currently investigating polymer hydrogels as alternative materials, these by definition contain large amounts of water and are not compatible with the need for a lightweight, easily stored dry bandage that could be efficiently distributed to warfighters and medics.[22, 23] There remains a need for more broadly applicable hemostat agents and dressings that can withstand high arterial pressure and stop bleeding more rapidly while retaining portability and usability of the system in a resorbable form that does not require later removal and also addressing the special needs of military patients for extended care in the field.

1.4 Layer-by-layer assembly

Drug release coatings with high densities of biologic drugs, biomacromolecules, or other biomedical components can be assembled using a water-based method known as alternating electrostatic layer-by-layer (LBL) or polyelectrolyte multilayer assembly [24, 25] . Films are formed through the alternating adsorption of positively and negatively charged polymer monolayers at room conditions. Total film thicknesses range from a few nm to 10 microns. Many aspects including molecular weight, charge density, hydrophobicity, steric hindrance, and strength of secondary interactions can affect both the film buildup and overall film structure[26-30]. LbL assembly is versatile, allowing the incorporation and controlled release of a broad range of functional polymers and other charged species including antibiotics, anti-inflammatory drugs, chemotherapeutics, growth factors, and nucleic acids[31-39]. Automated Spray-LbL methods have

reduced process times down to seconds per process cycle[40], making the process ideal for conformally coating porous mats and matrices such as wound dressings while maintaining pore size and structure.

Various hemostatic layer-by-layer systems have been examined to reduce bleeding. Previously a hydrogen bonding based LbL system was used to apply thrombin to bandages[41]. While these bandages were successful in promoting hemostasis, the inclusion of thrombin as the primary hemostat requires cold storage and severely limits the long term stability of dressings. Another benefit of these LbL systems is the ability to build in additional functionality to the systems. The existing thrombin LbL system has been modified to also allow for the sustained delivery of antibiotics released from the film[42]. This shows the unique ability of LbL to target multiple problems with a single system, in this case promoting hemostasis and then preventing infection in a wound. Previous work using the self-assembling peptide RADA16 has shown promise as an existing hemostat LbL system[43].

1.5 Self-assembling peptide nanofibers

Self-assembled peptide materials have shown great promise in biological applications[44]. These peptides are able to self-assemble through the alternation of positive and negative amino acid groups along a more hydrophobic backbone. The placement of the charges allow the peptides to align with each other to form nanofibers. As these fibers grow, they entangle with each other and are able to gel in solution at high enough concentrations. Many iterations of these self-assembling peptides have been developed and RADA16 and IEIK13 are two peptides that show great promise as hemostats[45]. RADA16 (RADARADARADARADA) is 16 amino acid peptide consisting of the sequence arginine-alanine-aspartic acid-alanine repeated four times. IEIK13 (IEIKIEIKIEIKI) is 13 amino acid peptide consisting of the sequence isoleucine-glutamic acid-isoleucine-lysine repeated three times with an additional isoleucine at the end. The different amino acids used in each peptide lead to differences in hydrophobicity of the peptides and different gel

properties. The increased hydrophobicity of IEIK13 with respect to RADA16 leads to a stiffer gel being formed and allows IEIK13 to gel at concentrations much lower than RADA16. While both peptides are stable and resistant to degradation, IEIK13 has shown the ability to maintain its structure even through autoclaving[46].

Both RADA16 and IEIK13 can self-assemble into a β-sheet structure to form individual nanofibers that generate a nanofiber scaffold that resembles natural fibrin clots with 1-100 nm pore sizes[47]. The peptide nanofiber scaffold, when delivered as a solution to wounds, has been demonstrated to be a superb material for stopping bleeding in multiple types of wounds of several tissues in less than 10 seconds[48]. These nanofiber scaffolds have been tested in many types of animals, including mice, rats, rabbits, and pigs[49]. These peptide materials have been used as scaffolds to promote cellular growth and wound healing. The synthetic nature of these materials allows for excellent biocompatibility without the issues that can arise from biologically sourced materials. Additionally, RADA16 has already been developed into a commercial hemostat (PuraStat®) and has shown great efficacy when applied directly as a peptide gel[44]. Previous work on RADA16 has demonstrated that these peptides are able to be applied to three dimensional substrates in LbL films with high loading. It has been shown that these films are extremely stable, retaining the ability to form a peptide gel even after 6 months at 60°C. It was also shown that these films were capable of reducing blood loss in a swine skin puncture model[43]. While previous LbL systems have already examined the use of RADA16, much less has been done to study IEIK13. IEIK13 provides a potentially more potent peptide material to examine as a hemostat.

Self-assembling peptides have shown great effectiveness in promoting hemostasis[43, 44, 48]. Previous work has demonstrated that the hemostatic properties of self-assembling peptides is highly dependent on their ability to form nanofibers and gel in solution. It has been proposed that the peptide nanofibers promote hemostasis by acting as a net that collects and concentrates red blood cells, platelets, and even clotting factors which leads to the acceleration of clot formation[43, 50].

1.6 Tissue adhesive molecules

The ability of the hemostatic dressing to adhere to the wound surface becomes extremely important when dealing with non-compressible wounds. In these cases hemostasis can be more readily achieved without the need for pressure with fast adhesion of the dressing to the wound area[51]. Various wound sealing adhesives have been shown to effectively provide both hemostasis and promote better wound healing. Adhesion can be achieved both through the use of ionic charge interactions and with crosslinking polymers that bind strongly to the tissue[52-54]. Materials like chitosan which present free amine groups that can interact with tissues and exhibit muco-adhesive properties that have been shown to be effective in different forms, including within a tissue binding hydrogel[55-57]. Chitosan can be adhesive through positive charge promotes strong interaction with negatively charged wound surfaces as well as hydrogen bonding with extracellular matrix components. It also promotes strong aggregation and activation of platelets in blood[58, 59]. Catechol groups can interact through a combination of hydrogen bonding, π-π stacking interactions, and covalent bonding with organic surfaces[60]. Collagen adhesion is driven by specific interaction with cell receptors. This also provides adhesion and activation of platelets in blood[61, 62]. Laminin Contains globular binding domains for both cellular adhesion as well as adhesion to extracellular matrix molecules[63, 64]. Poly(acrylic acid) grafted with N-hydroxysuccinimide ester (Paac-NHS ester) has carboxylic acid groups that can interact with the tissue surface through electrostatic interactions and hydrogen bonding, as well as NHS ester groups that can form covalent bonds with exposed primary amine groups on the tissue surface[65]. Other forms or modes of adhesion can be achieved through rapid covalent bonding to tissue, such as the formation of bonds to the surface with catechol groups, much as is observed with the adhesion of mussels. Incorporation of these chemical motifs into the LbL film can be used as a means of achieving a

rapid hemostat that also exhibits enhanced muco-adhesive properties, thus enabling multiple properties of the LbL coating to greatly enhance the hemostatic activity of the dressing.

1.7 Scope and Outline

The primary objective of this thesis was to use the self-assembling peptides RADA16 and IEIK13 to develop lightweight, stable, and biocompatible hemostatic dressings. While previous work has been conducted using RADA16 in layer-by-layer, IEIK13 has yet to be studied in these systems. These new LbL film systems have been designed to address some of the shortcomings of existing hemostat materials.

Chapter 2 outlines the generation and optimization of LbL systems containing RADA16 or IEIK13. Additionally, preliminary pilot testing was conducted that motivated further work with developing new LbL formulations.

Chapter 3 looks at the mechanism through which the peptide nanofibers and other LbL components may induce clotting and reduce blood loss from a wound. We examine different levels of clot formation, from individual clotting factors and platelets to plasma and whole blood interactions.

Chapter 4 examines the effect of building in adhesive molecules into the LbL systems. Catechol functional groups and chitosan containing systems were combined with peptide nanofiber LbL systems to improve adhesion between hemostatic dressings and wound tissue. The improvement in adhesive force was measured and future in vivo studies are recommended.

Chapter 5 provides a summary of the conclusions from this work as well as discussing future work and directions for the hemostatic peptide LbL systems.

1.8 References

1. Bellamy, R.F., Pedersen, D.C. & Deguzman, L.R. ORGAN BLOOD-FLOW AND THE CAUSE OF DEATH FOLLOWING MASSIVE HEMORRHAGE. *Circulatory Shock* **14**, 113-127 (1984).
2. Katzenell, U., Ash, N., Tapia, A.L., Campino, G.A. & Glassberg, E. Analysis of the causes of death of casualties in field military setting. *Mil Med* **177**, 1065-1068 (2012).
3. Hong, C., Olsen, B.D. & Hammond, P.T. A review of treatments for non-compressible torso hemorrhage (NCTH) and internal bleeding. *Biomaterials* **283**, 121432 (2022).
4. Chambers, J.A. et al. "Stop the Bleed": A U.S. Military Installation's Model for Implementation of a Rapid Hemorrhage Control Program. *Mil Med* **184**, 67-71 (2019).
5. Sobrino, J. & Shafi, S. Timing and causes of death after injuries. *Proceedings* **26**, 120-123 (2013).
6. Adams, R.L.C. & Bird, R.J. Review article: Coagulation cascade and therapeutics update: Relevance to nephrology. Part 1: Overview of coagulation, thrombophilias and history of anticoagulants. *Nephrology* **14**, 462-470 (2009).
7. Mackman, N. The role of tissue factor and factor VIIa in hemostasis. *Anesthesia and analgesia* **108**, 1447-1452 (2009).
8. Brummel-Ziedins, K., Vossen, C.Y., Rosendaal, F.R., Umezaki, K. & Mann, K.G. The plasma hemostatic proteome: thrombin generation in healthy individuals. *Journal of thrombosis and haemostasis : JTH* **3**, 1472-1481 (2005).
9. Howard, P.R., Bovill, E.G., Pike, J., Church, W.R. & Tracy, R.P. Factor VII antigen levels in a healthy blood donor population. *Thrombosis and haemostasis* **72**, 21-27 (1994).
10. Hellstern, P., Beeck, H., Fellhauer, A., Fischer, A. & Faller-Stockl, B. Measurement of factor VII and of activated factor VII in healthy individuals and in prothrombin complex concentrates. *Thrombosis research* **86**, 493-504 (1997).
11. Souid, A.-K. in Pediatric Emergency Medicine. (eds. J.M. Baren, S.G. Rothrock, J.A. Brennan & L. Brown) 917-926 (W.B. Saunders, Philadelphia; 2008).
12. Gulati, D., Novak, A. & Stanworth, S.J. Common haemostasis issues in major bleeding and critical illness. *Clinical medicine* **18**, 320-323 (2018).
13. Pusateri, A.E. et al. Making sense of the preclinical literature on advanced hemostatic products. *J Trauma* **60**, 674-682 (2006).
14. Spotnitz, W.D. & Burks, S. Hemostats, Sealants, and Adhesives II: Update As Well As How and When to Use the Components of the Surgical Toolbox. *Clinical and Applied Thrombosis-Hemostasis* **16**, 497-514 (2010).
15. Spotnitz, W.D. & Burks, S. Hemostats, sealants, and adhesives: components of the surgical toolbox. *Transfusion* **48**, 1502-1516 (2008).
16. Dai, C.L., Liu, C.S., Wei, J., Hong, H. & Zhao, Q.H. Molecular imprinted macroporous chitosan coated mesoporous silica xerogels for hemorrhage control. *Biomaterials* **31**, 7620-7630 (2010).
17. Malmquist, J.P., Clemens, S.C., Oien, H.J. & Wilson, S.L. Hemostasis of oral surgery wounds with the HemCon Dental Dressing. *J Oral Maxil Surg* **66**, 1177-1183 (2008).
18. Khoshmohabat, H., Paydar, S., Kazemi, H.M. & Dalfardi, B. Overview of Agents Used for Emergency Hemostasis. *Trauma Mon* **21** (2016).
19. Rhee, P. et al. QuikClot use in trauma for hemorrhage control: Case series of 103 documented uses. *J Trauma* **64**, 1093-1099 (2008).
20. Arnaud, F. et al. Exothermic reaction in zeolite hemostatic dressings: QuikClot ACS and ACS+(R). *Ann Biomed Eng* **36**, 1708-1713 (2008).
21. Granville-Chapman, J., Jacobs, N. & Midwinter, M.J. Pre-hospital haemostatic dressings: A systematic review. *Injury* **42**, 447-459 (2011).

22. Casey, B.J. et al. FVII Dependent Coagulation Activation in Citrated Plasma by Polymer Hydrogels. *Biomacromolecules* **11**, 3248-3255 (2010).
23. Raymond, J., Metcalfe, A., Salazkin, I. & Schwarz, A. Temporary vascular occlusion with poloxamer 407. *Biomaterials* **25**, 3983-3989 (2004).
24. Decher, G. Fuzzy Nanoassemblies: Toward Layered Polymeric Multicomposites. *Science* **277**, 1232 (1997).
25. Hammond, P.T. Form and Function in Multilayer Assembly: New Applications at the Nanoscale. *Advanced Materials* **16**, 1271-1293 (2004).
26. Shiratori, S.S. & Rubner, M.F. pH-dependent thickness behavior of sequentially adsorbed layers of weak polyelectrolytes. *Macromolecules* **33**, 4213-4219 (2000).
27. Gilbert, J.B., Rubner, M.F. & Cohen, R.E. Depth-profiling X-ray photoelectron spectroscopy (XPS) analysis of interlayer diffusion in polyelectrolyte multilayers. *P Natl Acad Sci USA* **110**, 6651-6656 (2013).
28. Xu, L., Ankner, J.F. & Sukhishvili, S.A. Steric Effects in Ionic Pairing and Polyelectrolyte Interdiffusion within Multilayered Films: A Neutron Reflectometry Study. *Macromolecules* **44**, 6518-6524 (2011).
29. Sui, Z.J., Salloum, D. & Schlenoff, J.B. Effect of molecular weight on the construction of polyelectrolyte multilayers: Stripping versus sticking. *Langmuir* **19**, 2491-2495 (2003).
30. Clark, S.L. & Hammond, P.T. The role of secondary interactions in selective electrostatic multilayer deposition. *Langmuir* **16**, 10206-10214 (2000).
31. Shah, N.J., Hong, J., Hyder, M.N. & Hammond, P.T. Osteophilic Multilayer Coatings for Accelerated Bone Tissue Growth. *Adv Mater* **24**, 1445-1450 (2012).
32. Shukla, A. et al. Controlling the release of peptide antimicrobial agents from surfaces. *Biomaterials* **31**, 2348-2357 (2010).
33. Moskowitz, J.S. et al. The effectiveness of the controlled release of gentamicin from polyelectrolyte multilayers in the treatment of Staphylococcus aureus infection in a rabbit bone model. *Biomaterials* **31**, 6019-6030 (2010).
34. Shukla, A., Fuller, R.C. & Hammond, P.T. Design of multi-drug release coatings targeting infection and inflammation. *J Control Release* **155**, 159-166 (2011).
35. DeMuth, P.C., Su, X.F., Samuel, R.E., Hammond, P.T. & Irvine, D.J. Nano-Layered Microneedles for Transcutaneous Delivery of Polymer Nanoparticles and Plasmid DNA. *Adv Mater* **22**, 4851-+ (2010).
36. Macdonald, M.L. et al. Tissue integration of growth factor-eluting layer-by-layer polyelectrolyte multilayer coated implants. *Biomaterials* **32**, 1446-1453 (2011).
37. Samuel, R.E. et al. Osteoconductive protamine-based polyelectrolyte multilayer functionalized surfaces. *Biomaterials* **32**, 7491-7502 (2011).
38. Min, J., Braatz, R.D. & Hammond, P.T. Tunable staged release of therapeutics from layer-by-layer coatings with clay interlayer barrier. *Biomaterials* **35**, 2507-2517 (2014).
39. Min, J.H. et al. Designer Dual Therapy Nanolayered Implant Coatings Eradicate Biofilms and Accelerate Bone Tissue Repair. *Acs Nano* **10**, 4441-4450 (2016).
40. Krogman, K.C., Lowery, J.L., Zacharia, N.S., Rutledge, G.C. & Hammond, P.T. Spraying asymmetry into functional membranes layer-by-layer. *Nat Mater* **8**, 512-518 (2009).
41. Shukla, A., Fang, J.C., Puranam, S., Jensen, F.R. & Hammond, P.T. Hemostatic Multilayer Coatings. *Adv Mater* **24**, 492-+ (2012).
42. Hsu, B.B. et al. Multifunctional Self-Assembled Films for Rapid Hemostat and Sustained Anti-infective Delivery. *Acs Biomater Sci Eng* **1**, 148-156 (2015).
43. Hsu, B.B. et al. Clotting Mimicry from Robust Hemostatic Bandages Based on Self-Assembling Peptides. *Acs Nano* **9**, 9394-9406 (2015).
44. Gelain, F., Luo, Z., Rioult, M. & Zhang, S. Self-assembling peptide scaffolds in the clinic. *NPJ Regenerative medicine* **6**, 9 (2021).

45. Verbraeken, B. et al. Efficacy and histopathological effects of self-assembling peptides RADA16 and IEIK13 in neurosurgical hemostasis. *Nanomedicine : nanotechnology, biology, and medicine* **40**, 102485 (2022).
46. GIL, E.S., GILBERT, K. & Mehta, M., Edn. C07K 7/08 (2006.01), A61L 27/22 (2006.01), A61K 38/12 (2006.01), A61L 27/54 (2006.01), A61L 27/58 (2006.01). (ed. W.I.P. Organization) (2015).
47. Zhang, H., Luo, H. & Zhao, X. Mechanistic Study of Self-Assembling Peptide RADA16-I in Formation of Nanofibers and Hydrogels. *Journal of Nanotechnology in Engineering and Medicine* **1** (2009).
48. Ellis-Behnke, R.G. et al. Nano hemostat solution: immediate hemostasis at the nanoscale. *Nanomedicine : nanotechnology, biology, and medicine* **2**, 207-215 (2006).
49. Ellis-Behnke, R. At the nanoscale: nanohemostat, a new class of hemostatic agent. *Wires Nanomed Nanobi* **3**, 70-78 (2011).
50. Luo, Z., Wang, S. & Zhang, S. Fabrication of self-assembling D-form peptide nanofiber scaffold d-EAK16 for rapid hemostasis. *Biomaterials* **32**, 2013-2020 (2011).
51. Kheirabadi, B. Evaluation of topical hemostatic agents for combat wound treatment. *U.S. Army Medical Department journal*, 25-37 (2011).
52. Min, Y.J. & Hammond, P.T. Catechol-Modified Polyions in Layer-by-Layer Assembly to Enhance Stability and Sustain Release of Biomolecules: A Bioinspired Approach. *Chem Mater* **23**, 5349-5357 (2011).
53. Spicer, C.D. et al. Synthesis of Phospho-Amino Acid Analogues as Tissue Adhesive Cement Additives. *Acs Central Sci* **6**, 226-231 (2020).
54. Taboada, G.M. et al. Overcoming the translational barriers of tissue adhesives. *Nat Rev Mater* **5**, 310-329 (2020).
55. Bouten, P.J.M. et al. The chemistry of tissue adhesive materials. *Prog Polym Sci* **39**, 1375-1405 (2014).
56. Du, X.C. et al. Anti-Infective and Pro-Coagulant Chitosan-Based Hydrogel Tissue Adhesive for Sutureless Wound Closure. *Biomacromolecules* **21**, 1243-1253 (2020).
57. Pang, J.H. et al. Mechanically and functionally strengthened tissue adhesive of chitin whisker complexed chitosan/dextran derivatives based hydrogel. *Carbohyd Polym* **237** (2020).
58. Narimane Mati-Baouche, P.-H.E., Helene de Baynast, Guillaume Pierre, Cedric Delattre, Philippe Michaud Chitosan as an adhesive. *European Polymer Journal* **60**, 198-212 (2014).
59. Chou, T.C., Fu, E., Wu, C.J. & Yeh, J.H. Chitosan enhances platelet adhesion and aggregation. *Biochem Bioph Res Co* **302**, 480-483 (2003).
60. Saiz-Poseu, J., Mancebo-Aracil, J., Nador, F., Busque, F. & Ruiz-Molina, D. The Chemistry behind Catechol-Based Adhesion. *Angew Chem Int Edit* **58**, 696-714 (2019).
61. Heino, J. The collagen family members as cell adhesion proteins. *Bioessays* **29**, 1001-1010 (2007).
62. Morton, L.F. et al. Conformation-dependent platelet adhesion to collagen involving integrin alpha 2 beta 1-mediated and other mechanisms: multiple alpha 2 beta 1-recognition sites in collagen type I. *The Biochemical journal* **299 (Pt 3)**, 791-797 (1994).
63. Hohenester, E. Structural biology of laminins. *Essays Biochem* **63**, 285-295 (2019).
64. Aumailley, M. The laminin family. *Cell Adhes Migr* **7**, 48-55 (2013).
65. Yuk, H. et al. Dry double-sided tape for adhesion of wet tissues and devices. *Nature* **575**, 169-174 (2019).

Chapter 2. Generation and Optimization of Layer-by-Layer Films Containing the Self-Assembling Peptides RADA16 and IEIK13

2.1 Introduction

Self-assembling peptide nanofibers show great promise as a potential ideal hemostat[1-4], an example being the peptides RADA16 and IEIK13[5]. When working with self-assembled materials, the past treatment and states of the material can have an impact on the current structure and function. Specifically with self-assembling peptide nanofibers, the fibers length and shape can be dependent on the formation conditions[6]. While stable fibers form in acidic conditions, it has been shown that irregular aggregates can form at a neutral pH[7]. In an effort to improve reproducibility of all materials, methods were developed to clear out the self-assembled materials' past conditions and start fresh with only newly formed fibers.

Layer-by-layer (LbL) assembly is a versatile method to create films containing many different functional species. The incorporation and controlled release of a broad range of functional polymers and other charged species including antibiotics, anti-inflammatory drugs, chemotherapeutics, growth factors, and nucleic acids can be achieved[8-16]. LbL films can be constructed through many different interactions including electrostatic interactions and hydrogen bonding interactions[17, 18]. Generally speaking, the weaker the interactions used to build the film, the less stable the resulting film will be. When a film is unstable or constructed under conditions different from the release conditions, it will fall apart rapidly[18].

Previous work has shown methods to create layer-by-layer films containing the self-assembling peptide RADA16[19]. However, no previously published work has shown the ability to produce LbL films containing IEIK13. Many aspects including molecular weight, charge density, hydrophobicity, steric hindrance, and strength of secondary interactions can affect both the film buildup and overall film structure[20-24]. While both peptides can be treated similarly, optimization was necessary to increase reproducibility and loading of peptides within the films.

Spray layer-by-layer setups provide a much more rapid way to apply an LbL film to a substrate and can be much more rapidly translatable than dip LbL due to the speed of application and the ability to spray on virtually any substrate[25, 26]. However, this process relies on a different mechanism than traditional dip LbL, primarily acting through kinetic entrapment rather than equilibrium adsorption and can have relatively poor efficiency with materials[26].

Chapter Scope: This study covers the development of an IEIK13 layer-by-layer film as well as various optimizations conducted to standardize solution and material preparation. Additionally, the methods to produce the layer-by-layer sponge samples used in subsequent studies are described. General characterization of these samples is described in this chapter.

2.2 Methods

2.2.1 Materials

Self-assembling peptides solutions of 1.5 wt% RADA16 and IEIK13 were generous donations from 3-D Matrix Medical Technology. Hyaluronic acid (MW = 2 MDa) was obtained from Lifecore Biomedical. Collegenase (Type I) was purchased from Sigma-Aldrich. Human whole blood (EDTA anticoagulated) was obtained from Hemacare, and washed and pooled 10% rabbit red blood cells (RBCs) were obtained from Lampire Biological Laboratories. Solutions of 1% (10 mg/mL) RADA16-I were a generous donation from 3DMatrix. Fluorescently labeled RADA16-I (RADA16-IFAM) was functionalized by 5-carboxyfluorescein at the N-terminus through a -Gly-Gly- linker and synthesized by the MIT Biopolymers Laboratory. Surgifoam gelatin sponges (8cm x 12.5cm x 10mm) were purchased from McKesson. Chitosan (MW = 15 kDa) was purchased from Polysciences, Inc.

2.2.2 Solution preparation

1.5 wt% peptide gel was diluted to 1 mg/mL or 0.1 mg/mL using 10mM HCl. This solution was then stirred overnight. Afterward the solutions were sonicated for 1 hour using a bath sonicator and immediately filtered through a 0.2 μm PES membrane. The resulting solution was

stored at room temperature overnight to allow the peptide fibers to reassemble. Solutions of Hyaluronic acid were dissolved into 10mM HCl and stirred overnight.

2.2.3 Dip layer-by-layer

Film assembly conditions for electrostatic films were based on previously published work with RADA16[19]. Silicon wafer substrates were cut into pieces approximately 25mm by 6.5mm. These wafers were cleaned using isopropanol, followed by methanol, and finally water before being air dried. Immediately prior to layering, the wafers were plasma treated (Harrick PDC-32G) for at least 10 minutes and then immediately placed onto a slide stainer for Layer-by-Layer film assembly. Silicon slides were immersed into 1 mg/mL peptide (RADA16 or IEIK13) for 10 minutes, followed by immersion into 3 separate wash baths of 10mM HCl for 1 minute each, then into 1 mg/mL HA in 10mM HCl for 10 minutes, and again into 3 separate wash baths of 10 mM HCl for 1 minute each. This constituted one bilayer and the process was repeated for a given number of n bilayers. An additional formulation for a hydrogen bonding based film was created using 1 minute adsorption times in ethanol instead of the 10mM HCl. These hydrogen boding films also used tannic acid (TA) in place of HA.

2.2.4 Film thickness

Methods for measuring film thickness were adapted from previously published work[19, 27]. Thickness of films deposited onto silicon substrates were measured using a Profilometer (Dektak 150 Profilometer). A razor was used to scratch two lines in the film lengthwise approximately 1.5-2mm apart. These scored areas were used to level the resulting data and the step-height was calculated by comparing the razor scored area with the average height of the area in between the two scratches. A data point was collected from three separate spots along the film for each sample and then averaged.

2.2.5 Film adsorption equilibrium time

Methods for QCMD were adapted from previously published work[28]. Gold coated crystals were used in a quartz crystal microbalance with dissipation (QCMD) at the MIT Materials

Research Laboratory to conduct a flow based layer by layer formulation. Crystals were equilibrated in 10mM HCl and then layered by flowing 1 mg/mL peptide (RADA16 or IEIK13) until the frequency change leveled off (approximately 30 minutes). Then 10mM HCl was flowed as a wash solution for 30 minutes. Afterward, 1mg/mL HA was flowed until the frequency change leveled off (approximately 30 min) followed by another 30 minute wash step. This process consisted of one bilayer and was repeated for 2-5 bilayers.

2.2.6 Atomic force microscopy (AFM)

Cleaned silicon slides were placed in solutions of 1mg/mL RADA16 or IEIK13 for a period of 10 minutes. Afterward, the slides were removed, air dried and imaged on a Veeco Nanoscope V with Dimension 3100 AFM in tapping mode.

2.2.7 Spray layer-by-layer

Methods for spray LbL systems were adapted from previously published work[19]. Large gelatin sponges (8cm x 12.5cm x 10mm) were coated using an automated film assembly instrument (Svaya). The sprayer was calibrated to a 0.25mL/s flow rate at 15PSI. House vacuum was applied through a regulator to around 50% strength (Approximately -45kPa closed pressure). Bilayer formulations were created with the following steps: 0.1mg/mL peptide (RADA16 or IEIK13) in 10mM HCl for 3 seconds, wait time for 5 seconds, rinse with 10mM HCl for 3 seconds, dry time for 8 seconds, 0.1 mg/mL polyanion in 10mM HCl for 3 seconds, wait time for 5 seconds, rinse with 10mM HCl for 3 seconds, dry time for 8 seconds. In summary: peptide (3s), wait (5s), wash (3s), dry (8s), polyanion (3s), wait (5s), wash (3s), dry (8s). This made up one bilayer and was repeated for n bilayers with a 60 minute air dry time added after every 10 bilayers.

Even coverage of Sponge samples was examined by spraying fluorescently labeled peptide solutions for the LbL process. Afterward the sponge samples were imaged using an In Vivo Imaging System (IVIS) at λ_{ex} = 465 nm; λ_{em} = 520 nm.

2.2.8 Peptide release study

Methods for the release of LbL films from gelatin substrates were adapted from previously published work[19]. For release studies, films containing either labeled RADA16 or labeled IEIK13 were generated. This was done by adding fluorescently labeled peptide in a 1:20 ratio with unlabeled peptide. Release of film coated sponges were done by placing pieces of the sponge sample into 1mL of PBS at 37°C. At each time point 300 µL was removed and replaced with fresh, prewarmed PBS. Fluorescence (λ_{ex} = 480 nm; λ_{em} = 525 nm) of collected samples were measured and compared with a standard curve for RADA16 or IEIK13. Total loading was obtained by adding 100 µL of 10mg/mL Collagenase (Type I) and then incubating samples for at least 24hr to allow the sponge substrate to be digested. Then fluorescence was measured and concentration was calculated as described above.

2.3 Results and Discussion

2.3.1 Layer-by-layer film framework

These layer-by-layer (LbL) films were constructed using electrostatic films using a framework similar to previously published work with RADA16[19]. **Figure 2.1** shows the structure of each component used in the films as well as the three dimensional gelatin sponge substrate used to produce hemostatic bandages. At neutral pH, both RADA16 and IEIK13 have a net neutral charge and therefore would be poor electrostatic LbL components. However, by using a an acidic 10 mM HCl solution at around pH 2, the peptides skew toward having a net positive charge and can be treated as a polycation. This low pH is also necessary to promote the formation of peptide nanofibers[7]. Hyaluronic Acid (HA) with a molecular weight of 2 MDa maintains a negative charge in 10 mM HCl and can be used as a polyanion in LbL films built under these conditions. The two electrostatic films were created by alternating peptide, either RADA16 or IEIK13, with HA to produce bilayers as described in the methods. An LbL film consisting of n bilayers of alternating RADA16 and hyaluronic acid (HA) is denoted as $(RADA/HA)_n$. Similarly, an LbL film of n bilayers alternating between IEIK13 and HA is denoted as $(IEIK/HA)_n$. These LbL systems were first

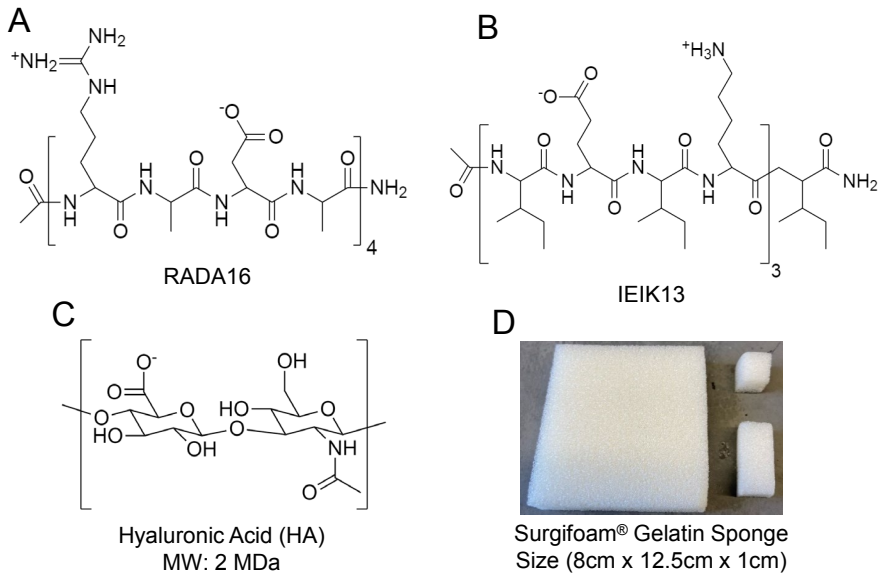

Figure 2.1 Layer by Layer film components. *(A) Self-assembling peptide RADA16 used as a polycation, (B) Self-assembling peptide IEIK13 used as a polycation, (C) Hyaluronic Acid (MW 2MDa) used as a polyanion, (D) Surgifoam gelatin sponge substrate.*

examined as dip LbL systems built on silicon slides and later applied to a three dimensional gelatin sponge substrate (**Figure 2.1D**) for evaluation as a hemostat.

2.3.2 Optimizing solution preparation

The Layer-by-Layer (LbL) films were generated using electrostatic interactions. It has been documented that the self-assembling peptides RADA16 and IEIK13 both form a hydrogel based on peptide concentration and salt concentration in solution. Previous work has shown that dissolving these peptides into 10 mM HCl increases the solubility of the peptides without introducing enough salt to cause gelation[6].

In an effort to examine what state the peptides were in when adsorbing to the surface, solutions of both RADA16 and IEIK13 were adsorbed onto silicon slides and examined under atomic force microscopy (AFM). **Figure 2.2** showed that both peptides do indeed adsorb as fibers onto the surface and within LbL films. We then examined methods to break up the peptide fibers into smaller pieces. Previous work has shown that sonication is sufficient to break up most of the

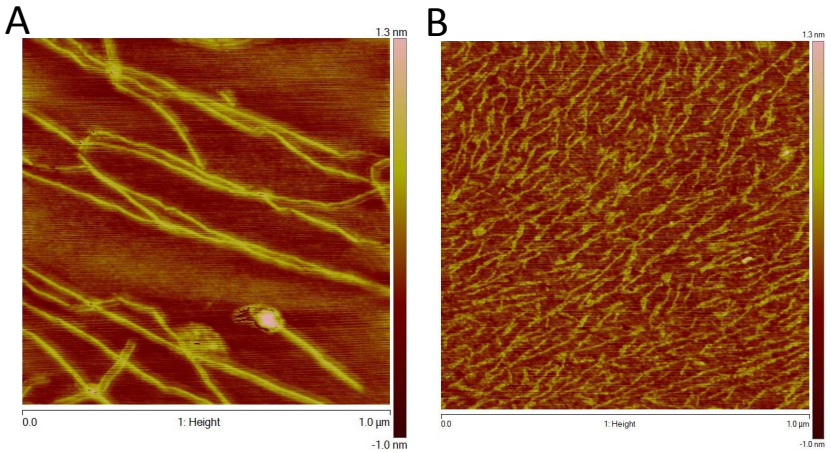

Figure 2.2 Peptide nanofiber adsorption structure. *Representative AFM images of peptide nanofibers adsorbed on silicon. (A) RADA16 peptide nanofibers, (B) IEIK13 peptide nanofibers. Images 1 µm x 1 µm.*

peptide fibers in solution[6]. After sonicating the peptide solution, we examined how long it takes for the fibers to reform into a steady state. To examine this, peptide solutions of both RADA16 and IEIK13 were placed on a TEM grid at various time points after sonication. (**Figure 2.3**). These images showed that 24 hours was sufficient to reform peptide fibers to a similar length as the non-sonicated fibers. This result is supported by previous measurements of RADA16 fibers after sonication using AFM[29]. Rheology on RADA16 and IEIK13 has also showed a viscosity recovery between 12-48hrs after fiber breakup[6]. Additionally, these samples (particularly the IEIK13 solutions) showed some larger fiber clumps that did not break up from the sonication. This lead to the idea of filtering the solutions immediately after sonication, allowing the broken up fibers to move through the filter and removing any larger fiber clumps that did not break down. With the new method of dissolving into 10mM HCl, sonicating for one hour and then filtering, better reproducibility was observed in the construction of LbL films. (**Figure 2.4**)

2.3.3 Optimizing slide preparation

To look at the effects of slide treatment, silicon slides cleaned with piranha solution were compared with slides cleaned with isopropanol, methanol, and water. Results showed no significant difference between piranha treated slides and the alcohol cleaned slides for $(RADA/HA)_{50}$ bilayer films. **Figure 2.4** shows the mass, thickness, and roughness of the various

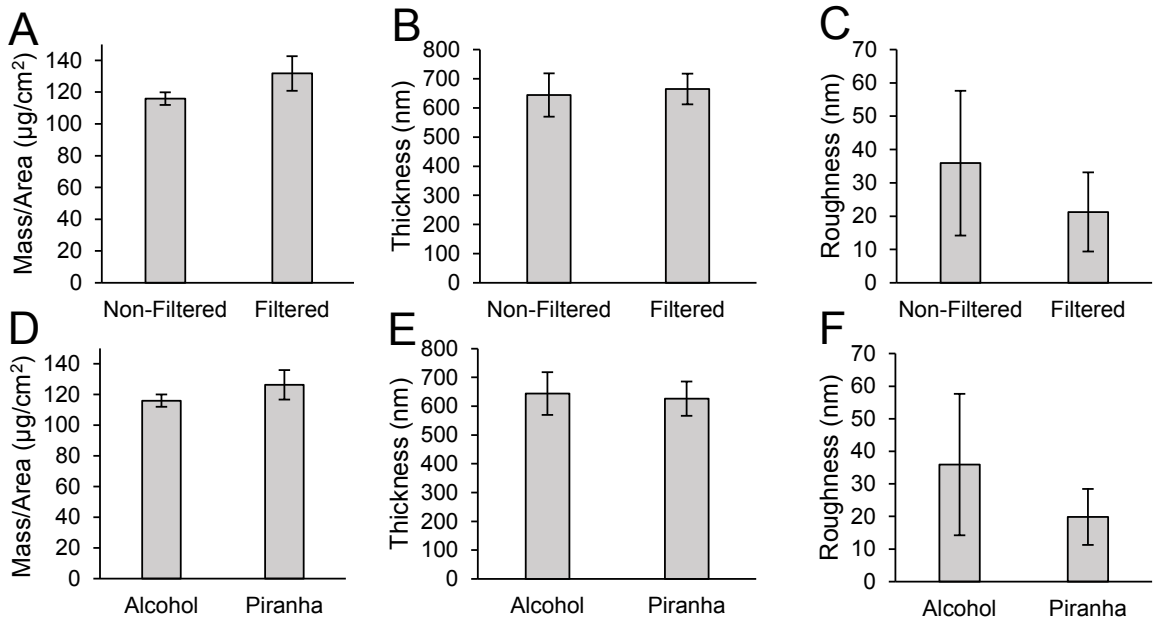

Figure 2.4 Effects of changing LbL preparation methods. *(A)-(C) (n=9) Effect of filtering peptide solutions on (A) Mass deposition, (B) Film thickness, and (C) Film Roughness of LbL films. (D)-(F) Comparison of alcohol slide treatment (n=9) to Piranha treated slides (n=6) on (D) mass deposition, (E) film thickness, and (F) Film roughness of LbL films. All slides comparing $(RADA/HA)_{50}$ films. Data for non-filtered and alcohol are from the same samples and were reproduced for comparison.*

substrate treatments. This result was supported by previous LbL work in which a methanol and water cleaning treatment was sufficient to prepare silicon wafers for layering[27]. Because of the lack of difference the alcohol rinsing process was used moving forward to eliminate the use of hazardous materials (piranha solution).

2.3.4 Optimizing dip LbL conditions

Adhesion time for dip LbL films was examined using a Quartz Crystal Microbalance with Dissipation (QCMD) adapted from previously published work[28]. With this method we were able to examine the equilibrium adsorption time for films. (**Figure 2.5**). This experiment showed that we were able to achieve around 90% of maximum adsorption in 10-15 minutes. This allowed for reduced sample production time compared with previous work[19]. A similar result was found for IEIK/HA films. To confirm these results, $(RADA/HA)_{10}$ films were constructed using 10 and 15 minute dip adsorption times. The results showed that while there was a small increase in thickness

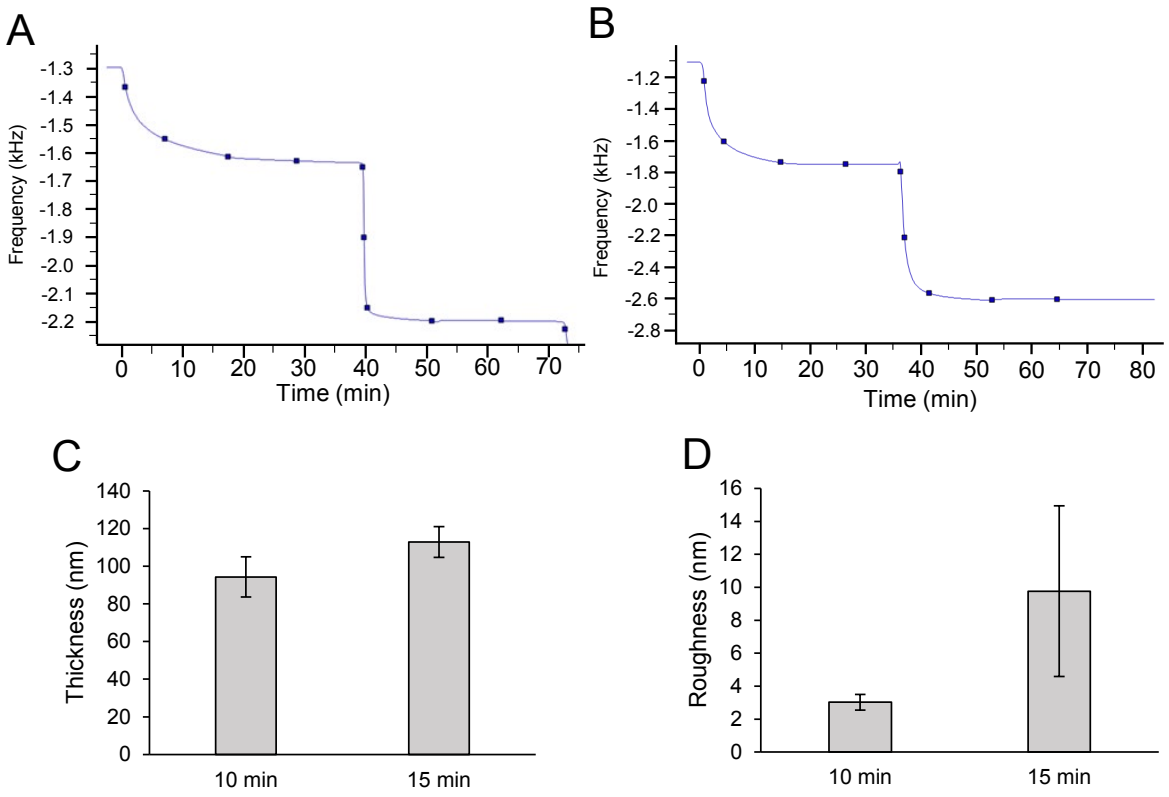

Figure 2.5 Optimization of film deposition time. *(A),(B) QCMD frequency change with time corresponding to a mass increase from film deposition. Each shows the 2nd bilayer absorption for (A) (RADA/HA) system or (B) (IEIK/HA) system. (C),(D) Dip LbL films for $(RADA/HA)_{10}$ (n=3) showing the effect of changing dipping time on (C) Film thickness and (D) film roughness of LbL films.*

for the 15 minute dip time, it was not significant and was also accompanied by a large increase in roughness. It was ultimately decided that the extra dip adsorption time was not necessary so 10 minute dip times were used moving forward. Using the optimized dip LbL conditions for the electrostatic film system, growth curves for (RADA/HA) and (IEIK/HA) films were produced. IEIK13 films tend to be thinner than RADA16 films. This result could be due to increased steric hindrance from the stiffer IEIK13 fibers[22].

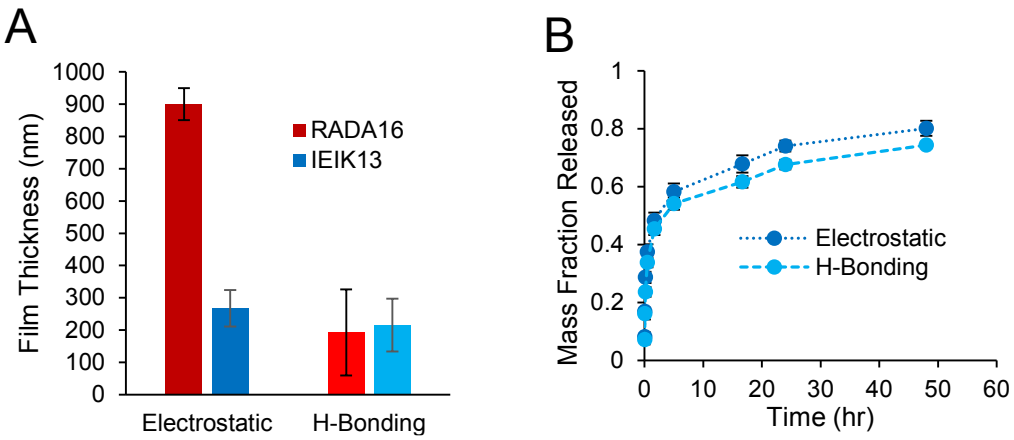

Figure 2.6 Comparison of Electrostatic and Hydrogen bonding LbL systems. *(A) film thickness at 100 bilayers for electrostatic based peptide/hyaluronic acid (HA) LbL films and hydrogen bonding based peptide/tannic acid (TA) LbL films. (B) mass fraction release from IEIK13 50 bilayer films. Electrostatic films* $(RADA/HA)_{200}$ *and* $(IEIK/HA)_{200}$*, hydrogen bonding films* $(RADA/TA)_{200}$ *and* $(IEIK/TA)_{200}$*.*

Hydrogen bonding based films were examined in the hopes that the weaker hydrogen bonding interactions would allow the film to break up faster and the peptide fibers to release more rapidly. Tannic acid (TA) has been shown previously to work well in hydrogen bonding based films[28]. Solution conditions had to be adapted to promote film growth with the finding that $(peptide/TA)_n$ films would not grow in water, likely due to water itself being a more favorable hydrogen bonding partner than either the peptides or tannic acid. Ethanol has been shown to weaken the hydrogen bonding of water[30]. Different water and ethanol mixtures were tested with no LbL film growth. However, film assembly did occur in a solution of pure ethanol Film thickness of $(RADA/TA)_{100}$ and $(IEIK/TA)_{100}$ films were compared against $(RADA/HA)_{100}$ and $(IEIK/HA)_{100}$ films constructed using the same dipping protocol (1 min adsorption with two 1 min washes). Then labeled IEIK13 films were constructed to look for any changes in the release rate. **Figure 2.6** shows the results. No significant change in the release rate of IEIK13 was observed in the hydrogen bonding film compared with the electrostatic film. This, coupled with the poor loading and unnecessary hazard of working with pure ethanol, led to the hydrogen bonding films being dropped.

2.3.5 Optimizing spray LbL conditions

Spray Layer-by-Layer has been shown to be a successful method for applying LbL films to three dimensional, biocompatible substrates[19, 27, 28]. To optimize the production of LbL coated sponge samples, several changes were made to the existing spray LBL apparatus. First, a new sample holder was designed using Autodesk Inventor and 3D printed. This new holder allowed for full size sponges to be sprayed with a uniform vacuum pulled through. (**Figure A.2**) Additionally, controls were placed on the vacuum system used to pull air and solution spray through the sponge samples. A vacuum regulator was placed on the house vacuum line to control for day to day fluctuations in the house vacuum pressure. Using fluorescently labeled peptides, we were also able to examine coverage across the entire sponge surface. Coverage of the LbL coating was examined on films constructed with fluorescently labeled peptides. With this we were not only able to see fairly even coverage across the entire sponge surface (**Figure 2.7**), but also that almost all of the LbL film was deposited directly on the front facing surface (**Figure 2.8**). This means that when the sponge is applied to a wound, all loaded peptide material will be directly in contact with the wound surface when placed against the bleeding source. This result is beneficial

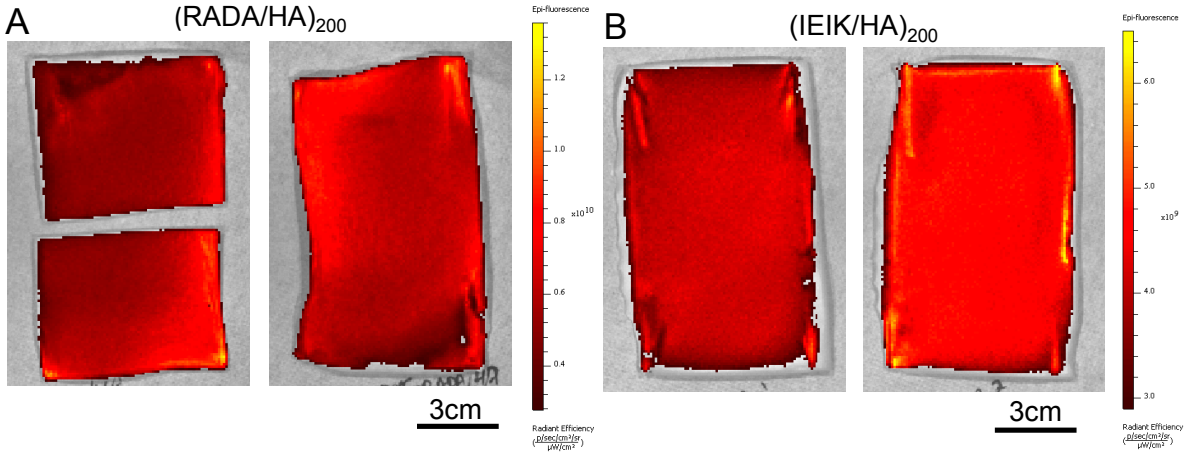

Figure 2.7 Spray LbL film coverage of gelatin sponges. *Composite IVIS images of gelatin sponges coated with LbL films containing fluorescently labeled peptides. (A) Active side of $(RADA/HA)_{200}$ sponges. (B) Active side of $(IEIK/HA)_{200}$ sponges, scale bars represent 3cm. Two replicate sponges are shown for each film treatment.*

as previous work with self-assembling peptides has highlighted the importance of contact with the site of injury for the fibers to promote hemostasis[19].

2.3.6 Total peptide loading

Total loading on RADA/HA and IEIK/HA coated sponges was normalized to either the mass of sponge released or the area of the active side of the sponge released. Values are given **Figure 2.9**. Mass normalized loadings of approximately 2.6 ug RADA/mg sponge and 1.9ug IEIK/mg sponge were calculated. Area normalized loadings of 29 ug RADA/cm^2 coated surface and 22 ug IEIK/cm^2 coated surface were calculated. Extrapolating the area loading for an entire sponge (approximately 100cm^2) gives a value of 2.95 mg RADA16 on each $(RADA/HA)_{200}$ sponge and

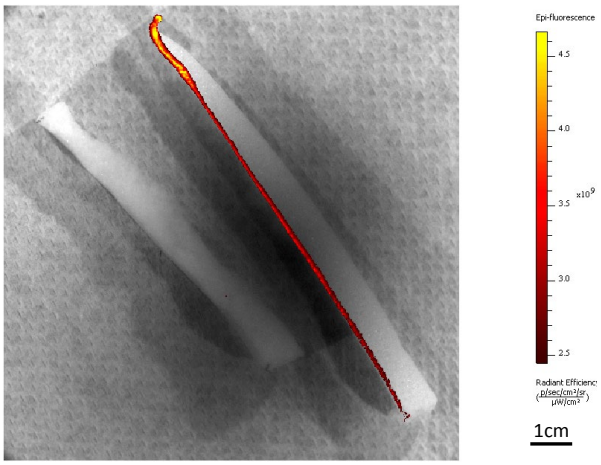

Figure 2.8 Depth of spray LbL film penetration into gelatin sponges. *IVIS image of cross section of an uncoated gelatin sponge (left) and a $(RADA16/HA)_{200}$ coated sponge (right). The cross section shows almost all peptide material is deposited on the front facing surface. Scale bar represents 1 cm.*

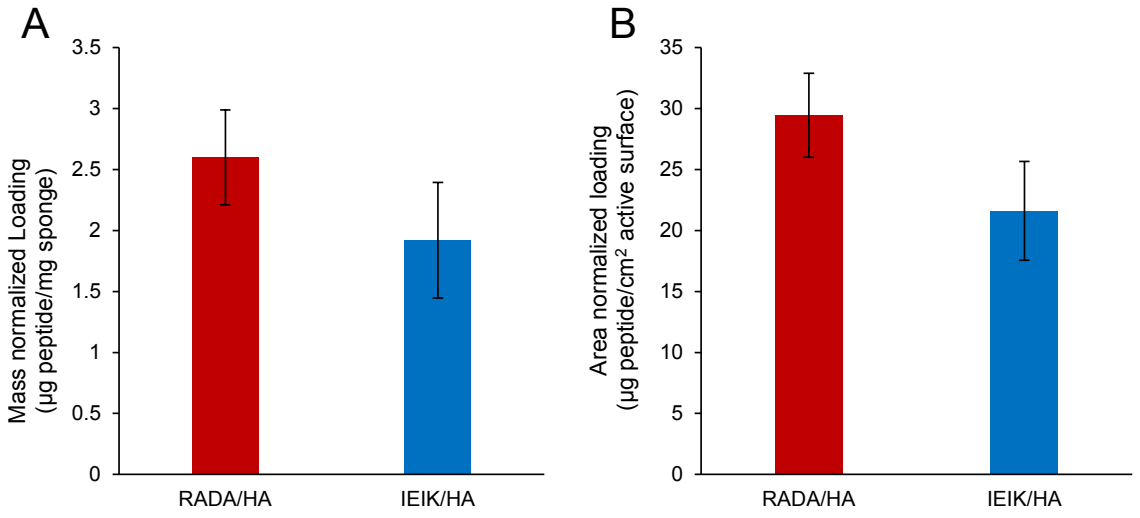

Figure 2.9 Normalized loading of peptide LbL films on gelatin sponges. *(A) Mass normalized loading, mass of peptide deposited divided by the mass of sponge. (B) Active surface area normalized loading, mass of peptide loaded divided by the coated side sponge area. All films were 200 bilayers: $(RADA/HA)_{200}$ and $(IEIK/HA)_{200}$.*

2.16 mg IEIK13 on each $(IEIK/HA)_{200}$ sponge. To produce each sponge approximately 150 mL of 0.1g/mL peptide solution is sprayed for a maximum possible loading of 15mg peptide per sponge. Therefore the encapsulation efficiency for the sponge samples is approximately 19.6% for RADA16 and 14.4% for IEIK13. The low encapsulation efficiency is not unexpected because much of the sprayed solution never makes it to the sponge surface. Other researchers have shown ways to improve this efficiency by changing the spray orientation or recovering and recycling peptide solution that does not make it onto the sample[26].

2.3.7 In vivo pilot testing of hemostatic bandages in swine liver injury model

To examine if these self-assembling peptide LbL systems could promote hemostasis, *in vivo* pilot tests were conducted. LbL formulations were tested *in vivo* in a swine grade IV/V liver injury model in collaboration with the Army Institute of Surgical Research (AISR)[31]. Two separate

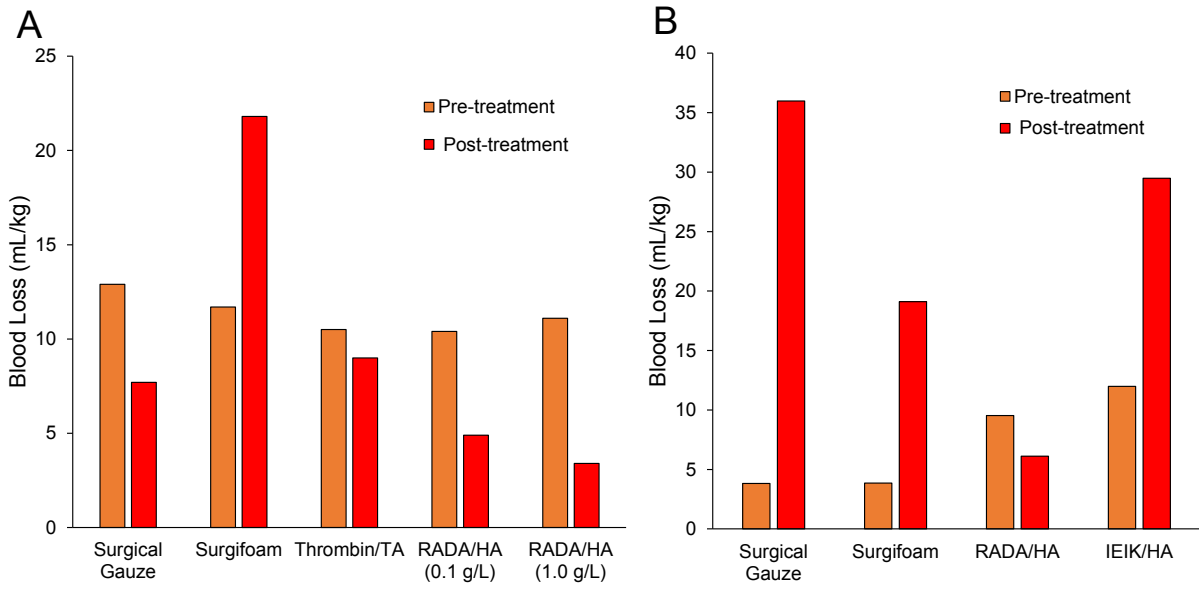

Figure 2.10 Pilot testing in swine liver injury model. *Blood loss results from pilot testing in a swine grade IV/V liver injury model. (A) Pilot test (n=1) comparing surgifoam gelatin sponges coated with either a $(Thrombin/Tannic\ Acid)_{200}$ film or $(RADA/Hyaluronic\ Acid)_{200}$ film. RADA16 films were created using solutions with a polyelectrolyte concentration of either 0.1 g/L or 1.0 g/L. (B) Pilot test (n=1) comparing RADA16 and IEIK13 LbL coated surgifoam gelatin sponges. In both tests, surgical gauze was used as a control and uncoated surgifoam was used as a vehicle control. Blood loss was normalized to the mass of the animal. Pre-treatment blood loss represents the severity of the injury, post-treatment blood loss represents the effect of the applied treatment.*

pilot tests (n=1 for each treatment) were conducted (**Figure 2.10**). The first test compared $(RADA/HA)_{200}$ films created at two different solution concentrations against gauze, a substrate control, and a previously published thrombin and tannic acid LbL system based on hydrogen bonding interactions. The $(Thrombin/TA)_{200}$ films had shown promotion of hemostasis in the literature[28]. While no significance can be drawn from the results of this pilot test (**Figure 2.10A**), it showed some promise for reduced blood loss from the $(RADA/HA)_{200}$ films. Additionally, the lack of improvement from the $(RADA/HA)_{200}$ films created from 10x more concentrated stock solutions seems to indicate that even the lower concentration films are sufficient.

The second pilot test (n=1 for all groups) was conducted to compare the RADA16 based system with the IEIK13 based system in a more severe model (**Figure 2.10B**). In this pilot test, slight coagulopathy was induced through hemodilution to reduce clotting ability in the animal. This test indicated that the $(RADA/HA)_{200}$ films were similarly successful to the first test. However, $(IEIK/HA)_{200}$ films did not show the same reduction in blood loss. This validation test reinforced the previous findings for RADA16 films while showing that something was potentially preventing the $(IEIK/HA)_{200}$ films from promoting hemostasis. This lack of efficacy could be due to slightly lower peptide loading on IEIK13 coated sponges or possibly due to morphology differences between the two peptides. It is also possible that the results were a side of effect of the increased hydrophobicity of IEIK13 fibers over RADA16 fibers, leading to slower release of the fibers from the film or potentially reduced interaction between the film and the wound surface. It was observed during these tests that stronger adhesion between the dressing and the wound surface seemed to correlate with reduced blood loss from the injury. While it is difficult to draw meaningful conclusions without replicates, the testing did seem to indicate that $(RADA/HA)_{200}$ can be successful at promoting hemostasis and there may be a connection between dressing adhesion and improved hemostasis.

2.4 Conclusions:

All of the work done in this study helped to improve reproducibility and maximize loading of peptide into the layer-by-layer (LbL) samples. Solution preparation was optimized to using 10 mM HCl, stirring all solutions overnight, then sonicating RADA16, IEIK13, and Chitosan solutions, filtering them immediately, and allowing them to sit overnight again for fibers to reform. It was shown that both peptides adsorb into films already formed into nanofibers. Dip LbL was optimized for proper slide cleaning and proper dipping times of 10 minutes. Hydrogen bonding based LbL films were examined using tannic acid in ethanol. However, they failed to speed up film release and were not pursued. Spray LbL was optimized through the design of a new sample holder, a controlled vacuum pressure, and alignment of the spray nozzles for even coverage across the entire sponge. Loading and encapsulation efficiencies were shown to be at a level expected for the spray LbL process. All of these steps in sample development and optimization led to better reproducibility and consistency in LbL samples used throughout the rest of this work. Finally pilot testing helped to indicate that these films are capable of showing improvement in blood loss and a possible correlation between blood loss and adhesion strength between the wound and the dressing. This observation led to the development of adhesive LbL formulations discussed in Chapter 4.

2.5 References:

1. Ellis-Behnke, R.G. et al. Nano hemostat solution: immediate hemostasis at the nanoscale. *Nanomedicine : nanotechnology, biology, and medicine* **2**, 207-215 (2006).
2. Ellis-Behnke, R. At the nanoscale: nanohemostat, a new class of hemostatic agent. *Wires Nanomed Nanobi* **3**, 70-78 (2011).
3. Gelain, F., Luo, Z., Rioult, M. & Zhang, S. Self-assembling peptide scaffolds in the clinic. *NPJ Regenerative medicine* **6**, 9 (2021).
4. Sankar, S. et al. Clinical Use of the Self-Assembling Peptide RADA16: A Review of Current and Future Trends in Biomedicine. *Frontiers in Bioengineering and Biotechnology* **9** (2021).
5. Verbraeken, B. et al. Efficacy and histopathological effects of self-assembling peptides RADA16 and IEIK13 in neurosurgical hemostasis. *Nanomedicine : nanotechnology, biology, and medicine* **40**, 102485 (2022).
6. GIL, E.S., GILBERT, K. & Mehta, M., Edn. C07K 7/08 (2006.01), A61L 27/22 (2006.01), A61K 38/12 (2006.01), A61L 27/54 (2006.01), A61L 27/58 (2006.01). (ed. W.I.P. Organization) (2015).
7. Zhang, H., Luo, H. & Zhao, X. Mechanistic Study of Self-Assembling Peptide RADA16-I in Formation of Nanofibers and Hydrogels. *Journal of Nanotechnology in Engineering and Medicine* **1** (2009).
8. Shah, N.J., Hong, J., Hyder, M.N. & Hammond, P.T. Osteophilic Multilayer Coatings for Accelerated Bone Tissue Growth. *Adv Mater* **24**, 1445-1450 (2012).
9. Shukla, A. et al. Controlling the release of peptide antimicrobial agents from surfaces. *Biomaterials* **31**, 2348-2357 (2010).
10. Moskowitz, J.S. et al. The effectiveness of the controlled release of gentamicin from polyelectrolyte multilayers in the treatment of Staphylococcus aureus infection in a rabbit bone model. *Biomaterials* **31**, 6019-6030 (2010).
11. Shukla, A., Fuller, R.C. & Hammond, P.T. Design of multi-drug release coatings targeting infection and inflammation. *J Control Release* **155**, 159-166 (2011).
12. DeMuth, P.C., Su, X.F., Samuel, R.E., Hammond, P.T. & Irvine, D.J. Nano-Layered Microneedles for Transcutaneous Delivery of Polymer Nanoparticles and Plasmid DNA. *Adv Mater* **22**, 4851-+ (2010).
13. Macdonald, M.L. et al. Tissue integration of growth factor-eluting layer-by-layer polyelectrolyte multilayer coated implants. *Biomaterials* **32**, 1446-1453 (2011).
14. Samuel, R.E. et al. Osteoconductive protamine-based polyelectrolyte multilayer functionalized surfaces. *Biomaterials* **32**, 7491-7502 (2011).
15. Min, J., Braatz, R.D. & Hammond, P.T. Tunable staged release of therapeutics from layer-by-layer coatings with clay interlayer barrier. *Biomaterials* **35**, 2507-2517 (2014).
16. Min, J.H. et al. Designer Dual Therapy Nanolayered Implant Coatings Eradicate Biofilms and Accelerate Bone Tissue Repair. *Acs Nano* **10**, 4441-4450 (2016).
17. Hammond, P.T. Form and function in multilayer assembly: New applications at the nanoscale. *Adv Mater* **16**, 1271-1293 (2004).
18. Kim, B.S., Lee, H., Min, Y.H., Poon, Z. & Hammond, P.T. Hydrogen-bonded multilayer of pH-responsive polymeric micelles with tannic acid for surface drug delivery. *Chem Commun*, 4194-4196 (2009).
19. Hsu, B.B. et al. Clotting Mimicry from Robust Hemostatic Bandages Based on Self-Assembling Peptides. *Acs Nano* **9**, 9394-9406 (2015).
20. Shiratori, S.S. & Rubner, M.F. pH-dependent thickness behavior of sequentially adsorbed layers of weak polyelectrolytes. *Macromolecules* **33**, 4213-4219 (2000).

21. Gilbert, J.B., Rubner, M.F. & Cohen, R.E. Depth-profiling X-ray photoelectron spectroscopy (XPS) analysis of interlayer diffusion in polyelectrolyte multilayers. *P Natl Acad Sci USA* **110**, 6651-6656 (2013).
22. Xu, L., Ankner, J.F. & Sukhishvili, S.A. Steric Effects in Ionic Pairing and Polyelectrolyte Interdiffusion within Multilayered Films: A Neutron Reflectometry Study. *Macromolecules* **44**, 6518-6524 (2011).
23. Sui, Z.J., Salloum, D. & Schlenoff, J.B. Effect of molecular weight on the construction of polyelectrolyte multilayers: Stripping versus sticking. *Langmuir* **19**, 2491-2495 (2003).
24. Clark, S.L. & Hammond, P.T. The role of secondary interactions in selective electrostatic multilayer deposition. *Langmuir* **16**, 10206-10214 (2000).
25. Krogman, K.C., Lowery, J.L., Zacharia, N.S., Rutledge, G.C. & Hammond, P.T. Spraying asymmetry into functional membranes layer-by-layer. *Nat Mater* **8**, 512-518 (2009).
26. Hsu, B.B., Hagerman, S.R. & Hammond, P.T. Rapid and efficient sprayed multilayer films for controlled drug delivery. *Journal of Applied Polymer Science* **133** (2016).
27. Monteiro, I.P., Shukla, A., Marques, A.P., Reis, R.L. & Hammond, P.T. Spray-assisted layer-by-layer assembly on hyaluronic acid scaffolds for skin tissue engineering. *Journal of biomedical materials research. Part A* **103**, 330-340 (2015).
28. Shukla, A., Fang, J.C., Puranam, S., Jensen, F.R. & Hammond, P.T. Hemostatic Multilayer Coatings. *Adv Mater* **24**, 492-+ (2012).
29. Wang, T., Zhong, X., Wang, S., Lv, F. & Zhao, X. Molecular mechanisms of RADA16-1 peptide on fast stop bleeding in rat models. *International journal of molecular sciences* **13**, 15279-15290 (2012).
30. Burikov, S., Dolenko, T., Patsaeva, S., Starokurov, Y. & Yuzhakov, V. Raman and IR spectroscopy research on hydrogen bonding in water-ethanol systems. *Mol Phys* **108**, 2427-2436 (2010).
31. Delgado, A.V. et al. A novel biologic hemostatic dressing (fibrin patch) reduces blood loss and resuscitation volume and improves survival in hypothermic, coagulopathic Swine with grade V liver injury. *J Trauma* **64**, 75-80 (2008).

Chapter 3. Mechanistic Study of Peptide LbL Film Hemostatic Interactions

3.1 Introduction

Blood loss due to injury is one of the leading causes of death among US military warfighters[1]. The majority of preventable battlefield deaths were due to hemorrhage[2, 3]. In addition to military deaths, trauma related hemorrhage is the leading cause of death for patients between the ages of 1-46[4, 5]. While many different hemostat materials have been developed[6, 7], no materials have checked every criteria for the ideal hemostat: easy to apply, no negative side effects, long term shelf stability, thermal stability, cost effective, and bioabsorbable[8].

A possible solution to the ideal hemostat is through the use of self-assembling peptide nanofibers. Self-assembling peptide nanofibers have been used extensively to promote rapid hemostasis[9-13]. Many products currently exist in the form of a high concentration peptide gel that is applied directly to the source of bleeding[11, 12]. Other work has been done previously with RADA16 to apply it in a dry state to various substrates using layer-by-layer (LbL)[14]. The hypothesized mechanism of action is that by physically catching blood components in peptide gel, the red blood cells, platelets, and other clotting factors are concentrated. The increase in local concentration of these factors then facilitates a more rapid clot formation. Essentially the peptide gel acts as an artificial clot that is then strengthened by the formation of the natural clot. This mechanism has been supported through examining dependence of gel formation[15] and clot structure via AFM[16], histology[17], and SEM[14]. Contrasting with this physical catching interaction, the peptide fibers have been shown to be relatively biocompatible and inert when it comes to cellular interactions[11]. Because of the difficulty in directly testing this mechanical mechanism, we decided to examine smaller interactions with aspects of clot formation. A lack of direct effects on clot formation or clotting factors in vitro could support the hypothesis through the exclusion of these interactions.

Hemostasis is the process by which blood clots and blood loss at a wound stops. It is generally broken down into two complimentary processes; primary and secondary hemostasis. In

primary hemostasis, a platelet plug is formed at the wound site. The wound causes the exposure of collagen to platelets which become activated and stick to collagen and von Willebrand Factor. These activated platelets are then able to bind to fibrinogen in the blood, leading to the formation of the platelet plug[3]. Secondary hemostasis describes the formation of a fibrin clot through a process often described as the clotting cascade. The clotting cascade involves two pathways of activation; the intrinsic pathway and the extrinsic pathway. The intrinsic pathway is activated by contact of the blood to a negatively charged surface and acts through coagulation factors XII, XI, IX, VII, and V. The extrinsic pathway is activated by the wound causing exposure of tissue factor to the blood and activating factor VII[18]. Both processes ultimately lead to the activation of factor X which is responsible for converting prothrombin into the active form thrombin. Thrombin is then responsible for converting fibrinogen into fibrin as well as further activating platelets. Fibrin then polymerizes and leads to the formation of the fibrin clot which is able to form around the original platelet plug[3, 18].

Layer-by-layer (LbL) assembly can be used to create films containing many different functional species[19, 20]. A broad range of functional polymers and other charged species including antibiotics, anti-inflammatory drugs, chemotherapeutics, growth factors, and nucleic acids can be incorporated with controlled release[20-29]. This method can be used through traditional dipping methods or through a spray LbL apparatus. Spray LbL allows for the application of films to three dimensional, biocompatible substrates[30, 31] and has already been used previously to apply the self-assembling peptide RADA16 to porous substrates[14].

3.2 Methods

3.2.1 Materials

Factor IXa Activity Assay Kit (ab204727), Factor VII Human Chromogenic Activity Kit (ab108830), Tissue Factor Activity Assay Kit (ab108906), and Thrombin Activity Assay Kit (ab197006) were purchased from Abcam. Anticoagulated human whole blood was purchased from Research Blood Components. CyQUANT LDH Cytotoxicity Assay Kit was purchased from

ThermoFisher Scientific. Washed and pooled 10% rabbit red blood cells (RBCs) were obtained from Lampire Biological Laboratories.

3.2.2 Solution preparation

1.5 wt% peptide gel was diluted to 1 mg/mL or 0.1 mg/mL using 10mM HCl. This solution was then stirred overnight. Afterward the solutions were sonicated for 1 hour using a bath sonicator and immediately filtered through a 0.2 μm PES membrane. The resulting solution was stored at room temperature overnight to allow the peptide fibers to reassemble. Solutions of Hyaluronic acid were dissolved into 10mM HCl and stirred overnight.

3.2.3 Spray LbL film generation

Methods for spray LbL systems were adapted from previously published work[14]. Large gelatin sponges (8cm x 12.5cm x 10mm) were coated using an automated film assembly instrument (Svaya). The sprayer was calibrated to a 0.25mL/s flow rate at 15PSI. House vacuum was applied through a regulator to around 50% strength (Approximately -45kPa closed pressure). Bilayer formulations were created with the following steps: 0.1mg/mL peptide (RADA16 or IEIK13) in 10mM HCl for 3 seconds, wait time for 5 seconds, rinse with 10mM HCl for 3 seconds, dry time for 8 seconds, 0.1 mg/mL polyanion in 10mM HCl for 3 seconds, wait time for 5 seconds, rinse with 10mM HCl for 3 seconds, dry time for 8 seconds. In summary: peptide (3s), wait (5s), wash (3s), dry (8s), polyanion (3s), wait (5s), wash (3s), dry (8s). This made up one bilayer and was repeated for n bilayers with a 60 minute air dry time added after every 10 bilayers.

3.2.4 LbL release

Methods for the release of LbL films from gelatin substrates were adapted from previously published work[14]. Released LbL formulations were generated by cutting 1cm^2 (of the LbL coated side) pieces of sponge (approximately 15-20 mg of sponge sample) into 1 mL of 1xPBS. 100 uL of 10mg/mL Collagenase (Type I) was added and the samples were incubated for at least 24hr to allow the sponge substrate to be digested.

3.2.5 Clotting Assays

3.2.5.1 Generation of plasma samples

Platelet rich plasma (PRP) was obtained by centrifuging whole blood, following previously published protocols[32]. Platelet poor plasma (PPP) was obtained by centrifuging the platelet rich plasma (PRP) at approximately 2000 RPM for at least 10 min[33]. Sample Solutions were then diluted 1/10 into either PRP or PPP and incubated for at least 10 minutes. Sample solutions were a vehicle control (10mM HCl for stock solutions and 1xPBS with approximately 15mg of degraded gelatin sponge dissolved), 1mg/mL LbL stock solution in 10mM HCl, or released LbL film formulation in 1x PBS.

3.2.5.2 Platelet aggregation via lactate dehydrogenase (LDH)

To determine platelet interaction and binding, a lactate dehydrogenase (LDH) assay was modified from the literature[33]. The platelet rich plasma was then split up into two containers. ADPT was added to one of the containers to activate the platelets. Stock solutions of 1mg/mL LbL component in 10mM HCl or solution released from an LbL coated sponge were diluted 1/10 into either the activated platelet plasma or the non-activated platelet plasma for at least 10 minutes. Platelets were activated through the addition of adenosine diphosphate (ADP) at a concentration of 10 μM. The plasma was then diluted to ½ concentration and placed into a 96 well plate. The plates are allowed to incubate for a period of time and then each well is gently washed at least 3 times to rinse out any material that did not bind and settle to the bottom of the wells. Following this, the LDH assay was performed following the kit instructions to obtain a measure of the number of platelets that settled out of solution. The wells were measured on a plate reader at absorbance of 490nm and 680nm using the 680nm absorbance as a reference wavelength. Comparing non-activated and activated platelets allows us to examine nonspecific binding from the non-activated platelets as a baseline and any additional specific binding from the activated platelets.[33]

3.2.5.3 Factor IXa activity

Platelet poor plasma samples were generated in the same way as described above. These plasma samples were then diluted 10x in FIXa Assay buffer and run in a 96 well plate following the kit directions. Fluorescent results were plotted and the slope of fluorescence over time was used to calculate Factor IXa activity. Each sample was then compared to the appropriate vehicle control to obtain the fold change in Factor IXa Activity.

3.2.5.4 Factor VII human chromogenic activity

Platelet poor plasma samples were generated in the same way as described above. These plasma samples were diluted 30x with the assay diluent before being run in a 96 well plate following the kit directions. Absorbance results were plotted and the slope of the absorbance change over time was used to calculate Factor VII activity. Each sample was then compared with the appropriate vehicle control to obtain the fold change in Factor VII Activity.

3.2.5.5 Tissue factor activity

Platelet poor plasma samples were generated in the same way as described above. These plasma samples were then diluted 2x with kit Sample Diluent and run in a 96 well plate following the kit directions. Absorbance results were plotted and the slope of the absorbance change over time was used to calculate Tissue Factor activity. Each sample was then compared with the appropriate vehicle control to obtain the fold change in Tissue Factor Activity

3.2.5.6 Thrombin activity

Platelet poor plasma samples were generated in the same way as described above. These plasma samples were then diluted 2x with kit Thrombin Assay Buffer and run in a 96 well plate following the kit directions. Fluorescence results were plotted and the slope of the fluorescence change over time was used to calculate Thrombin activity. Each sample was then compared with the appropriate vehicle control to obtain the fold change in Thrombin Activity

3.2.6 Plasma clot formation absorbance assay

Protocols for the clot formation absorbance assay were adapted from previously published methods in the literature[34]. Platelet rich plasma (PRP) was used to measure changes in clot

formation speed through an absorbance assay in a 96 well plate. Samples were diluted 10 times into PRP. The wells of a 96 well plate were loaded with 10 µL of 100 mM $CaCl_2$ solution, then 90 µL of PRP samples were added to each well using a multichannel pipette. 6 replicates were collected. The plate was then measured in a Tecan plate reader for absorbance at 620 nm. Measurements were taken every minute for 2 hours or until all wells had clotted. The time of the maximum slope was measured for each well as the time of clot formation.

3.2.7 Hemostasis analyzer

Clotting experiments using whole blood were conducted using a Stago STart4 Hemostasis analyzer. The activated partial thromboplastin time (aPPT) test setting was used with a 3 minute incubation and the maximum clot time raised to 600 seconds. Samples were produced by diluting either stock solutions or film releasate 10 fold into whole blood. The blood and sample were then gently mixed and 450 µL of the blood sample was added to each well. Each test has 4 wells; two were used for a vehicle control and two were used for the intended sample. Each set of 4 wells had magnetic beads added and then placed in the incubator wells at 37°C for at least 3 minutes. The samples were then placed in the test wells and 50 µL of 100mM $CaCl_2$ solution was added. At the moment the calcium was added, the timer was started. After a clot formed, the magnetic bead stopped moving and the equipment registered a clot time. To account for changes in the blood clotting behavior over the course of the tests, each sample was compared only with the control from the same test. Vehicle controls were the same as described for the plasma samples (10mM HCl for stock solutions and 1xPBS with approximately 15mg of degraded gelatin sponge dissolved).

3.2.8 In vitro gelation assay

Peptide gelation was tested using methods following previous published work[14]. 95 µL of peptide dissolved in PBS diluted from stocks or released from films were added to 96-well microtiter plates with V shaped wells. Then 10 µL of 10% rabbit RBCs was added. The wells were

sealed with a clear adhesive film and agitated at ~900 rpm for 15 min. Plates were incubated at 4 °C for at least 4 h prior to observing results.

3.2.9 Thromboelastography (TEG)

Thromboelastography (TEG) was conducted using a TEG 5000 (Haemonetics). Native TEG was run using untreated cups and pins and only adding $CaCl_2$ solution. Samples were run by diluting peptide stocks into citrated whole blood. Each test contained a vehicle control (DI H_2O) as well as a non-clotting control for both the sample and the vehicle control.

3.3 Results and Discussion:

3.3.1 Gelation in vitro

Previous work using self-assembling peptides for hemostasis has highlighted the importance of gel formation for hemostatic efficacy[15]. To examine the gelation threshold, stock solutions of RADA16 and IEIK13 were examined in a V-well Clotting Assay (**Figure 3.1**). This showed that RADA16 is able to form a gel at concentrations as low as 50 ug/mL and IEIK13 is able to form a gel at concentrations as low as 12.5 ug/mL. This result confirms previous work in

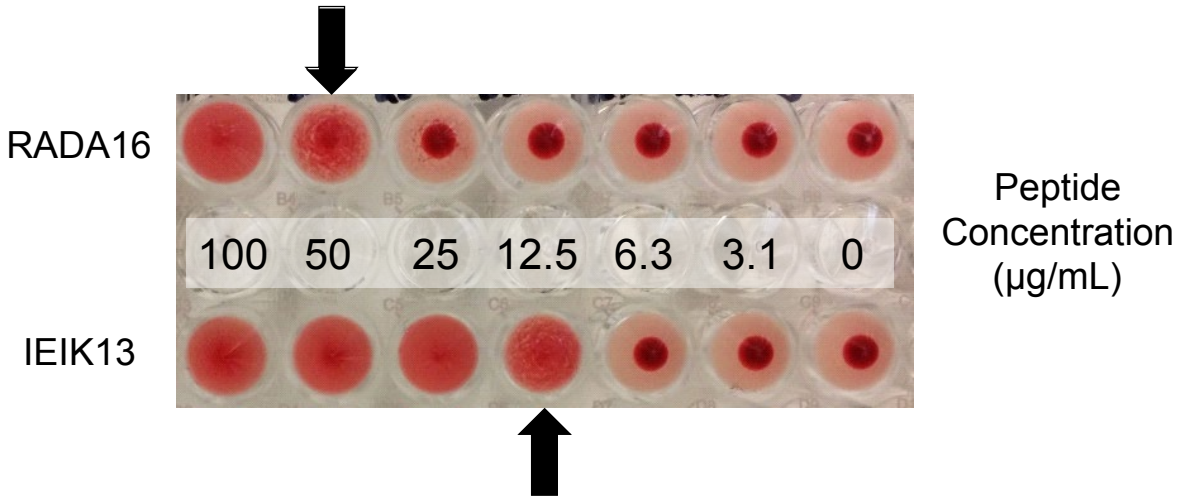

Figure 3.1 V-well clotting assay of RADA16 and IEIK13 in PBS. *Gel formation assay mixing red blood cells with PBS containing different amounts of peptide RADA16 or IEIK13. When a gel is present in solution, red blood cells remain suspended and the color is spread throughout the well. When no gel is present, the red blood cells settle to the bottom creating a dark spot in the middle of the well. Arrows mark the gelation threshold for RADA16 (top) and IEIK13 (bottom).*

the literature and highlights that the increased hydrophobicity and stiffness of the IEIK13 gel translates to gelation at lower concentrations[14, 35]. The ability to form a stiffer gel even at lower concentrations highlights the potential benefit of incorporating IEIK13 into LbL film bandages.

3.3.2 Interaction with individual clotting factors

In an effort to examine possible non-mechanical methods that the peptide nanofibers accelerate hemostasis, effect on the activity of several different clotting factors was examined (**Figure 3.2**). No significant differences in factor IXa or tissue factor were observed for any of the stock solutions or film releasates. Only factor VII showed a significant decrease with the stock solutions IEIK13 and HA. The $(RADA/HA)_{200}$ film releasate showed a significant increase in factor VII activity. In the thrombin activity assay, no significant differences in activity were observed from the stock solutions. However, both the RADA16 and IEIK13 released film solutions seem to show a significant decrease in thrombin activity. The assay results for both factor VII activity and thrombin activity do not seem to show agreement between the stock solution results and the film releasate results. It is possible that this is due to a synergistic effect from the LbL formulations or possibly due to varying degrees of sponge substrate digestion. It is worth noting that the levels of these clotting factors in healthy patients can vary considerably. Thrombin levels can range as much as 4.5 fold[36]. Factor VII levels can range from 60-140%[37]. Factor VII clotting activity can range from 65-160 U/100mL, activated factor VII levels can range from 30-170 mU/mL[38], and factor IX can range from 0.5-1.5 U/mL[39]. Even variations outside this range can still show normal clot behavior *in vitro*. For example, activated partial thromboplastin time (aPTT) does not become effected by factor IX levels until they drop below 0.35 U/mL[39].

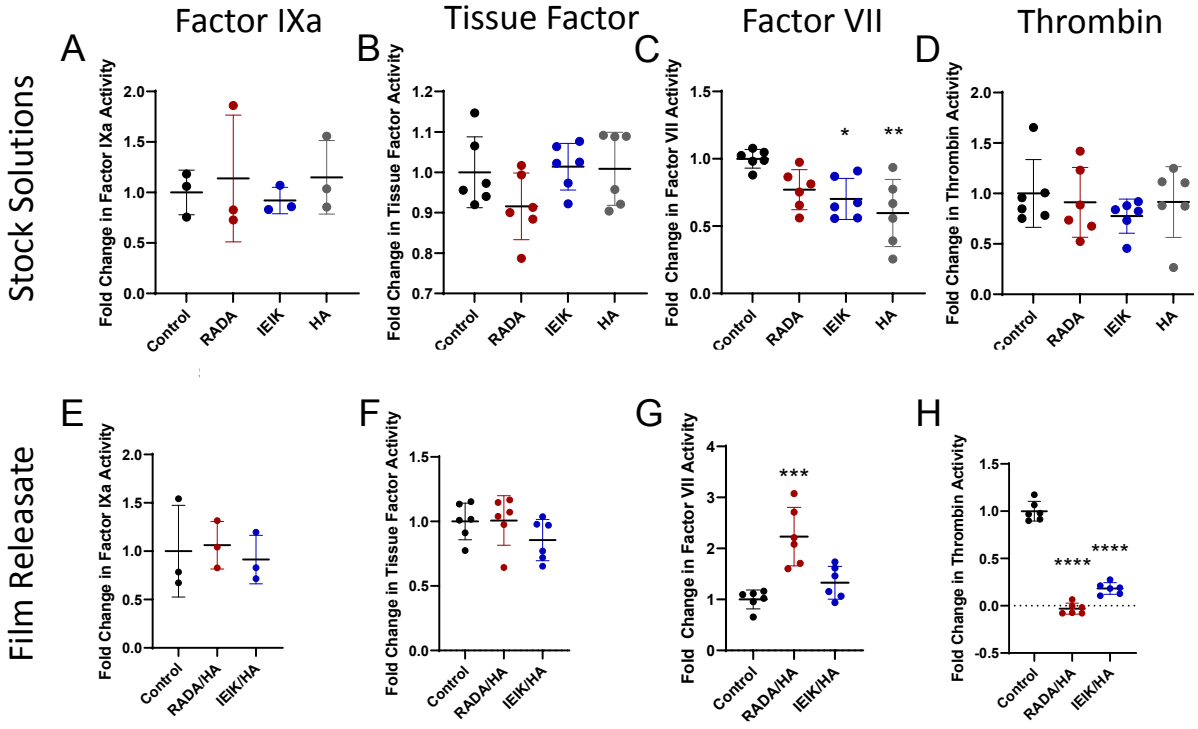

Figure 3.2 Effects of LbL films on clotting factor activity. Fold Change in (A) factor IXa activity, (C) factor VII activity, (E) tissue factor activity, (G) thrombin activity with stock solutions of LbL components. Stock solutions are 1mg/mL added 1:10 with platelet poor plasma. Control for stock solutions is the vehicle control of 10mM HCl. Fold Change in (B) factor IXa activity, (D) factor VII activity, (F) tissue factor activity, (H) thrombin activity with solutions released from LbL formulations. Film releasates are added 1:10 with platelet poor plasma. Control for film releasate is the vehicle control of 1xPBS with gelatin sponge digested by collagenase. RADA/HA is $(RADA/HA)_{200}$, IEIK/HA is $(IEIK/HA)_{200}$. Statistical analysis conducted comparing each sample to the vehicle control using ordinary one way anova with Dunnett multiple comparison correction. (* $P \leq 0.05$, ** $P \leq 0.01$, *** $P \leq 0.001$, **** $P \leq 0.0001$).

Platelets play a vital role in hemostasis[3] so it was important to examine the interactions of both activated and non-activated platelets with the peptides. When examining interactions with platelets, some significant changes in platelet aggregation were observed (**Figure 3.3**). In the platelet aggregation assay, non-specific aggregation was examined through non-activated platelet interactions. Activated platelet aggregation was examined by first activating platelets with ADP, then measuring for aggregation. Specific binding and aggregation of activated platelets was measured by normalizing the activated platelet values to the non-activated platelet values to

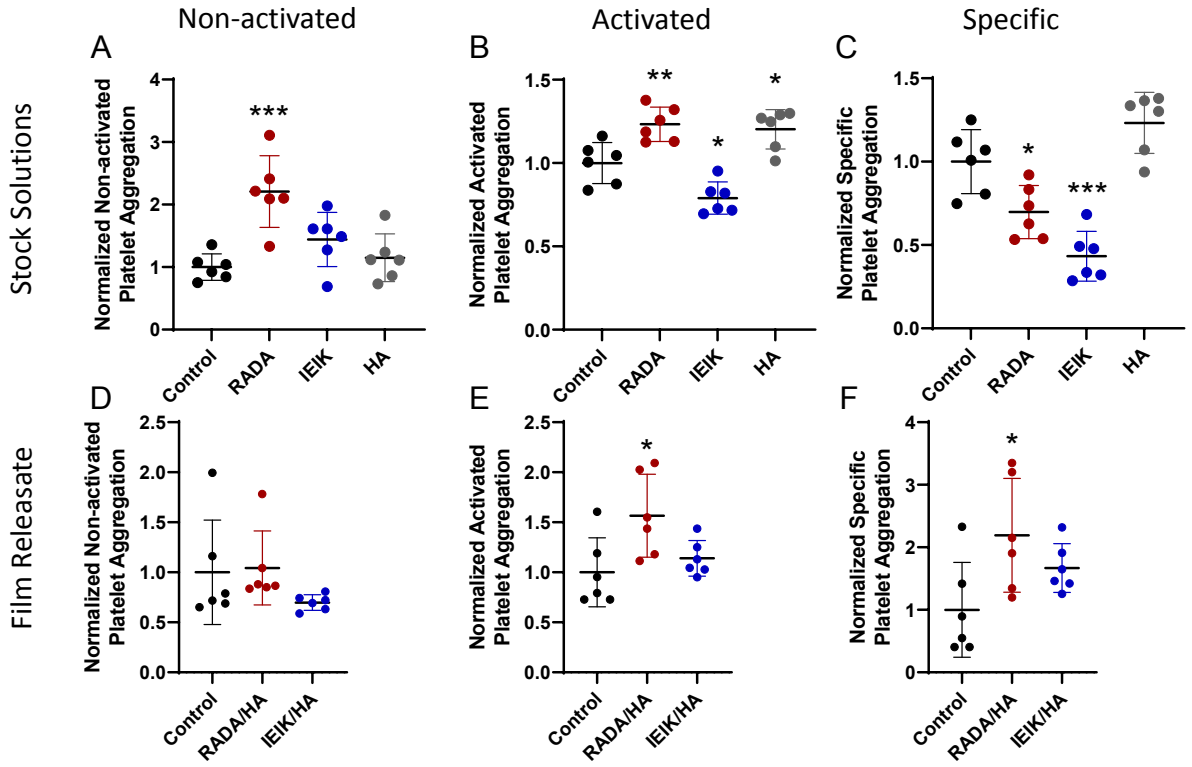

Figure 3.3 Effects of LbL films on *platelet aggregation.* *Platelet aggregation results showing fold change from vehicle control for aggregation of (A,D) non-activated platelets, (B,E) activated platelets, and (C,F) specific aggregation of platelets calculated as the activated platelet value minus the non-activated platelets. (A-C) shows results from stock solutions of 1mg/mL added 1:10 with platelet rich plasma. The vehicle control is 10mM HCl. (D-F) shows results from released sponge samples added 1:10 with platelet rich plasma and the vehicle control is 1xPBS with gelatin sponge digested by collagenase. RADA/HA is $(RADA/HA)_{200}$ and IEIK/HA is $(IEIK/HA)_{200}$.* Statistical analysis conducted comparing each sample to the vehicle control using ordinary one way anova with Dunnett multiple comparison correction. (* P ≤ 0.05, ** P ≤ 0.01, *** P ≤ 0.001, **** P ≤ 0.0001).

account for any non-specific binding as described in the literature[33]. RADA16 stocks showed increased aggregation of non-activated platelets and a small decrease in specific platelet aggregation. IEIK13 stock solutions showed no change in non-specific aggregation, but similarly to RADA16 showed a decrease in specific platelet aggregation. Hyaluronic acid stock solutions showed no significant differences in non-specific or specific platelet aggregation. Material released from (RADA/HA) showed a slight increase in specific platelet aggregation and (IEIK/HA)

releasate showed no significant changes over the control. These results indicate that the effects from the LbL films and components on platelet aggregation and binding are relatively small.

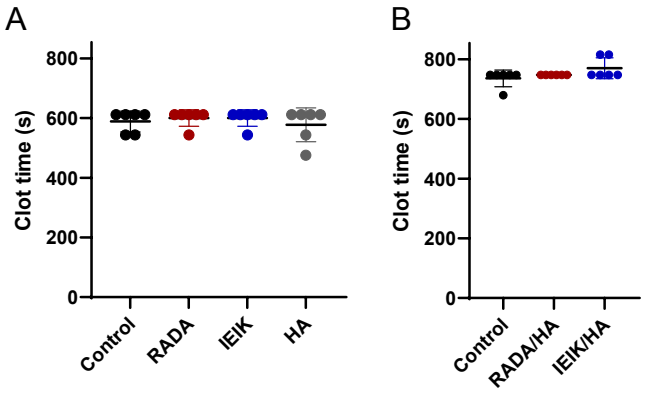

Figure 3.4 Effects of LbL films on platelet rich plasma clot time. Absorbance assay to measure clot formation time in platelet rich plasma for (A) stock solutions and (B) film releasate samples. Stock solutions are 1mg/mL added 1:10 with platelet rich plasma. Material released from sponge samples added 1:10 with platelet rich plasma. The vehicle control for stock solutions is 10mM HCl. The vehicle control for film releasate is 1xPBS with gelatin sponge digested by collagenase. *RADA/HA is* $(RADA/HA)_{200}$ *and IEIK/HA is* $(IEIK/HA)_{200}$. Statistical analysis conducted comparing each sample to the vehicle control using ordinary one way anova with Dunnett multiple comparison correction. (* $P \leq 0.05$, ** $P \leq 0.01$, *** $P \leq 0.001$, **** $P \leq 0.0001$).

3.3.3 Interaction with Plasma Clots

After observing variations in clotting factor activity and platelet aggregations, we examined whether or not these changes could affect the formation of clots in platelet rich plasma (PRP) in an effort to look for more macro scale changes in clot formation rate (**Figure 3.4**). When comparing both stock solutions and material released from films to vehicle controls, no significant differences were observed in any of the materials. This is supported by previous research claiming that small variations in clotting factor activity does not necessarily translate to changes in clot assay results[39].

3.3.4 Interaction with whole blood clot

Moving up another layer in complexity, clot formation time was measured using whole blood. By using the hemostasis analyzer to measure clot time, interactions between the LbL film components and whole blood could be examined (**Figure 3.5**). The results showed no significant effects from any of the components or film releasates on the clot formation time. Because the clot time of whole blood can change over time, each test was self-contained and only the controls and

samples within a single test were compared. These results agreed with the previous results using PRP, suggesting that even though some significant effects were observed on clotting factor activity, they do not seem strong enough to effect the clot formation on a larger scale.

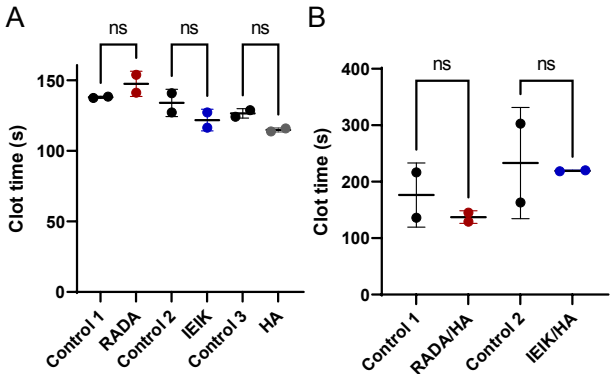

Figure 3.5 Effects of LbL films on whole blood clot time. *Mechanical measurement of clot formation time in whole blood for (A) stock solutions and (B) film releasate samples. Stock solutions are 1mg/mL added 1:10 with citrated whole blood. Stock solutions are 1mg/mL added 1:10 with platelet rich plasma. Material released from sponge samples added 1:10 with citrated whole blood. The vehicle control for stock solutions is 10mM HCl. The vehicle control for film releasate is 1xPBS with gelatin sponge digested by collagenase. RADA/HA is* $(RADA/HA)_{200}$ *and IEIK/HA is* $(IEIK/HA)_{200}$*. Statistical analysis conducted comparing each sample to the vehicle control within each individual test using ordinary one way anova with Šídák's multiple comparisons correction. Each test was compared within each individual test, bars show which samples are compared. (ns=not significant, * P ≤ 0.05, ** P ≤ 0.01, *** P ≤ 0.001, **** P ≤ 0.0001).*

To further examine effects of the peptides on whole blood clot formation, thromboelastography was used. This testing method allowed for the measurement of how RADA16 and IEIK13 affect both the speed of clot formation and the strength of the clot. **Figure 3.6** shows the results from TEG experiments. Each test was conducted with 2 clotting channels and two nonclotting control channels. These controls test whether the citrated blood is capable of clotting without calcium being added. The lack of any clot formation shows that both RADA16 and IEIK13 are not capable of triggering clotting spontaneously. Additionally, a vehicle control (1xPBS) was added to ensure any differences observed are the result of the added peptide. This showed no difference in time to clot formation or the strength of the clot formed when either RADA16 or IEIK13 were added. These results again highlight that the difference observed at the clotting factor scale do not translate into changes in clot formation at the plasma or whole blood scale. This indicates that the hemostasis mechanism is not due to peptides or LbL films signaling or changing the activity of

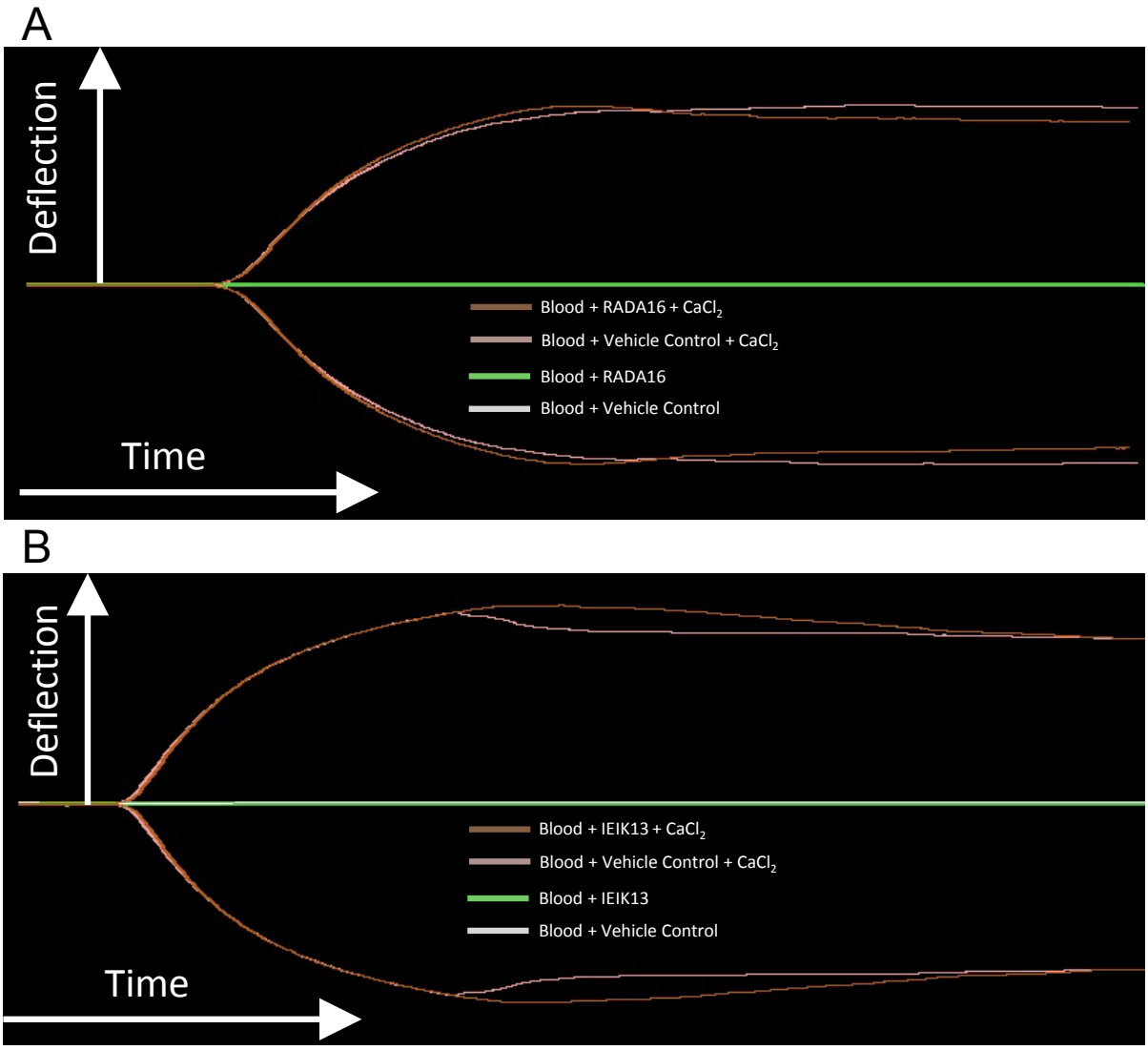

Figure 3.6 Peptide effects on whole blood clot formation and strength. *Thromboelastography mechanical measurement of clot formation and strength for A) RADA16 and B) IEIK13. movement away from the center line denotes deflection of the measurement pin as a result of clot formation. A larger deflection is the result of a stiffer clot. Clot formation is triggered by the addition of $CaCl_2$ solution for clotting samples or saline solution for non-clotting samples. The vehicle control is deionized water. Brown- Clotting Blood with 150ug/mL Peptide, Pink- Clotting Blood with Vehicle Control, Green- Non-clotting Blood with 150ug/mL Peptide, White- Non-clotting Blood with Vehicle Control.*

various clotting factors to promote hemostasis. The mechanical hemostasis mechanism put forth in the literature does not depend on specific signaling or binding of blood components, but rather the physical entrapment of blood components into the peptide hydrogel[14-17]. This mechanism is difficult to directly observe *in vitro* without the presence of flow to drive blood components into the

peptide hydrogel, so it is expected that no significant differences would be observed in the absence of flowing conditions. Future experiments to observe the self-assembling peptide nanofiber mechanism will need to operate under flowing conditions to properly validate the mechanism reported in the literature.

3.4 Conclusions

Examining possible mechanisms for RADA16 and IEIK13 to accelerate hemostasis has shown that both peptides as well as hyaluronic acid (HA) have little effect on the activity of Factor IXa, Factor VII, Tissue Factor, or Thrombin. Some effects on thrombin activity were observed from the films released from RADA/HA and IEIK/HA films showing that there could be some more effects from the LbL formulation. However, this measured decrease in thrombin activity does not seem to play much of a role in overall clot formation. When examining effects on clot formation speed in plasma or whole blood, no significant differences were observed from LbL films or peptide stock solutions. Examining the clot strength with RADA16 and IEIK13 stock solutions also showed no difference observed from the presence of either peptide. All of this data suggests that the differences observed in clotting factor activity and platelet aggregation were not significant enough to impact clot formation and therefore unlikely to be the mechanism to promote hemostasis. The hypothesis from the literature is that these self-assembling peptide LbL formulations do not directly act on the clot mechanism and it is believed that the acceleration in hemostasis is due to the peptide gel forming and physically catching and therefore concentrating blood components and clotting factors. The true mechanism for RADA16 and IEIK13 requires further study and could be directly explored using in vitro clotting experiments under flow.

3.5 References

1. Bellamy, R.F., Pedersen, D.C. & Deguzman, L.R. ORGAN BLOOD-FLOW AND THE CAUSE OF DEATH FOLLOWING MASSIVE HEMORRHAGE. *Circulatory Shock* **14**, 113-127 (1984).
2. Katzenell, U., Ash, N., Tapia, A.L., Campino, G.A. & Glassberg, E. Analysis of the causes of death of casualties in field military setting. *Mil Med* **177**, 1065-1068 (2012).
3. Hong, C., Olsen, B.D. & Hammond, P.T. A review of treatments for non-compressible torso hemorrhage (NCTH) and internal bleeding. *Biomaterials* **283**, 121432 (2022).
4. Chambers, J.A. et al. "Stop the Bleed": A U.S. Military Installation's Model for Implementation of a Rapid Hemorrhage Control Program. *Mil Med* **184**, 67-71 (2019).
5. Sobrino, J. & Shafi, S. Timing and causes of death after injuries. *Proceedings* **26**, 120-123 (2013).
6. Spotnitz, W.D. & Burks, S. Hemostats, Sealants, and Adhesives II: Update As Well As How and When to Use the Components of the Surgical Toolbox. *Clinical and Applied Thrombosis-Hemostasis* **16**, 497-514 (2010).
7. Spotnitz, W.D. & Burks, S. Hemostats, sealants, and adhesives: components of the surgical toolbox. *Transfusion* **48**, 1502-1516 (2008).
8. Pusateri, A.E. et al. Making sense of the preclinical literature on advanced hemostatic products. *J Trauma* **60**, 674-682 (2006).
9. Ellis-Behnke, R.G. et al. Nano hemostat solution: immediate hemostasis at the nanoscale. *Nanomedicine : nanotechnology, biology, and medicine* **2**, 207-215 (2006).
10. Ellis-Behnke, R. At the nanoscale: nanohemostat, a new class of hemostatic agent. *Wires Nanomed Nanobi* **3**, 70-78 (2011).
11. Gelain, F., Luo, Z., Rioult, M. & Zhang, S. Self-assembling peptide scaffolds in the clinic. *NPJ Regenerative medicine* **6**, 9 (2021).
12. Sankar, S. et al. Clinical Use of the Self-Assembling Peptide RADA16: A Review of Current and Future Trends in Biomedicine. *Frontiers in Bioengineering and Biotechnology* **9** (2021).
13. Verbraeken, B. et al. Efficacy and histopathological effects of self-assembling peptides RADA16 and IEIK13 in neurosurgical hemostasis. *Nanomedicine : nanotechnology, biology, and medicine* **40**, 102485 (2022).
14. Hsu, B.B. et al. Clotting Mimicry from Robust Hemostatic Bandages Based on Self-Assembling Peptides. *Acs Nano* **9**, 9394-9406 (2015).
15. Luo, Z., Wang, S. & Zhang, S. Fabrication of self-assembling D-form peptide nanofiber scaffold d-EAK16 for rapid hemostasis. *Biomaterials* **32**, 2013-2020 (2011).
16. Wang, T., Zhong, X., Wang, S., Lv, F. & Zhao, X. Molecular mechanisms of RADA16-1 peptide on fast stop bleeding in rat models. *International journal of molecular sciences* **13**, 15279-15290 (2012).
17. Song, H., Zhang, L. & Zhao, X. Hemostatic efficacy of biological self-assembling peptide nanofibers in a rat kidney model. *Macromolecular bioscience* **10**, 33-39 (2010).
18. Adams, R.L.C. & Bird, R.J. Review article: Coagulation cascade and therapeutics update: Relevance to nephrology. Part 1: Overview of coagulation, thrombophilias and history of anticoagulants. *Nephrology* **14**, 462-470 (2009).
19. Hammond, P.T. Form and function in multilayer assembly: New applications at the nanoscale. *Adv Mater* **16**, 1271-1293 (2004).
20. Kim, B.S., Lee, H., Min, Y.H., Poon, Z. & Hammond, P.T. Hydrogen-bonded multilayer of pH-responsive polymeric micelles with tannic acid for surface drug delivery. *Chem Commun*, 4194-4196 (2009).
21. Shah, N.J., Hong, J., Hyder, M.N. & Hammond, P.T. Osteophilic Multilayer Coatings for Accelerated Bone Tissue Growth. *Adv Mater* **24**, 1445-1450 (2012).

22. Shukla, A. et al. Controlling the release of peptide antimicrobial agents from surfaces. *Biomaterials* **31**, 2348-2357 (2010).
23. Moskowitz, J.S. et al. The effectiveness of the controlled release of gentamicin from polyelectrolyte multilayers in the treatment of Staphylococcus aureus infection in a rabbit bone model. *Biomaterials* **31**, 6019-6030 (2010).
24. Shukla, A., Fuller, R.C. & Hammond, P.T. Design of multi-drug release coatings targeting infection and inflammation. *J Control Release* **155**, 159-166 (2011).
25. DeMuth, P.C., Su, X.F., Samuel, R.E., Hammond, P.T. & Irvine, D.J. Nano-Layered Microneedles for Transcutaneous Delivery of Polymer Nanoparticles and Plasmid DNA. *Adv Mater* **22**, 4851-+ (2010).
26. Macdonald, M.L. et al. Tissue integration of growth factor-eluting layer-by-layer polyelectrolyte multilayer coated implants. *Biomaterials* **32**, 1446-1453 (2011).
27. Samuel, R.E. et al. Osteoconductive protamine-based polyelectrolyte multilayer functionalized surfaces. *Biomaterials* **32**, 7491-7502 (2011).
28. Min, J., Braatz, R.D. & Hammond, P.T. Tunable staged release of therapeutics from layer-by-layer coatings with clay interlayer barrier. *Biomaterials* **35**, 2507-2517 (2014).
29. Min, J.H. et al. Designer Dual Therapy Nanolayered Implant Coatings Eradicate Biofilms and Accelerate Bone Tissue Repair. *Acs Nano* **10**, 4441-4450 (2016).
30. Krogman, K.C., Lowery, J.L., Zacharia, N.S., Rutledge, G.C. & Hammond, P.T. Spraying asymmetry into functional membranes layer-by-layer. *Nat Mater* **8**, 512-518 (2009).
31. Hsu, B.B., Hagerman, S.R. & Hammond, P.T. Rapid and efficient sprayed multilayer films for controlled drug delivery. *Journal of Applied Polymer Science* **133** (2016).
32. Gkikas, M. et al. Systemically Administered Hemostatic Nanoparticles for Identification and Treatment of Internal Bleeding. *Acs Biomater Sci Eng* **5**, 2563-2576 (2019).
33. Hong, C. et al. Modulating Nanoparticle Size to Understand Factors Affecting Hemostatic Efficacy and Maximize Survival in a Lethal Inferior Vena Cava Injury Model. *Acs Nano* **16**, 2494-2510 (2022).
34. Barrett, C.D. et al. Human neutrophil elastase mediates fibrinolysis shutdown through competitive degradation of plasminogen and generation of angiostatin. *The journal of trauma and acute care surgery* **83**, 1053-1061 (2017).
35. GIL, E.S., GILBERT, K. & Mehta, M., Edn. C07K 7/08 (2006.01), A61L 27/22 (2006.01), A61K 38/12 (2006.01), A61L 27/54 (2006.01), A61L 27/58 (2006.01). (ed. W.I.P. Organization) (2015).
36. Brummel-Ziedins, K., Vossen, C.Y., Rosendaal, F.R., Umezaki, K. & Mann, K.G. The plasma hemostatic proteome: thrombin generation in healthy individuals. *Journal of thrombosis and haemostasis : JTH* **3**, 1472-1481 (2005).
37. Howard, P.R., Bovill, E.G., Pike, J., Church, W.R. & Tracy, R.P. Factor VII antigen levels in a healthy blood donor population. *Thrombosis and haemostasis* **72**, 21-27 (1994).
38. Hellstern, P., Beeck, H., Fellhauer, A., Fischer, A. & Faller-Stockl, B. Measurement of factor VII and of activated factor VII in healthy individuals and in prothrombin complex concentrates. *Thrombosis research* **86**, 493-504 (1997).
39. Souid, A.-K. in Pediatric Emergency Medicine. (eds. J.M. Baren, S.G. Rothrock, J.A. Brennan & L. Brown) 917-926 (W.B. Saunders, Philadelphia; 2008).

Chapter 4. Development of LbL hemostatic films with the addition of tissue adhesive molecules.

4.1 Introduction

Hemorrhage due to trauma or injury remains a leading cause of death for both US military[1-3] and civilian populations[4, 5]. A great deal of hemostatic materials have been created and developed to address this issue[6, 7], however, none of these materials meet the criteria laid out for the ideal hemostat: simple application, no negative side effects, long term stability, thermal stability, cost effective, and bioabsorbable[8]. One possible solution to the ideal hemostat is through the use of self-assembling peptide nanofibers such as RADA16 and IEIK13. These peptides have been used extensively to promote rapid hemostasis and have shown excellent efficacy and biocompatibility[9-13]. These self-assembling peptides can be applied to biocompatible substrates through the use of layer-by-layer (LbL)[14]. LbL assembly is versatile and can be used to create films containing a variety of functional polymers and other charged species including antibiotics, anti-inflammatory drugs, chemotherapeutics, growth factors, and nucleic acids with controlled release[15-25]. LbL films can be constructed by dipping substrates into solutions or by spraying solutions directly onto three dimensional substrates[26, 27], allowing for the creation of LbL coated hemostatic bandages[14].

Non-compressible wounds can be difficult to properly treat with traditional hemostats[3]. In these cases, the ability of a wound dressing to interact with injured tissue can play an important role in how well the bandage is able to promote hemostasis. An impermeable dressing can't stop the bleeding from a wound if it can't interact with the tissue to form a seal around the bleeding source. Pilot testing of (RADA16/HA) and (IEIK13/HA) films in a swine severe liver injury model described in Chapter 2 helped motivate the interest in modulating the adhesion of the peptide LbL films. Anecdotally it seemed that the wound dressing was well adhered in tests where blood loss was reduced and poorly or not at all adhered in tests where blood loss was severe. This led to the hypothesis that the ability to interact with and adhere to the wound surface plays an important

role in promoting hemostasis. To this end, new LbL formulations were developed to incorporate materials that have been shown to be adhesive.

While there are many different types of tissue adhesive molecules available, we focused on two primary candidates; chitosan and catechols. Chitosan is a highly charged and sticky polycation that not only can interact with cellular tissue, but has hemostatic properties of its own[28-31]. Due to its highly charged nature, chitosan can be easily built into LbL formulations[24]. Catechols are capable of forming many different types of interactions including hydrogen bonding, covalent bonding, and pi-pi stacking[32]. These materials have even been shown to be a strong adhesive in wet environments and are part of the way mussels are able to glue themselves to underwater rocks in nature[33]. Luckily catechol groups can be functionalized onto a polyelectrolyte backbone to facilitate building into an LbL film[34-36].

4.2 Methods

4.2.1 Materials

Self-assembling peptides solutions of 1.5 wt% RADA16 and IEIK13 were generous donations from 3-D Matrix Medical Technology. Hyaluronic acid (MW = 2 MDa) was obtained from Lifecore Biomedical. Collegenase (Type I) was purchased from Sigma-Aldrich. Human whole blood (EDTA anticoagulated) was obtained from Hemacare, and washed and pooled 10% rabbit red blood cells (RBCs) were obtained from Lampire Biological Laboratories. Solutions of 1% (10 mg/mL) RADA16-I were a generous donation from 3DMatrix. Fluorescently labeled RADA16-I (RADA16-IFAM) was functionalized by 5-carboxyfluorescein at the N-terminus through a -Gly-Gly- linker and synthesized by the MIT Biopolymers Laboratory. Gelatin sponges were purchased from McKesson. Chitosan (MW = 15 kDa) was purchased from Polysciences, Inc. Factor IXa Activity Assay Kit (ab204727), Factor VII Human Chromogenic Activity Kit (ab108830), Tissue Factor Activity Assay Kit (ab108906), and Thrombin Activity Assay Kit (ab197006) were purchased from Abcam. Anticoagulated human whole blood was purchased from Research Blood

Components. CyQUANT LDH Cytotoxicity Assay Kit was purchased from ThermoFisher Scientific. Fresh animal muscle tissue was purchased from a local butcher. 50um Polymethylmethacrylate (PMMA) Films were purchased from Goodfellow.

4.2.2 Solution preparation

1.5 wt% peptide gel was diluted to 1 mg/mL or 0.1 mg/mL using 10mM HCl. These solutions were then stirred overnight. Afterward the solutions were sonicated for 1 hour using a bath sonicator and immediately filtered through a 0.2 μm PES membrane. The resulting solution was stored at room temperature overnight to allow the peptide fibers to reassemble. Solutions of Hyaluronic acid were dissolved into 10mM HCl and stirred overnight. Solutions of Chitosan were made using the same methods as the peptide solutions and solutions of HACA were made in the same way as HA solutions.

4.2.3 Synthesis of HACA

HACA was synthesized following an adaptation of a previously published protocol[36]. An example of volumes and masses is described here. 334 mg of 2 MDa Hyaluronic acid (HA) was dissolved into 116 mL of 0.1 M morpholineethanesulfonic acid buffer (MES) by stirring overnight. The solution was heated to 50°C and 338.7mg EDC and 101.2 mg of Sulfo-NHS were added. The solution was then pH adjusted to 4.5 using 1M HCl. 167.3 mL of Dopamine HCl was added to 13.9 mL of nitrogen purged DI water. The Dopamine solution was then added dropwise to the HA solution. The reaction mixture was kept at 50°C under nitrogen for approximately 15 hours. Afterward the solution was purified by dialysis for at least 5 days to remove unreacted materials. The solution was then frozen and lyophilized to obtain died powder of catechol modified Hyaluronic acid (HACA). The resulting powder was examined on NMR to determine the degree of functionalization.

4.2.4 Dip LbL

Film assembly conditions for electrostatic films were based on previously published work with RADA16[14]. Silicon wafer substrates were cut into pieces approximately 25mm by 6.5mm.

These wafers were cleaned using isopropanol, followed by methanol, and finally water before being air dried. Immediately prior to layering, the wafers were plasma treated (Harrick PDC-32G) for at least 10 minutes and then immediately placed onto a slide stainer for Layer-by-Layer film assembly. Silicon slides were immersed into 1 mg/mL peptide (RADA16 or IEIK13) for 10 minutes, followed by immersion into 3 separate wash baths of 10mM HCl for 1 minute each, then into 1 mg/mL HA in 10mM HCl for 10 minutes, and again into 3 separate wash baths of 10 mM HCl for 1 minute each. This constituted one bilayer and the process was repeated for a given number of n bilayers. For Chitosan containing films, a tetralayer formulation was used. The same process was used for solution and sample preparation. The tetralayer dipping protocol was as follows: Silicon slides were immersed into 1 mg/mL peptide (RADA16 or IEIK13) for 10 minutes, followed by immersion into 3 separate wash baths of 10mM HCl for 1 minute each, then into 1 mg/mL HA in 10mM HCl for 10 minutes, and again into 3 separate wash baths of 10 mM HCl for 1 minute each, then into a solution of 1 mg/mL Chitosan for 10 minutes, followed by immersion into 3 separate wash baths of 10mM HCl for 1 minute each, then into 1 mg/mL HA in 10mM HCl for 10 minutes, and again into 3 separate wash baths of 10 mM HCl for 1 minute each. This constitutes one tetralayer and the process was repeated for n tetralayers.

4.2.5 Sponge spray LbL

Methods for spray LbL systems were adapted from previously published work[14]. Large gelatin sponges (8cm x 12.5cm x 10mm) were coated using an automated film assembly instrument (Svaya). The sprayer was calibrated to a 0.25mL/s flow rate at 15PSI. House vacuum was applied through a regulator to around 50% strength. Bilayer formulations were created with the following steps: 0.1mg/mL peptide (RADA16 or IEIK13) in 10mM HCl for 3 seconds, wait time for 5 seconds, rinse with 10mM HCl for 3 seconds, dry time for 8 seconds, 0.1 mg/mL polyanion in 10mM HCl for 3 seconds, wait time for 5 seconds, rinse with 10mM HCl for 3 seconds, dry time for 8 seconds. In summary: peptide (3s), wait (5s), wash (3s), dry (8s), polyanion (3s), wait (5s), wash (3s), dry (8s). This made up one bilayer and was repeated for n bilayers with a 60

minute air dry time added after every 10 bilayers. For tetralayer formulations, the same process was followed except the peptide solution was alternated with 0.1mg/mL Chitosan in 10mM HCl. Briefly the process was: peptide (3s), wait (5s), wash (3s), dry (8s), polyanion (3s), wait (5s), wash (3s), dry (8s), chitosan (3s), wait (5s), wash (3s), dry (8s), HA (3s), wait (5s), wash (3s), dry (8s). This made up one tetralayer and was repeated for n tetralayers with a 60 minute air dry time added every 5 tetralayers.

Even coverage of Sponge samples was examined by spraying fluorescently labeled peptide solutions for the LbL process. Afterward the sponge samples were imaged using an In Vivo Imaging System (IVIS) at λ_{ex} = 465 nm; λ_{em} = 520 nm.

4.2.6 Film thickness

Methods for measuring film thickness were adapted from previously published work[14, 37]. Thickness of films deposited onto silicon substrates were measured using a Profilometer (Dektak 150 Profilometer). A razor was used to scratch two lines in the film lengthwise approximately 1.5-2mm apart. These scored areas were used to level the resulting data and the step-height was calculated by comparing the razor scored area with the average height of the area in between the two scratches. A data point was collected from three separate spots along the film for each sample and then averaged.

4.2.7 LbL film release

Methods for the release of LbL films from gelatin substrates were adapted from previously published work[14]. For release studies, films containing either labeled RADA16 or labeled IEIK13 were generated. This was done by adding fluorescently labeled peptide in a 1:20 ratio with unlabeled peptide. Release of film coated sponges were done by placing pieces of the sponge sample into 1mL of PBS at 37°C. At each time point 300 uL was removed and replaced with fresh, prewarmed PBS. Fluorescence (λ_{ex} = 480 nm; λ_{em} = 525 nm) of collected samples were measured and compared with a standard curve for RADA16 or IEIK13. Total loading was obtained by adding 100 uL of 10mg/mL Collagenase (Type I) and then incubating samples for at least 24hr to allow

the sponge substrate to be digested. Then fluorescence was measured and concentration was calculated as described above.

Released LbL formulations were generated by cutting 1cm^2 (of the LbL coated side) pieces of sponge (approximately 15-20 mg of sponge sample) into 1 mL of 1xPBS. 100 uL of 10mg/mL Collagenase (Type I) was added and the samples were incubated for at least 24hr to allow the sponge substrate to be digested.

4.2.8 Scanning electron microscopy (SEM)

Dry Sponge samples were sputter coated with 5-10 nm of Au prior to examination using a field-emission SEM (JEOL 6700F).

4.2.9 Clotting assays

4.2.9.1 Generation of plasma samples

Platelet rich plasma (PRP) was obtained by centrifuging whole blood, following previously published protocols[38]. Platelet poor plasma (PPP) was obtained by centrifuging the platelet rich plasma (PRP) at approximately 2000 RPM for at least 10 min[39]. Sample Solutions were then diluted 1/10 into either PRP or PPP and incubated for at least 10 minutes. Sample solutions were a vehicle control (10mM HCl for stock solutions and 1xPBS with approximately 15mg of degraded gelatin sponge dissolved) with either a 1mg/mL LbL stock solution in 10mM HCl, or released LbL film formulation in 1x PBS.

4.2.9.2 Platelet aggregation via lactate dehydrogenase (LDH)

To determine platelet interaction and binding, a lactate dehydrogenase (LDH) assay was modified from the literature[39]. The platelet rich plasma was then split up into two containers. ADPT was added to one of the containers to activate the platelets. Stock solutions of 1mg/mL LbL component in 10mM HCl or solution released from an LbL coated sponge were diluted 1/10 into either the activated platelet plasma or the non-activated platelet plasma for at least 10 minutes. The plasma was then diluted to half concentration and placed into a 96 well plate. The plates are

allowed to incubate for a period of time and then each well is gently washed at least 3 times to rinse out any material that did not bind and settle to the bottom of the wells. Following this, the LDH assay was performed following the kit instructions to obtain a measure of the number of platelets that settled out of solution. The wells were measured on a plate reader at absorbance of 490nm and 680nm using the 680nm absorbance as a reference wavelength. Comparing non-activated and activated platelets allows us to examine nonspecific binding from the non-activated platelets as a baseline and any additional specific binding from the activated platelets.

4.2.9.3 Factor IXa activity

Platelet poor plasma samples were generated in the same way as described above. These plasma samples were then diluted 10x in FIXa Assay buffer and run in a 96 well plate following the kit directions. Fluorescent results were plotted and the slope of fluorescence over time was used to calculate Factor IXa activity. Each sample was then compared to the appropriate vehicle control to obtain the fold change in Factor IXa Activity.

4.2.9.4 Factor VII human chromogenic activity

Platelet poor plasma samples were generated in the same way as described above. These plasma samples were diluted 30x with the assay diluent before being run in a 96 well plate following the kit directions. Absorbance results were plotted and the slope of the absorbance change over time was used to calculate Factor VII activity. Each sample was then compared with the appropriate vehicle control to obtain the fold change in Factor VII Activity.

4.2.9.5 Tissue factor activity

Platelet poor plasma samples were generated in the same way as described above. These plasma samples were then diluted 2x with kit Sample Diluent and run in a 96 well plate following the kit directions. Absorbance results were plotted and the slope of the absorbance change over time was used to calculate tissue factor activity. Each sample was then compared with the appropriate vehicle control to obtain the fold change in tissue factor activity

4.2.9.6 Thrombin activity

Platelet poor plasma samples were generated in the same way as described above. These plasma samples were then diluted 2x with kit Thrombin Assay Buffer and run in a 96 well plate following the kit directions. Fluorescence results were plotted and the slope of the fluorescence change over time was used to calculate thrombin activity. Each sample was then compared with the appropriate vehicle control to obtain the fold change in thrombin activity

4.2.10 Plasma clot formation absorbance assay

Protocols for the clot formation absorbance assay were adapted from previously published methods in the literature[40]. Platelet rich plasma (PRP) was used to measure changes in clot formation speed through an absorbance assay in a 96 well plate. Samples were diluted 10 times into PRP. The wells of a 96 well plate were loaded with 10 µL of 100 mM $CaCl_2$ solution, then 90 µL of PRP samples was added to each well using a multichannel pipette. 6 replicates were collected. The plate was then measured in a Tecan plate reader for absorbance at 620 nm. Measurements were taken every minute for 2 hours or until all wells had clotted. The time of the maximum slope was measured for each well as the time of clot formation.

4.2.11 Hemostasis analyzer

Clotting experiments using whole blood were conducted using a Stago STart4 Hemostasis analyzer. The activated partial thromboplastin time (aPPT) test setting was used with a 3 minute incubation and the maximum clot time raised to 600 seconds. Samples were produced by diluting either stock solutions or film releasate 10 fold into whole blood. The blood and sample were then gently mixed and 450 µL of the blood sample was added to each well. Each test had 4 wells, two were used for a vehicle control and two were used for the intended sample. Each set of 4 wells had magnetic beads added and then were placed in the incubator wells at 37°C for at least 3 minutes. The samples were then placed in the test wells and 50 µL of 100mM $CaCl_2$ solution was added. At the moment the calcium was added, the timer was started. After a clot formed, the magnetic bead stopped moving and the equipment registered a clot time. To account for changes in the blood clotting behavior over the course of the tests, each sample was compared only with

the control from the same test. Vehicle controls were the same as described for the plasma samples (10mM HCl for stock solutions and 1xPBS with approximately 15mg of degraded gelatin sponge dissolved).

4.2.12 Adhesion shear test

The shear test was conducted following an adaptation of the ASTM standard F2255 for a Lap-shear test[41]. Samples were generated by cutting 2cm x 5cm rectangles of both the sponge samples and tissue samples. A flexible but inelastic PMMA film was also cut into 2cm x 5cm pieces.. A thin layer of superglue was applied to the PMMA film and then the film was applied to either the back of the sponge sample or the muscle tissue. Samples were lightly misted with DI water just prior to application of the backing film for better adhesion. Any excess area not covered by the PMMA film was then trimmed off. The sponge samples and muscle tissue were wetted then placed end to end overlapping approximately 1cm. A 350g weight was placed on top of the sample to apply approximately 3.5N of force for 2 minutes. Then the weight was removed and the samples were wrapped in a damp paper towel, placed in a bag, and incubated at 37°C in a water bath for 1 hour. After the incubation time, the samples were removed and placed on a Zwick mechanical tester with the sponge sample on top for testing. After each test, the force of the sponge sample was recorded to remove effects from any difference in sponge mass. Pictures were then taken of the sponge and muscle tissue sample to accurately measure the contact area. The corrected force value was divided by the adhesion area to obtain the shear strength for the sample.

4.3 Results and Discussion

4.3.1 Different adhesion molecules and LbL formulations

New LbL adhesive formulations were generated based on the methods used to produce (RADA/HA) and (IEIK/HA) films. We were able to keep all solutions and concentrations the same to produce the new formulations. Catechol functionalized Hyaluronic Acid (HACA) was synthesized with a percent functionalization of 24-44%. The HACA reaction scheme and other

LbL film components are shown in **Figure 4.**1. HACA was then used in place of HA to generate (RADA/HACA) and (IEIK/HACA) films. Because chitosan (Chi) is a polycation and the peptide nanofibers act as a polycation in the LbL formulations, a tetralayer formulation was used to build chitosan into films. (RADA/HA/Chi/HA), abbreviated as (RADA/Chi), and (IEIK/HA/Chi/HA), abbreviated as (IEIK/Chi), films were constructed maintaining the same number of tetralayers as bilayers for the other formulations. This way, each sample had the same number of peptide layers in it.

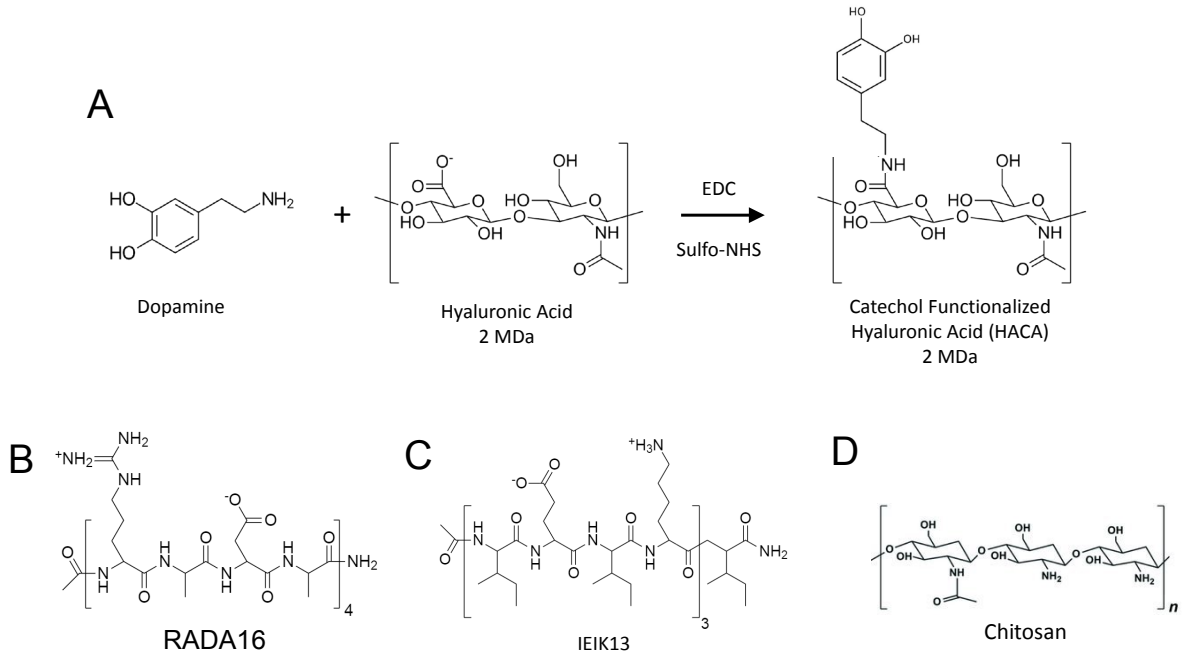

Figure 4.1 Reaction scheme and molecules for layer-by-layer film construction. *(A) Reaction scheme to synthesize catechol modified hyaluronic acid (HACA) using EDC/Sulfo-NHS chemistry. (B)-(D) Polycations for LbL films. (B) Self-assembling peptide RADA16, (C) self-assembling peptide IEIK13, (D) Chitosan. Hyaluronic acid (HA) (A middle) and catechol functionalized hyaluronic acid (HACA) (A right) are polyanions for LbL films.*

4.3.2 Film growth of adhesive formulations

Previous work has shown the ability to build stable LbL films with RADA16[14]. During assembly, acidic pH conditions (pH 2) were used to ensure the RADA16 aspartic acid side chains are neutral and the arginine side chains are cationic[42]. This is important both for the nanofiber assembly and allows the peptide to be used as a polycation for LbL film assembly[43, 44]. Adapting from the process to build $(RADA/HA)_n$ and $(IEIK/HA)_n$ films, dip layer-by-layer was performed on each of the newly generated adhesive LbL formulations. Films containing IEIK13 generated slightly thinner films than RADA16 based films. This result could be due to minor differences in fiber width or from steric hindrance of the stiffer IEIK13 nanofibers[43, 45]. Each film shows generally linear growth and the roughness is generally proportional to the film thickness indicating that each formulation is capable of building a stable LbL film.

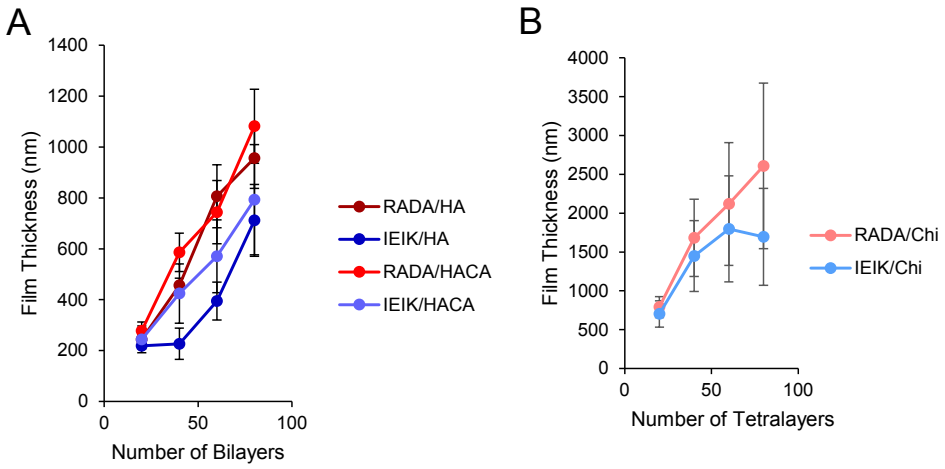

Figure 4.2 Film Growth of adhesive LbL formulations. *LbL film growth measured by film thickness for a given number of (A) bilayers or (B) tetralayers. (A) Bilayer films contain the self-assembling peptide RADA16 or IEIK13 as a polycation and either hyaluronic acid (HA) or catechol modified hyaluronic acid (HACA) as a polyanion. (B) Tetralayer films contain chitosan (Chi) and either RADA16 or IEIK13 as polycations and hyaluronic acid (HA) as the polyanion. Each formulation is listed as follows: RADA/HA-$(RADA/HA)_n$, RADA/HACA-$(RADA/HACA)_n$, RADA/Chi-$(RADA/HA/Chi/HA)_n$, IEIK/HA-$(IEIK/HA)_n$, IEIK/HACA-$(IEIK/HACA)_n$, IEIK/Chi-$(IEIK/HA/Chi/HA)_n$.*

4.3.3 Spray layer-by-layer adhesive formulations

After evaluating the stability of the adhesive LbL formulations, each dip LbL formulation was translated to a spray LbL system to apply films onto the gelatin sponge substrate. Spray LbL generally has a much lower film thickness due to lower concentration of polyelectrolytes in spray

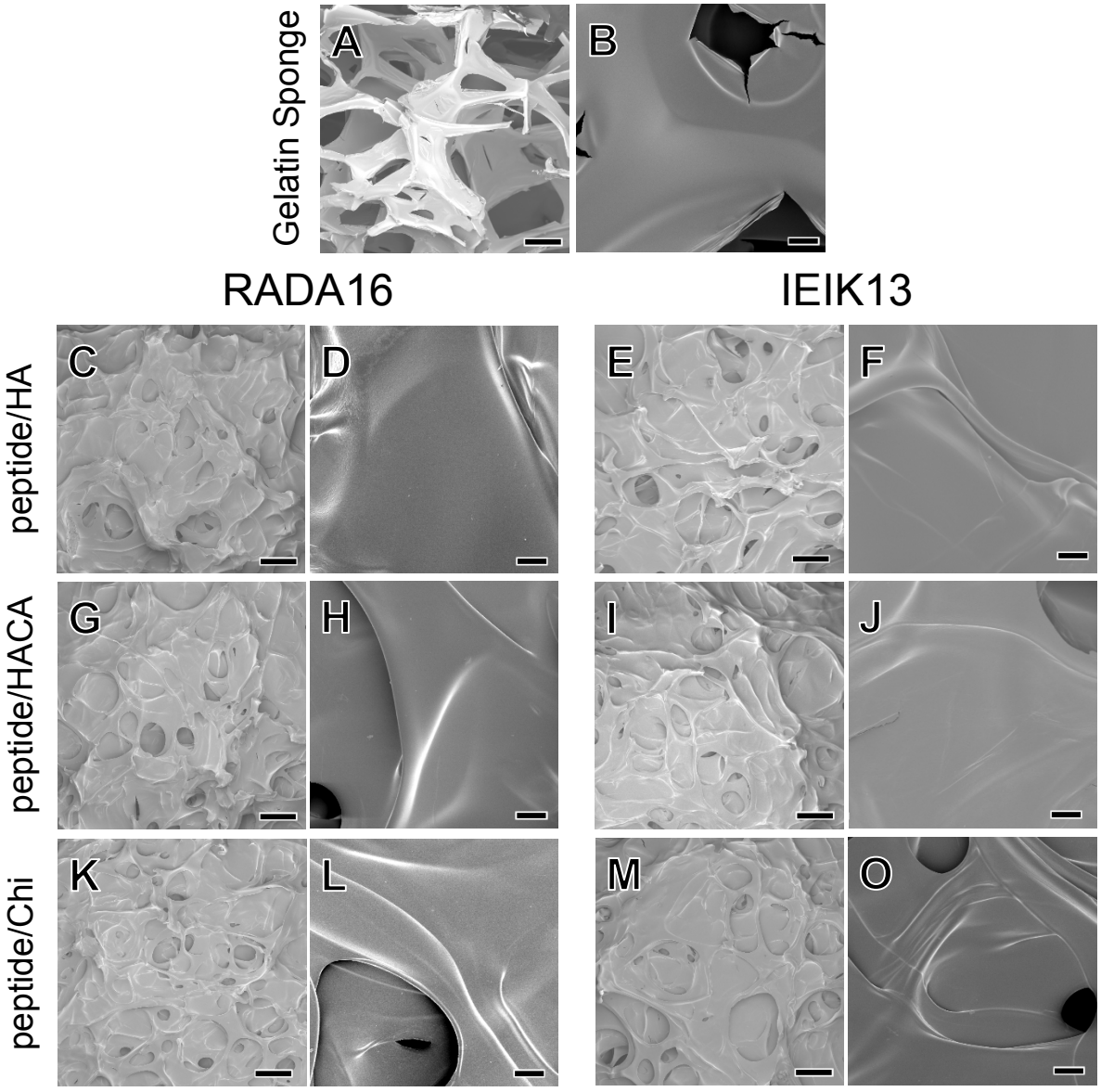

Figure 4.3 Surface morphology of LbL coated gelatin sponges. SEM imaging of uncoated and LbL coated gelatin sponges. (A,B) uncoated gelatin sponge substrate (C,D) $(RADA/HA)_{200}$,(E,F) $(IEIK/HA)_{200}$, (G,H) $(RADA/HACA)_{200}$, (I,J) $(IEIK/HACA)_{200}$, (K,L) $(RADA/Chi)_{200}$, (M,O) $(IEIK/Chi)_{200}$. Images show a collapse of the gelatin sponge structure from the spray LbL process that is conserved for all LbL film formulations. Scale bars represent 100 μm (A,C,E,G,I,K,M) and 10 μm (B,D,F,H,J,L,O).

solutions and reduced adsorption times from the spraying process. The resulting films were characterized using SEM (**Figure 4.3**) to observe changes in surface morphology. The structure of the gelatin sponge was observed to collapse partially from the repeated wetting and drying of the LbL spray process. This is likely due to a combination of the acidic solution conditions sprayed on the sponge, which has been shown to dissolve collagen[46], and the water surface tension during the drying steps. However, a similar amount of structural collapse was observed in all samples, and no significant differences between each of the LbL formulations were observed.

Fluorescently labeled RADA16 and IEIK13 were used to produce films to measure peptide loading and release from LbL films. Imaging of the entire sponges showed even coverage that was consistent between multiple samples (**Figure 4.4**). To measure how films would degrade in physiological conditions, sponge samples were placed in PBS at 37°C. The change in conditions from LbL assembly (low pH) alters the charges and interactions between the film components and the substrate to facilitate the breakup. Release profiles showed that IEIK13 films release

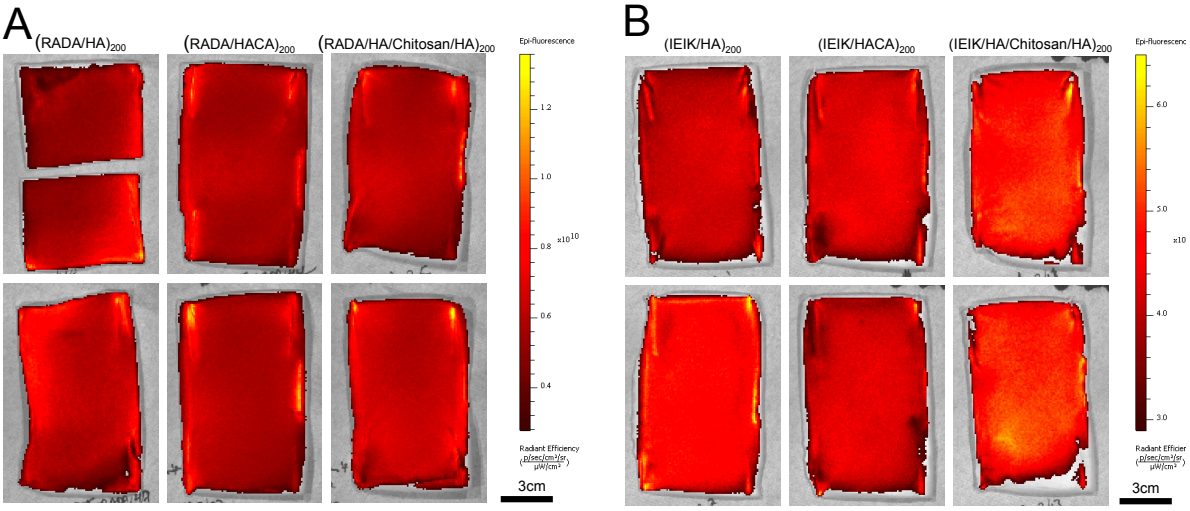

Figure 4.4 Peptide coverage of spray LbL coated sponge samples. *Composite IVIS images of LbL coated gelatin sponge samples containing fluorescently labeled self assembling peptides. Color intensity denotes the peptide concentration. (A) RADA LbL formulations (B) IEIK LbL formulations. Each column shows multiple samples of the same formulation. Two replicate sponges are shown for each film treatment. $(RADA/HA)_{200}$ and $(IEIK/HA)_{200}$ images reproduced from Figure 2.7.*

more slowly than RADA16 based films (**Figure 4.5**). In the first three hours of release, RADA16 based films released around 40% of the total RADA16 whereas IEIK13 based films only released around 10% of the total IEIK13. This result is likely due to the increased hydrophobicity and gel stiffness of IEIK13 acting as an additional barrier to release[43]. The addition of fetal bovine serum (FBS) to the release solution promoted a more rapid film breakup for all films due which has also been reported for LbL film release previously[14]. Total loading of peptides were calculated for each of the different LbL formulations normalized to either the mass of the sponge (**Figure 4.5A**) or the area of the LbL coated side (**Figure 4.5B**). Extrapolating the area loading for an entire sponge (approximately 100cm^2) and spraying approximately 15mg or peptide per sponge allows an

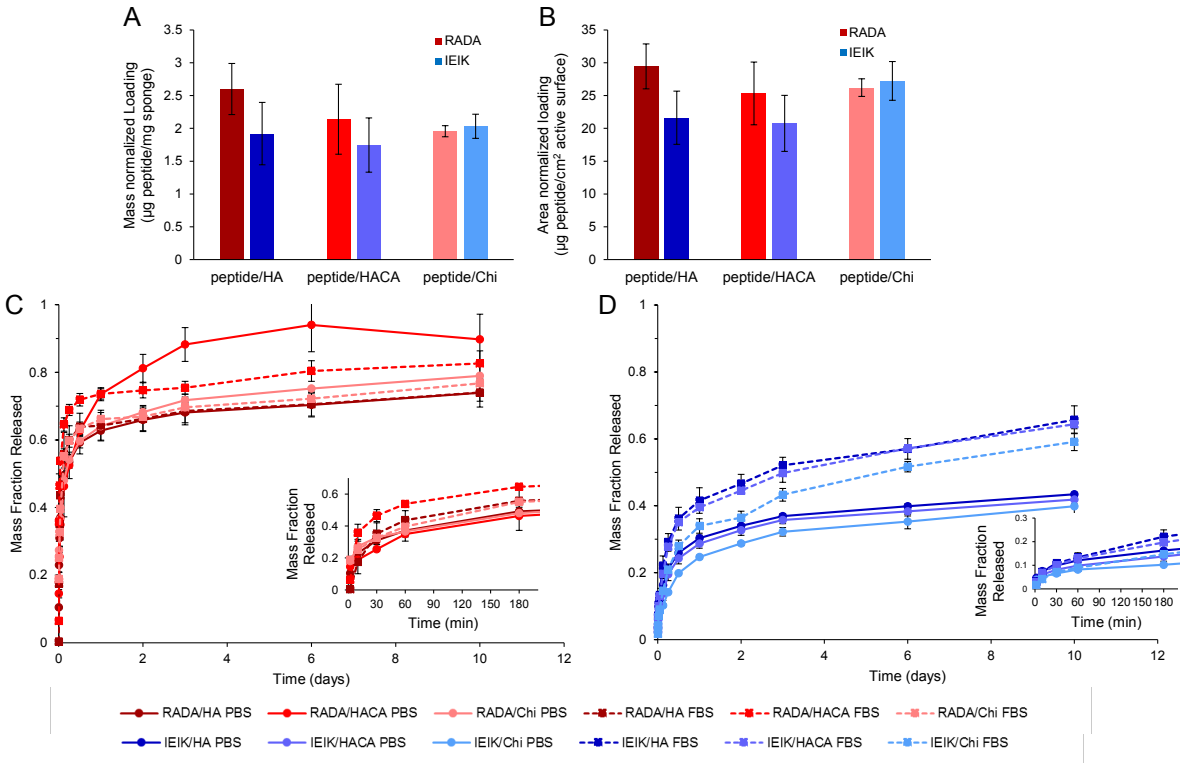

Figure 4.5 Total loading and release of LbL coated gelatin sponges. *(A) Mass normalized total loading of LbL film formulations, mass of loaded peptide normalized to the mass of gelatin sponge substrate. (B) Area normalized total loading of LbL film formulations, mass of loaded peptide normalized to the area of the active LbL coated sponge surface. (C) Mass fraction of released RADA16 in PBS (solid line) and FBS (dashed line). (C, insert) mass fraction of RADA16 released over the first 3 hours. (D) Mass fraction of released IEIK13 in PBS (solid line) and FBS (dashed line). (D,insert) mass fraction of IEIK13 released over the first 3 hours. Total loadings obtained by digesting sponge samples with collagenase.*

encapsulation efficiency to be calculated. The encapsulation efficiency for each formulation is approximately 19.6% for $(RADA/HA)_{200}$, 16.9% for $(RADA/HACA)_{200}$, 17.5% for $(RADA/HA/Chi/HA)_{200}$, 14.4% for $(IEIK/HA)_{200}$, 13.8% for $(IEIK/HACA)_{200}$, and 18.2% for $(IEIK/HA/Chi/HA)_{200}$. The efficiency for each LbL film formulation remains fairly consistent for each film formulation with RADA16 based films containing slightly more peptide than IEIK13 based films.

4.3.4 Interactions of individual adhesive components

Each of the new LbL film components as well as released material from each of the formulations were tested in each of the individual clotting factor assays along with the original LbL formulations described in Chapter 3 (**Figure 4.6**). Significant effects on tissue factor activity, factor VII activity, and thrombin activity were observed with stock solutions of HACA and chitosan. All RADA16 based films showed an increase in factor VII activity and all film formulations showed a drastic decrease in thrombin activity. There do not seem to be consistent trends between effects from the stock solutions and material released from LbL films showing that the effects observed in these clotting factor assays are unlikely to be the cause of hemostasis acceleration by peptide LbL films. Additionally, the levels and activity of these different clotting factors can range considerably even within healthy patients without having a significant effect on bleeding times[47-50].

Platelet activation and aggregation plays an important role in hemostasis[3]. The new adhesive LbL film components and formulations were tested for their interactions with platelets similarly to Chapter 3. When examining interactions with platelets, some significant changes in platelet aggregation were observed (**Figure 4.7**). In the platelet aggregation assay, non-specific aggregation was examined through non-activated platelet interactions. Activated platelet aggregation was examined by first activating platelets with ADP, then measuring for aggregation. Specific binding and aggregation of activated platelets was measured by normalizing the activated platelet values to the non-activated platelet values to account for any non-specific binding as

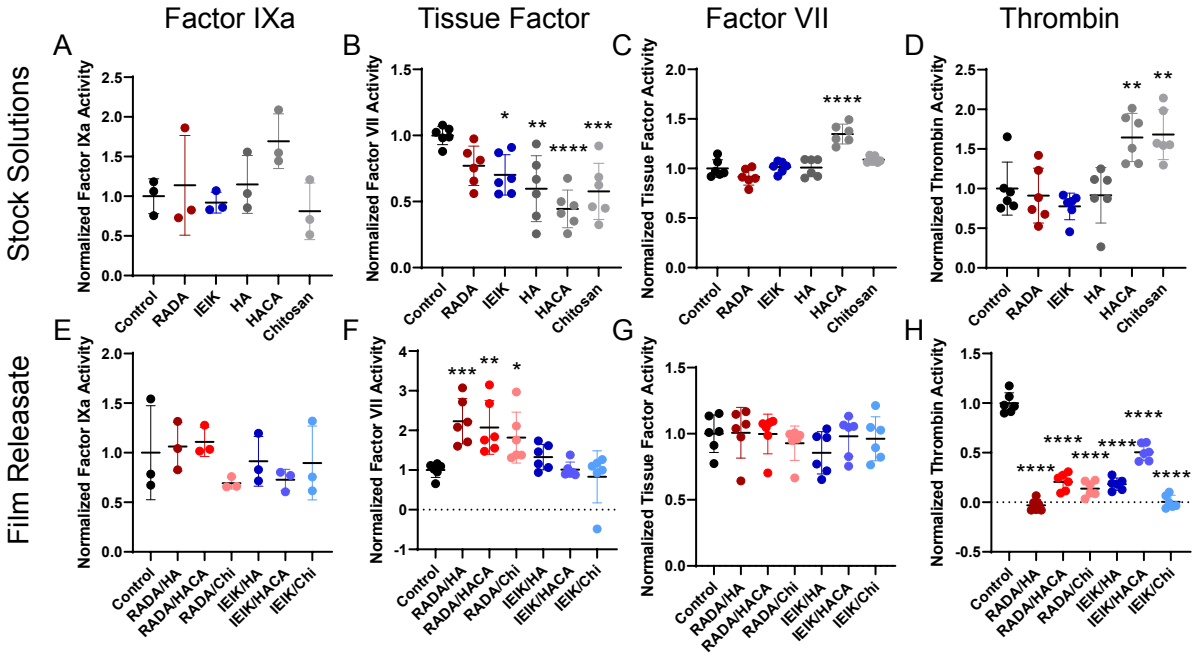

Figure 4.6 Effects of LbL films on clotting factor activity. *Fold Change in (A) factor IXa activity, (B) factor VII activity, (C) tissue factor activity, (D) thrombin activity with stock solutions of LbL components. Stock solutions are 1mg/mL added 1:10 with platelet poor plasma. Control is the vehicle control of 10mM HCl. Fold Change in (E) factor IXa activity, (F) factor VII activity, (G) tissue factor activity, (H) thrombin activity with solutions released from LbL formulations. Film releasates are added 1:10 with platelet poor plasma. Control is the vehicle control of 1xPBS with gelatin sponge digested by collagenase. RADA/HA is* $(RADA/HA)_{200}$*, RADA/HACA is* $(RADA/HACA)_{200}$*, RADA/Chi is* $(RADA/HA/Chitosan/HA)_{200}$*, IEIK/HA is* $(IEIK/HA)_{200}$*, IEIK/HACA is* $(IEIK/HACA)_{200}$*, IEIK/Chi is* $(IEIK/HA/Chitosan/HA)_{200}$*. Results for Stock Solution Control, RADA, IEIK, HA, Film Release Contol, RADA/HA, and IEIK/HA reproduced from figure 3.2. Statistical analysis conducted comparing each sample to the vehicle control using ordinary one way anova with Dunnett multiple comparison correction. (* P ≤ 0.05, ** P ≤ 0.01, *** P ≤ 0.001, **** P ≤ 0.0001).*

described in the literature[39]. Minor variations in platelet aggregation were observed with chitosan stocks slightly decreasing the aggregation of activated platelets. This result is surprising because chitosan is generally believed to attract and bind with platelets[31]. Only IEIK/Chi film releasate showed increased aggregation of both non-activated and activated platelets. In general, the effects of both the stock solutions and LbL film materials had relatively small effects on platelet aggregation.

These materials were then tested for effects on clot formation time in both platelet rich plasma and whole blood following the same protocol as Chapter 3 (**Figure 4.8**). The addition of

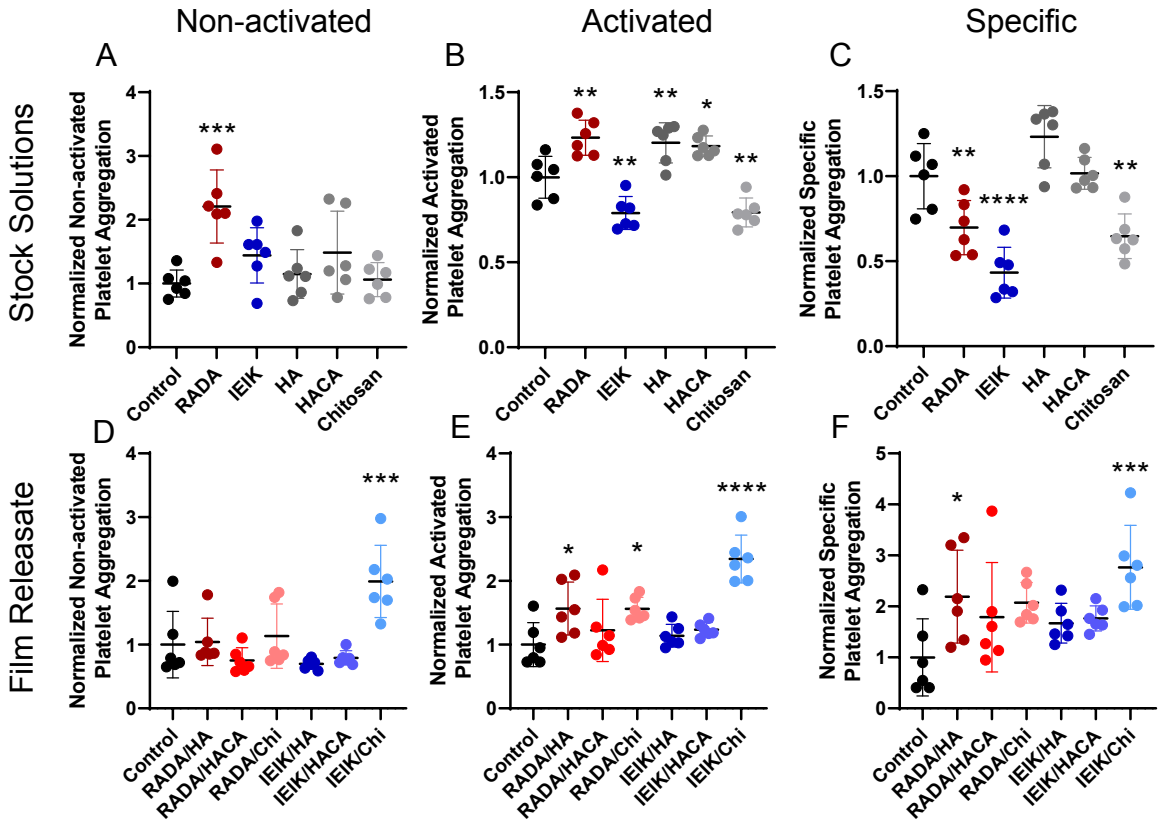

Figure 4.7 Effects of LbL films on platelet aggregation. *Platelet aggregation results showing fold change from vehicle control for aggregation of (A,D) non-activated platelets, (B,E) activated platelets, and (C,F) specific aggregation of platelets calculated as the activated platelet value minus the non-activated platelet. (A-C) shows results from stock solutions of 1mg/mL added 1:10 with platelet rich plasma. The vehicle control is 10mM HCl. (D-F) shows results from released sponge samples added 1:10 with platelet rich plasma and the vehicle control is 1xPBS with gelatin sponge digested by collagenase. RADA/HA is $(RADA/HA)_{200}$, RADA/HACA is $(RADA/HACA)_{200}$, RADA/Chi is $(RADA/HA/Chitosan/HA)_{200}$, IEIK/HA is $(IEIK/HA)_{200}$, IEIK/HACA is $(IEIK/HACA)_{200}$, IEIK/Chi is $(IEIK/HA/Chitosan/HA)_{200}$. Stock Solution Control, RADA, IEIK, HA, Film Release Contol, RADA/HA, and IEIK/HA reproduced from figure 3.3. Statistical analysis conducted comparing each sample to the vehicle control using ordinary one way anova with Dunnett multiple comparison correction. (* $P \leq 0.05$, ** $P \leq 0.01$, *** $P \leq 0.001$, **** $P \leq 0.0001$).*

the adhesive LbL film components did seem to have a small effect on clotting time with chitosan stocks showing a decrease in clot time and IEIK/Chi film samples showing a decrease in clot time. In whole blood, no significant changes in clot time were observed except for chitosan stock solutions showing a large increase in clot time. This result is again surprising because of chitosan's strong interactions with platelets in blood[31]. This result could be due to limiting the

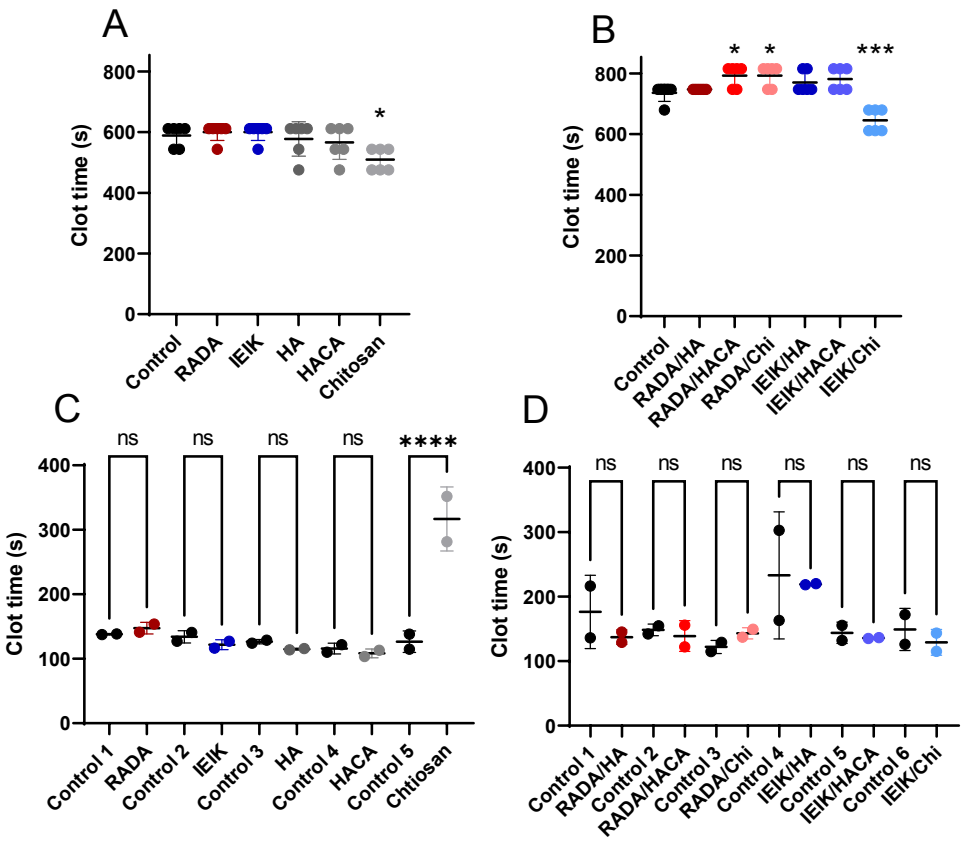

Figure 4.8 Effects of LbL films on clot formation time. *(A,B) Absorbance assay to measure clot formation time in platelet rich plasma for (A) stock solutions and (B) film releasate samples. (A) Stock solutions are 1mg/mL added 1:10 with platelet rich plasma and the vehicle control is 10mM HCl. (B) Material released from sponge samples added 1:10 with platelet rich plasma and the vehicle control is 1xPBS with gelatin sponge digested by collagenase. (C,D) Mechanical measurement of clot formation time in whole blood for (C) stock solutions and (D) film releasate samples. (C) Stock solutions are 1mg/mL added 1:10 with citrated whole blood and the vehicle control is 10mM HCl. (D) Material released from sponge samples added 1:10 with citrated whole blood and the vehicle control is 1xPBS with gelatin sponge digested by collagenase. RADA/HA is $(RADA/HA)_{200}$, RADA/HACA is $(RADA/HACA)_{200}$, RADA/Chi is $(RADA/HA/Chitosan/HA)_{200}$, IEIK/HA is $(IEIK/HA)_{200}$, IEIK/HACA is $(IEIK/HACA)_{200}$, IEIK/Chi is $(IEIK/HA/Chitosan/HA)_{200}$. (A,B) Stock Solution Control, RADA, IEIK, HA, Film Release Contol, RADA/HA, and IEIK/HA reproduced from figure 3.4. (C,D) Stock Solution Control, RADA, IEIK, HA, Film Release Contol, RADA/HA, and IEIK/HA reproduced from figure 3.5. (A,B) Statistical analysis conducted comparing each sample to the vehicle control using ordinary one way anova with Dunnett multiple comparison correction. (C,D) Statistical analysis conducted comparing each sample to the vehicle control within each individual test using ordinary one way anova with Šídák's multiple comparisons correction. Each test was compared within each individual test, bars show which samples are compared. (ns=not significant, * $P \leq 0.05$, ** $P \leq 0.01$, *** $P \leq 0.001$, **** $P \leq 0.0001$).*

mixing of calcium ions added to the blood to promote clotting if the chitosan promoted the generation of a platelet plug away from the clot detection area of the sample well. The lack of consistent trends in clot formation time is an indication that the mechanism of these adhesive LbL films is not dependent on any effects observed in the clotting factor or platelet aggregation assays. The hemostasis mechanism for the self-assembling peptide nanofibers described in the literature as a physical entrapment of blood components in the peptide hydrogel[14, 51-53] is not disproven by the data collected here. Additionally, it seems that the addition of the adhesive components HACA and chitosan into LbL films do not change the hemostatic mechanism at the level of whole blood clot time. It is possible that *in vitro* testing conditions for clot formation under flow may more directly test the physical hemostasis mechanism and future experiments should be conducted to evaluate the mechanism reported from the literature.

4.3.5 Shear force testing

After showing that the new layer-by-layer formulations were stable and without drastic changes in peptide loading or release, it was important to examine changes in adhesion strength from the addition of LbL films. Adhesion testing was conducted based on ASTM F2255 for lap-shear testing. The Shear test was optimized through several iterations testing various animal tissues and incubation times which can vary for different applications[41]. This optimization data is outlined in the Appendix. Shear force testing showed a significant increase in the shear strength of each formulation except for (IEIK/HACA) compared to untreated gelatin sponge as a control (**Figure 4.9**). This shows that the adhesive LbL formulations were able to make a significant improvement to the adhesive force of the LbL film. It is worth noting that the adhesion forces measured here are relatively small, but they are in an appropriate range to provide increased tissue interaction without damaging the tissue upon removal. Tissue adhesives themselves can also act to promote hemostasis and are commonly used in surgical applications[54]. Future testing will be necessary to confirm if this improvement in adhesive strength and tissue interaction will translate to more rapid hemostasis.

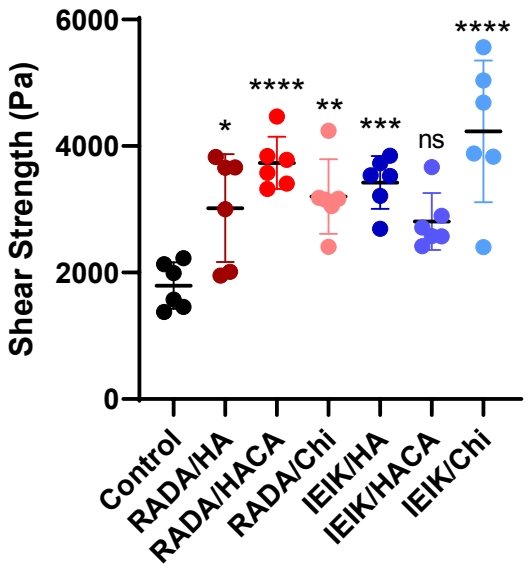

Figure 4.9 Adhesive strength of LbL coated sponges. *Mechanical test of shear force to measure the interfacial shear strength between sponge samples and porcine muscle tissue. RADA/HA is $(RADA/HA)_{200}$, RADA/HACA is $(RADA/HACA)_{200}$, RADA/Chi is $(RADA/HA/Chitosan/HA)_{200}$, IEIK/HA is $(IEIK/HA)_{200}$, IEIK/HACA is $(IEIK/HACA)_{200}$, IEIK/Chi is $(IEIK/HA/Chitosan/HA)_{200}$. n=6 for each formulation. Control is an uncoated gelatin sponge. Statistical analysis conducted comparing each sample to the vehicle control using ordinary one way anova with Dunnett multiple comparison correction. (* $P \leq 0.05$, ** $P \leq 0.01$, *** $P \leq 0.001$, **** $P \leq 0.0001$).*

4.4 Conclusions

LbL formulations were generated by building in adhesive components into the existing peptide LbL formulations. Catechol groups were functionalized onto hyaluronic acid to produce catechol modified HA (HACA). $(RADA/HACA)_n$ and $(IEIK/HACA)_n$ formulations were generated by replacing the HA bath with HACA. Chitosan was built into films using a tetralayer formulation with peptide and HA to create $(RADA/HA/Chi/HA)_n$ and $(IEIK/HA/Chi/HA)_n$ films. These new films showed steady growth and were translated into spray LbL systems. These LbL coated sponge systems showed peptide loadings of the same magnitude as the (peptide/HA) formulations and appropriate encapsulation efficiency. All formulations and components were tested for effects on the activity of several clotting factors as well as interactions with platelets and effects on clot times.

No consistent trends within the film formulations were observed in testing with whole blood indicating that the new LbL formulations do not introduce any drastic changes in blood interactions. Finally these formulations were tested for adhesive force in a shear test showing a significant increase in shear strength over control in almost all cases. This indicates that we were able to improve the tissue interaction of our samples by adding the adhesive LbL films. Further testing is necessary to truly examine if this increase in adhesive force will translate to reduced blood loss. A rat liver injury model was conducted with these formulations, however the data showed too much variation to show any conclusive differences. This data is outlined in the Appendix. A more refined animal model for blood loss will be necessary to properly evaluate any improvements in hemostasis efficacy. These RADA16 and IEIK13 based LbL films with the addition of tissue adhesive components HACA and chitosan have the potential to be a robust bioabsorbable hemostat in the future.

4.5 References

1. Bellamy, R.F., Pedersen, D.C. & Deguzman, L.R. ORGAN BLOOD-FLOW AND THE CAUSE OF DEATH FOLLOWING MASSIVE HEMORRHAGE. *Circulatory Shock* **14**, 113-127 (1984).
2. Katzenell, U., Ash, N., Tapia, A.L., Campino, G.A. & Glassberg, E. Analysis of the causes of death of casualties in field military setting. *Mil Med* **177**, 1065-1068 (2012).
3. Hong, C., Olsen, B.D. & Hammond, P.T. A review of treatments for non-compressible torso hemorrhage (NCTH) and internal bleeding. *Biomaterials* **283**, 121432 (2022).
4. Chambers, J.A. et al. "Stop the Bleed": A U.S. Military Installation's Model for Implementation of a Rapid Hemorrhage Control Program. *Mil Med* **184**, 67-71 (2019).
5. Sobrino, J. & Shafi, S. Timing and causes of death after injuries. *Proceedings* **26**, 120-123 (2013).
6. Spotnitz, W.D. & Burks, S. Hemostats, Sealants, and Adhesives II: Update As Well As How and When to Use the Components of the Surgical Toolbox. *Clinical and Applied Thrombosis-Hemostasis* **16**, 497-514 (2010).
7. Spotnitz, W.D. & Burks, S. Hemostats, sealants, and adhesives: components of the surgical toolbox. *Transfusion* **48**, 1502-1516 (2008).
8. Pusateri, A.E. et al. Making sense of the preclinical literature on advanced hemostatic products. *J Trauma* **60**, 674-682 (2006).
9. Ellis-Behnke, R.G. et al. Nano hemostat solution: immediate hemostasis at the nanoscale. *Nanomedicine : nanotechnology, biology, and medicine* **2**, 207-215 (2006).
10. Ellis-Behnke, R. At the nanoscale: nanohemostat, a new class of hemostatic agent. *Wires Nanomed Nanobi* **3**, 70-78 (2011).
11. Gelain, F., Luo, Z., Rioult, M. & Zhang, S. Self-assembling peptide scaffolds in the clinic. *NPJ Regenerative medicine* **6**, 9 (2021).
12. Sankar, S. et al. Clinical Use of the Self-Assembling Peptide RADA16: A Review of Current and Future Trends in Biomedicine. *Frontiers in Bioengineering and Biotechnology* **9** (2021).
13. Verbraeken, B. et al. Efficacy and histopathological effects of self-assembling peptides RADA16 and IEIK13 in neurosurgical hemostasis. *Nanomedicine : nanotechnology, biology, and medicine* **40**, 102485 (2022).
14. Hsu, B.B. et al. Clotting Mimicry from Robust Hemostatic Bandages Based on Self-Assembling Peptides. *Acs Nano* **9**, 9394-9406 (2015).
15. Hammond, P.T. Form and function in multilayer assembly: New applications at the nanoscale. *Adv Mater* **16**, 1271-1293 (2004).
16. Kim, B.S., Lee, H., Min, Y.H., Poon, Z. & Hammond, P.T. Hydrogen-bonded multilayer of pH-responsive polymeric micelles with tannic acid for surface drug delivery. *Chem Commun*, 4194-4196 (2009).
17. Shah, N.J., Hong, J., Hyder, M.N. & Hammond, P.T. Osteophilic Multilayer Coatings for Accelerated Bone Tissue Growth. *Adv Mater* **24**, 1445-1450 (2012).
18. Shukla, A. et al. Controlling the release of peptide antimicrobial agents from surfaces. *Biomaterials* **31**, 2348-2357 (2010).
19. Moskowitz, J.S. et al. The effectiveness of the controlled release of gentamicin from polyelectrolyte multilayers in the treatment of Staphylococcus aureus infection in a rabbit bone model. *Biomaterials* **31**, 6019-6030 (2010).
20. Shukla, A., Fuller, R.C. & Hammond, P.T. Design of multi-drug release coatings targeting infection and inflammation. *J Control Release* **155**, 159-166 (2011).
21. DeMuth, P.C., Su, X.F., Samuel, R.E., Hammond, P.T. & Irvine, D.J. Nano-Layered Microneedles for Transcutaneous Delivery of Polymer Nanoparticles and Plasmid DNA. *Adv Mater* **22**, 4851-+ (2010).

22. Macdonald, M.L. et al. Tissue integration of growth factor-eluting layer-by-layer polyelectrolyte multilayer coated implants. *Biomaterials* **32**, 1446-1453 (2011).
23. Samuel, R.E. et al. Osteoconductive protamine-based polyelectrolyte multilayer functionalized surfaces. *Biomaterials* **32**, 7491-7502 (2011).
24. Min, J., Braatz, R.D. & Hammond, P.T. Tunable staged release of therapeutics from layer-by-layer coatings with clay interlayer barrier. *Biomaterials* **35**, 2507-2517 (2014).
25. Min, J.H. et al. Designer Dual Therapy Nanolayered Implant Coatings Eradicate Biofilms and Accelerate Bone Tissue Repair. *Acs Nano* **10**, 4441-4450 (2016).
26. Krogman, K.C., Lowery, J.L., Zacharia, N.S., Rutledge, G.C. & Hammond, P.T. Spraying asymmetry into functional membranes layer-by-layer. *Nat Mater* **8**, 512-518 (2009).
27. Hsu, B.B., Hagerman, S.R. & Hammond, P.T. Rapid and efficient sprayed multilayer films for controlled drug delivery. *Journal of Applied Polymer Science* **133** (2016).
28. Dai, C.L., Liu, C.S., Wei, J., Hong, H. & Zhao, Q.H. Molecular imprinted macroporous chitosan coated mesoporous silica xerogels for hemorrhage control. *Biomaterials* **31**, 7620-7630 (2010).
29. Malmquist, J.P., Clemens, S.C., Oien, H.J. & Wilson, S.L. Hemostasis of oral surgery wounds with the HemCon Dental Dressing. *J Oral Maxil Surg* **66**, 1177-1183 (2008).
30. Narimane Mati-Baouche, P.-H.E., Helene de Baynast, Guillaume Pierre, Cedric Delattre, Philippe Michaud Chitosan as an adhesive. *European Polymer Journal* **60**, 198-212 (2014).
31. Chou, T.C., Fu, E., Wu, C.J. & Yeh, J.H. Chitosan enhances platelet adhesion and aggregation. *Biochem Bioph Res Co* **302**, 480-483 (2003).
32. Saiz-Poseu, J., Mancebo-Aracil, J., Nador, F., Busque, F. & Ruiz-Molina, D. The Chemistry behind Catechol-Based Adhesion. *Angew Chem Int Edit* **58**, 696-714 (2019).
33. Sun, C.J., Srivastava, A., Reifert, J.R. & Waite, J.H. Halogenated DOPA in a Marine Adhesive Protein. *The Journal of adhesion* **85**, 126 (2009).
34. Min, Y.J. & Hammond, P.T. Catechol-Modified Polyions in Layer-by-Layer Assembly to Enhance Stability and Sustain Release of Biomolecules: A Bioinspired Approach. *Chem Mater* **23**, 5349-5357 (2011).
35. Zhou, Y., Kang, L., Yue, Z., Liu, X. & Wallace, G.G. Composite Tissue Adhesive Containing Catechol-Modified Hyaluronic Acid and Poly-l-lysine. *ACS Applied Bio Materials* **3**, 628-638 (2020).
36. Zhou, Y., Yue, Z., Chen, Z. & Wallace, G. 3D Coaxial Printing Tough and Elastic Hydrogels for Tissue Engineering Using a Catechol Functionalized Ink System. *Advanced healthcare materials* **9**, e2001342 (2020).
37. Monteiro, I.P., Shukla, A., Marques, A.P., Reis, R.L. & Hammond, P.T. Spray-assisted layer-by-layer assembly on hyaluronic acid scaffolds for skin tissue engineering. *Journal of biomedical materials research. Part A* **103**, 330-340 (2015).
38. Gkikas, M. et al. Systemically Administered Hemostatic Nanoparticles for Identification and Treatment of Internal Bleeding. *Acs Biomater Sci Eng* **5**, 2563-2576 (2019).
39. Hong, C. et al. Modulating Nanoparticle Size to Understand Factors Affecting Hemostatic Efficacy and Maximize Survival in a Lethal Inferior Vena Cava Injury Model. *Acs Nano* **16**, 2494-2510 (2022).
40. Barrett, C.D. et al. Human neutrophil elastase mediates fibrinolysis shutdown through competitive degradation of plasminogen and generation of angiostatin. *The journal of trauma and acute care surgery* **83**, 1053-1061 (2017).
41. Yuk, H. et al. Dry double-sided tape for adhesion of wet tissues and devices. *Nature* **575**, 169-174 (2019).
42. Arosio, P., Owczarz, M., Wu, H., Butte, A. & Morbidelli, M. End-to-End Self-Assembly of RADA 16-I Nanofibrils in Aqueous Solutions. *Biophys J* **102**, 1617-1626 (2012).

43. GIL, E.S., GILBERT, K. & Mehta, M., Edn. C07K 7/08 (2006.01), A61L 27/22 (2006.01), A61K 38/12 (2006.01), A61L 27/54 (2006.01), A61L 27/58 (2006.01). (ed. W.I.P. Organization) (2015).
44. Zhang, H., Luo, H. & Zhao, X. Mechanistic Study of Self-Assembling Peptide RADA16-I in Formation of Nanofibers and Hydrogels. *Journal of Nanotechnology in Engineering and Medicine* **1** (2009).
45. Xu, L., Ankner, J.F. & Sukhishvili, S.A. Steric Effects in Ionic Pairing and Polyelectrolyte Interdiffusion within Multilayered Films: A Neutron Reflectometry Study. *Macromolecules* **44**, 6518-6524 (2011).
46. Lewandowska, K., Szulc, M. & Sionkowska, A. Effect of Solvent on the Hydrodynamic Properties of Collagen. *Polymers* **13** (2021).
47. Souid, A.-K. in Pediatric Emergency Medicine. (eds. J.M. Baren, S.G. Rothrock, J.A. Brennan & L. Brown) 917-926 (W.B. Saunders, Philadelphia; 2008).
48. Brummel-Ziedins, K., Vossen, C.Y., Rosendaal, F.R., Umezaki, K. & Mann, K.G. The plasma hemostatic proteome: thrombin generation in healthy individuals. *Journal of thrombosis and haemostasis : JTH* **3**, 1472-1481 (2005).
49. Howard, P.R., Bovill, E.G., Pike, J., Church, W.R. & Tracy, R.P. Factor VII antigen levels in a healthy blood donor population. *Thrombosis and haemostasis* **72**, 21-27 (1994).
50. Hellstern, P., Beeck, H., Fellhauer, A., Fischer, A. & Faller-Stockl, B. Measurement of factor VII and of activated factor VII in healthy individuals and in prothrombin complex concentrates. *Thrombosis research* **86**, 493-504 (1997).
51. Luo, Z., Wang, S. & Zhang, S. Fabrication of self-assembling D-form peptide nanofiber scaffold d-EAK16 for rapid hemostasis. *Biomaterials* **32**, 2013-2020 (2011).
52. Wang, T., Zhong, X., Wang, S., Lv, F. & Zhao, X. Molecular mechanisms of RADA16-1 peptide on fast stop bleeding in rat models. *International journal of molecular sciences* **13**, 15279-15290 (2012).
53. Song, H., Zhang, L. & Zhao, X. Hemostatic efficacy of biological self-assembling peptide nanofibers in a rat kidney model. *Macromolecular bioscience* **10**, 33-39 (2010).
54. Reece, T.B., Maxey, T.S. & Kron, I.L. A prospectus on tissue adhesives. *Am J Surg* **182**, 40S-44S (2001).

Chapter 5. Conclusions and Future Directions

5.1 Thesis Summary

Layer-by-layer (LbL) formulations using RADA16 and IEIK13 are promising approaches to promote hemostasis in a lightweight, stable, and resorbable dressing. This thesis presents the development and testing of new LbL formulations containing IEIK13 as well as the addition of the tissue adhesive components catechol groups and chitosan. We provide a look into possible mechanism of action for hemostasis as well as a measure of LbL film adhesion to tissue.

In Chapter 1, we reviewed existing hemostat solutions and highlighted where there is still room for improvement. LbL film assembly of RADA16 and IEIK13 was introduced as a promising solution to meet most if not all the criteria for the ideal hemostat.

In Chapter 2, characterization and optimization were carried out on LbL films containing RADA16 and IEIK13. Methods for handling and working with the peptide solutions were developed. Spray LbL systems were developed and used to coat resorbable gelatin sponges with LbL films.

In Chapter 3, we investigated the mechanism by which the self-assembling peptides RADA16 and IEIK13 are able to promote hemostasis. When examining platelet aggregation, no significant changes were observed with the peptides. Some minor effects on clotting factor activity were observed when incubating peptide solutions with plasma, however these were not significant enough to impact overall clot formation speed or strength in whole blood. We demonstrated that the peptide fibers are unlikely to promote clotting in the absence of flow.

In Chapter 4, we examined the importance of tissue adhesion for the treated dressings. New LbL formulations were developed that built in catechol groups or chitosan to enhance wound tissue interactions. An increase in adhesive shear force over untreated gelatin sponges was observed in almost all new formulations showing that the application of the LbL film did have a positive effect on the adhesive interactions with tissue.

5.2 Future Directions

5.2.1 Further investigation into hemostasis mechanism of RADA16 and IEIK13

In this thesis, we have made an effort to examine the mechanism in which RADA16 and IEIK13 are able to promote hemostasis. Previous work has generated the hypothesis that the peptide gel acts as an artificial fibrin clot, collecting blood components and creating a localized high concentration which leads more rapid hemostasis[1-4]. We examined various clotting factors and other in vitro clotting assays and were unable to show any direct effect on clot formation. While this can support the hypothesis through exclusion of possibilities, the lack of blood flow in vitro that is present in vivo prevents us from directly testing the hypothesis. An in vitro clotting test capable of simulating blood flow to and through the peptide gel would be able to either support or challenge the current mechanism hypothesis.

5.2.2 In vivo testing of LbL formulations

In this thesis, several different peptide LbL formulations were developed and characterized in vitro. It is difficult to know how promising these new formulations are without examining their effects on blood loss in vivo. While we were able to run a few promising pilot studies in a swine liver injury model, those studies lacked the numerical power to be able to show any conclusive results. Additionally, we have hypothesized that an increase in bandage tissue adhesion will translate to reduced blood loss in vivo, however we have not had the chance truly answer that question. A rat liver injury model was tested with the adhesive LbL formulations. However, the surgery proved to be too variable to make any conclusions from the results. In vivo testing of these hemostatic dressings is the clear next step to developing and progressing these hemostatic peptide systems.

5.2.3 Addition of other functionalities to hemostatic films

In this thesis, the ability to take an existing hemostatic LbL film formulation and modify it to include additional functionalities was outlined. In this case, tissue adhesive molecules chitosan

and a catechol-modified hyaluronic acid (HACA) were included into RADA16 and IEIK13 based films. Future work could examine adding other functionalities to the hemostatic films to address other aspects of wound care. This could include the addition of controlled release antibiotics[5, 6], painkillers, or tissue factors to promote wound healing[7]. Building other functionalities into the LbL films would take advantage of the versatility of layer-by-layer while allowing more specific wound situations to be targeted.

5.3 References:

1. Luo, Z., Wang, S. & Zhang, S. Fabrication of self-assembling D-form peptide nanofiber scaffold d-EAK16 for rapid hemostasis. *Biomaterials* **32**, 2013-2020 (2011).
2. Wang, T., Zhong, X., Wang, S., Lv, F. & Zhao, X. Molecular mechanisms of RADA16-1 peptide on fast stop bleeding in rat models. *International journal of molecular sciences* **13**, 15279-15290 (2012).
3. Song, H., Zhang, L. & Zhao, X. Hemostatic efficacy of biological self-assembling peptide nanofibers in a rat kidney model. *Macromolecular bioscience* **10**, 33-39 (2010).
4. Hsu, B.B. et al. Clotting Mimicry from Robust Hemostatic Bandages Based on Self-Assembling Peptides. *Acs Nano* **9**, 9394-9406 (2015).
5. Hsu, B.B. et al. Multifunctional Self-Assembled Films for Rapid Hemostat and Sustained Anti-infective Delivery. *Acs Biomater Sci Eng* **1**, 148-156 (2015).
6. Shukla, A., Fuller, R.C. & Hammond, P.T. Design of multi-drug release coatings targeting infection and inflammation. *J Control Release* **155**, 159-166 (2011).
7. Hammond, P.T. Building biomedical materials layer-by-layer. *Mater Today* **15**, 196-206 (2012).

Appendix. Supplemental Information

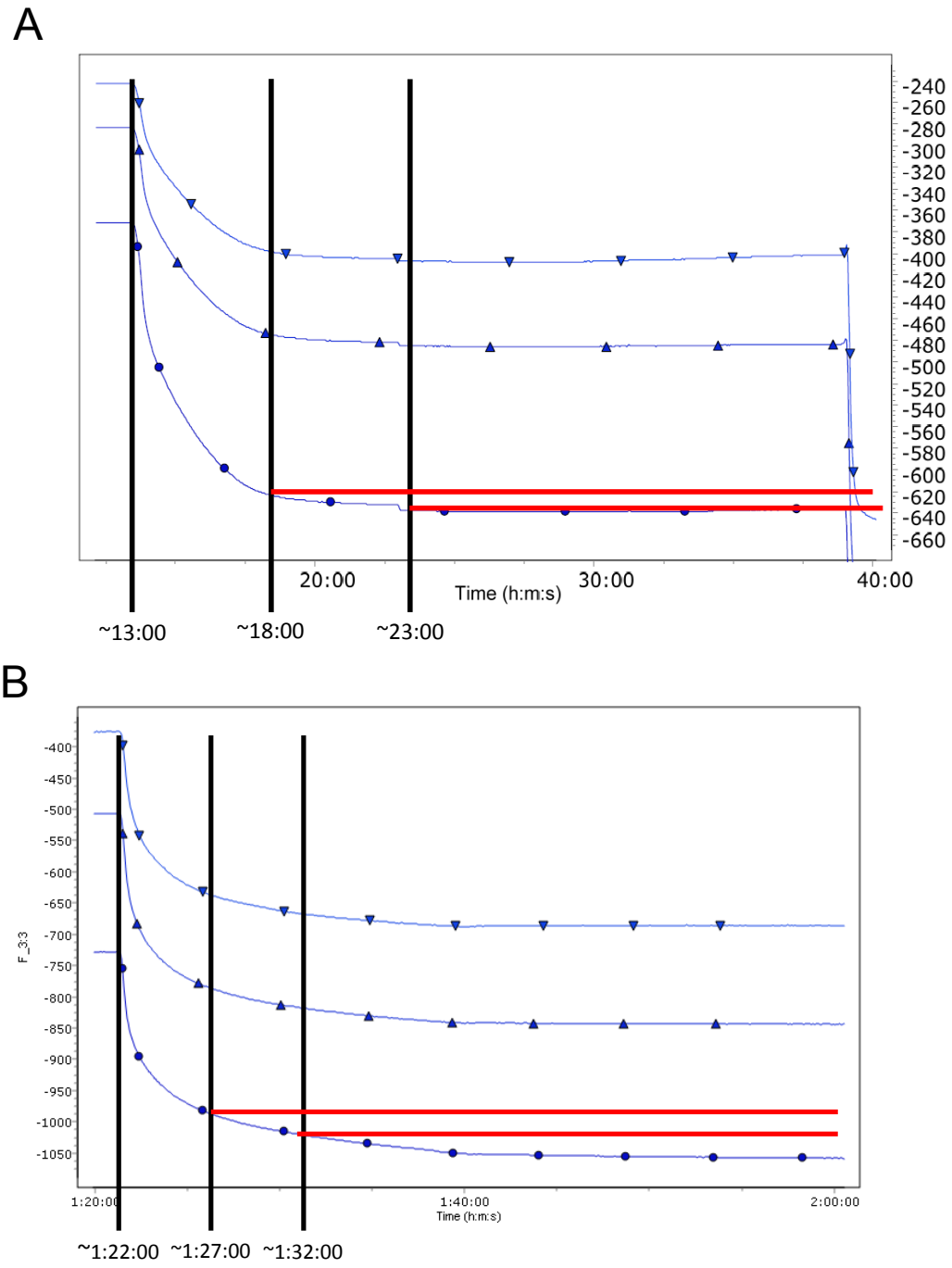

Figure A.1 Visual Depiction of Time to equilibrium adsorption for RADA16 in 10mM HCl. (A) shows the first bilayer of adsorption. (B) shows the second bilayer of adsorption. A decrease in frequency translates to deposited mass. Black lines represent the start of the adsorption, 5 minutes of adsorption, and 10 minutes of adsorption. Each curve represents a different resonance point on the crystal. The second Bilayer adsorption takes longer than the first.

(A)

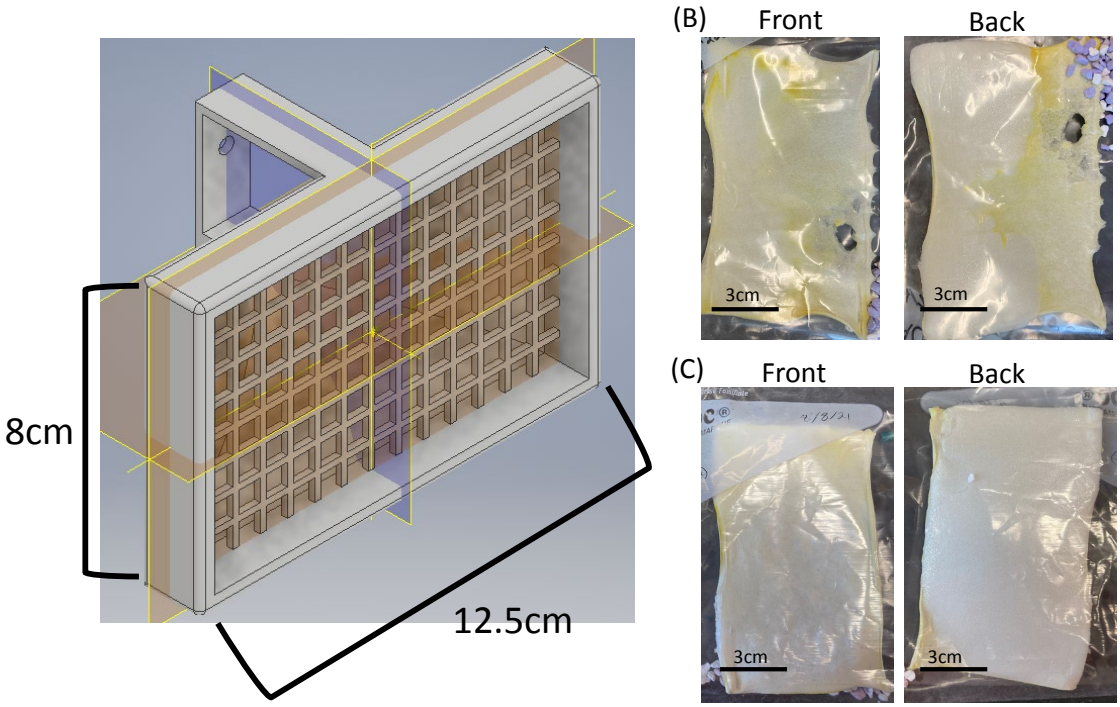

Figure A.2 Spray LbL setup optimization. (A) 3D model of sponge holder designed to hold and coat 8cm x 12.5cm x 10mm gelatin sponges. (B) LbL coated sponge front and back sprayed at full house vacuum pressure (Closed pressure of approximately -90kPa). (C) LbL coated sponge front and back sprayed at half house vacuum pressure (closed pressure of approximately -45kPa). The reduction in pressure helps keep the sponge from soaking through and being damaged after the LbL spraying process.

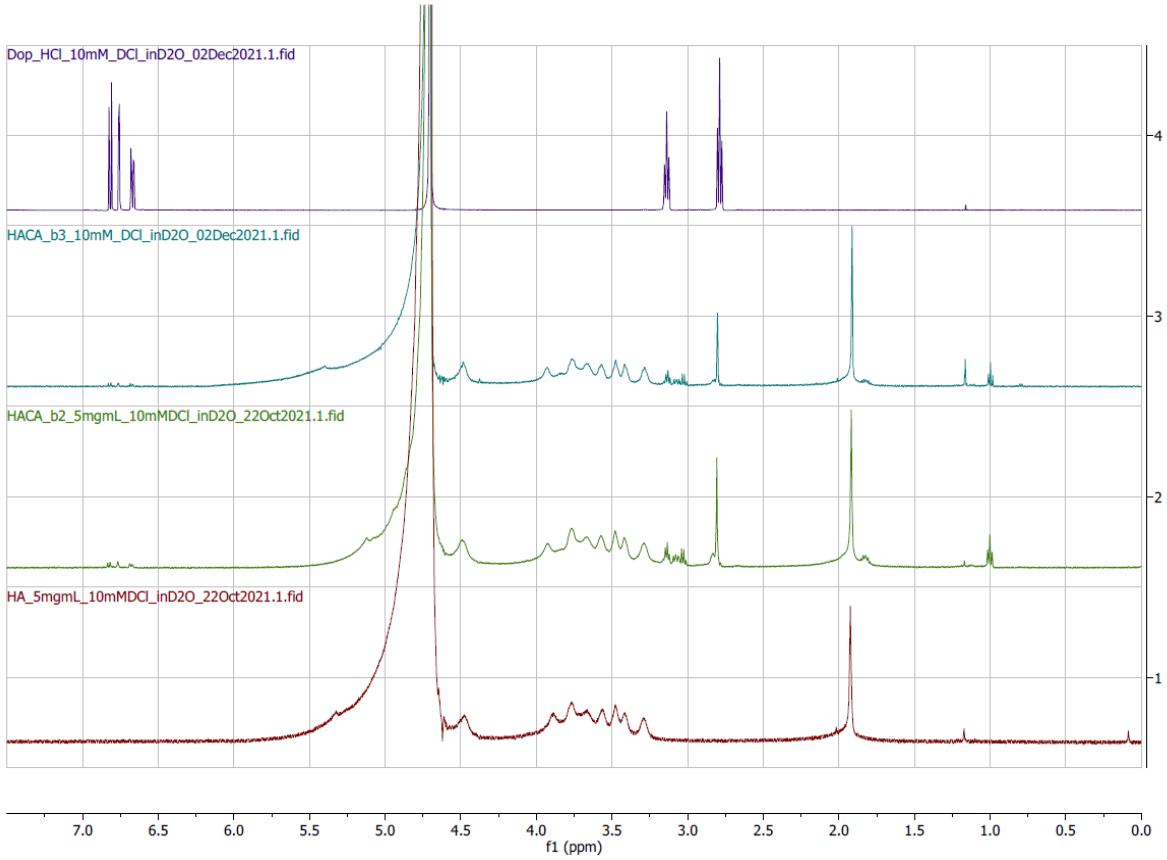

Figure A.3 NMR of different batches of catechol functionalized HA (HACA) used to determine the percent functionalization of hyaluronic acid side groups. NMR spectrum of Dopamine HCl (purple), HACA batch 3 (blue), HACA batch 3 (green), hyaluronic acid (HA) (red). Percent functionalization values for Batch 2 and Batch 3 are between 24-44% functionalization based on integration of different dopamine peaks.

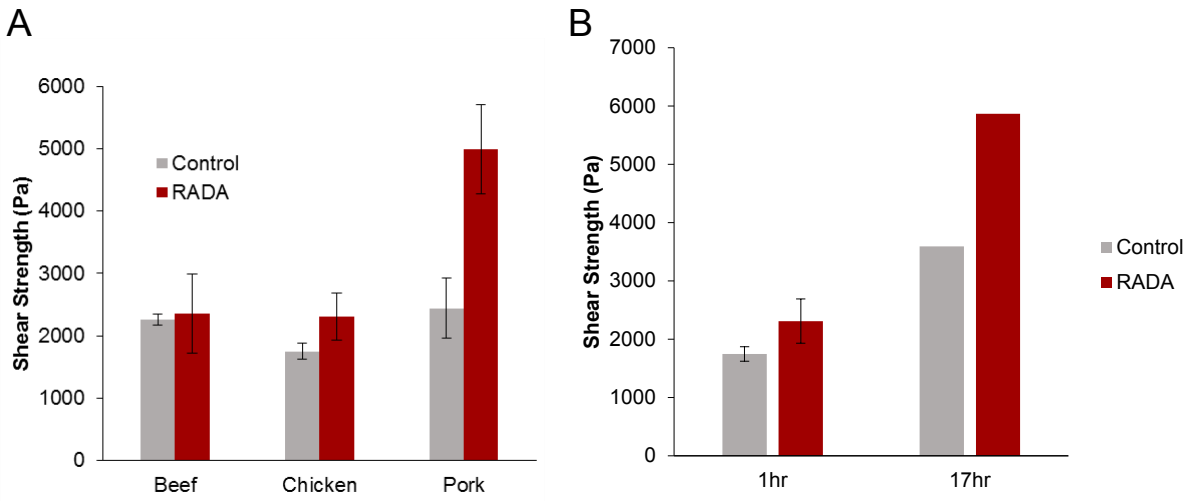

Figure A.4 Optimization of adhesion shear test methods. (A) Testing different types of muscle tissue in a shear force test. (B)Testing effect different amounts of contact time between the sponge sample and chicken muscle tissue on shear strength in a shear force test. Control is an uncoated gelatin sponge control. RADA is $(RADA/HA)_{200}$ sponges made using 0.5 g/L RADA16 and HA solutions. (A) n=3 for all samples, (B) n=3 for 1hr and n=1 for 17hr. Pork was selected moving forward because of the larger effect observed from the coated sponge samples. Longer contact time between tissue and sponge samples showed a larger adhesion force, but one hour was used to stay relevant to the bleeding application.

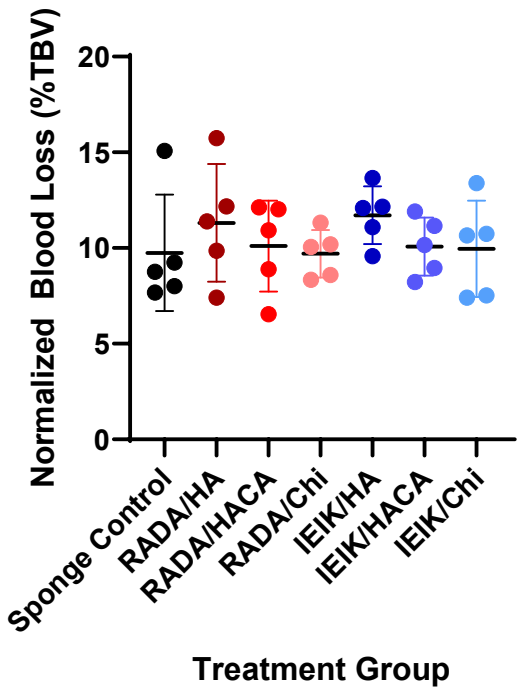

Figure A.5 Rat Liver injury test model. Testing adhesive LbL formulations in a rat liver injury model. N=5. Blood loss normalized to rat total blood volume. Sponge control is an uncoated gelatin sponge. *RADA/HA is $(RADA/HA)_{200}$, RADA/HACA is $(RADA/HACA)_{200}$, RADA/Chi is $(RADA/HA/Chitosan/HA)_{200}$, IEIK/HA is $(IEIK/HA)_{200}$, IEIK/HACA is $(IEIK/HACA)_{200}$, IEIK/Chi is $(IEIK/HA/Chitosan/HA)_{200}$.* Statistical analysis conducted comparing each sample to the sponge control using ordinary one way anova with Dunnett multiple comparison correction, no significant differences in blood loss were observed.

In vivo Rat liver injury model protocol: Rats were anesthetized by the inhalation of isoflurane. Anesthesia was maintained with a facial mask. The rat was then restrained and the midsection shaved. A 3 cm midline incision was made to open the abdominal cavity. An incision was made on the left medial lobe of the liver approximately 1 cm from the tip. The wound are was immediately covered with a dressing sample and light compression was applied for thirty seconds. Afterward, compression was ceased and the abdominal cavity was closed. After 1 hour, the abdominal cavity was reopened and blood loss was collected using preweighed gauze to soak up excess blood and blood clots The rats were then uthanized still under anesthesia by Fatal-Plus (pentobarbital) intracardiac injection at 100 mg/kg. Blood loss was normalized by total blood volume (TBV).

This injury model did not show significant effects from the LbL coated sponge samples due to a large amount of variation in the control samples. This test did highlight the importance of adhesion between the sponge sample and the wound surface. A test model with less variation in the control blood loss will be necessary to properly observe effects from the adhesive LbL film formulations.